The Astrophysical Journal, 698:43–74, 2009 June 10 doi:10.1088/0004-637X/698/1/43

JET BREAKS AND ENERGETICS OF *Swift* GAMMA-RAY BURST X-RAY AFTERGLOWS

J. L. Racusin[1], E. W. Liang[2,3], D. N. Burrows[1], A. Falcone[1], T. Sakamoto[4], B. B. Zhang[2], B. Zhang[2], P. Evans[5], and J. Osborne[5]

[1] Department of Astronomy & Astrophysics, The Pennsylvania State University, 525 Davey Lab, University Park, PA 16802, USA; racusin@astro.psu.edu
[2] Department of Physics, University of Nevada, Las Vegas, NV 89154, USA
[3] Department of Physics, Guangxi University, Nanning 530004, China
[4] Astrophysics Science Division, Code 661, NASA's Goddard Space Flight Center, 8800 Greenbelt Road, Greenbelt, MD 20771, USA
[5] Department of Physics and Astronomy, University of Leicester, Leicester, LE1 7RH, UK
Received 2008 December 24; accepted 2009 March 25; published 2009 May 19

ABSTRACT

We present a systematic temporal and spectral study of all *Swift*-X-ray Telescope observations of gamma-ray burst (GRB) afterglows discovered between 2005 January and 2007 December. After constructing and fitting all light curves and spectra to power-law models, we classify the components of each afterglow in terms of the canonical X-ray afterglow and test them against the closure relations of the forward shock models for a variety of parameter combinations. The closure relations are used to identify potential jet breaks with characteristics including the uniform jet model with and without lateral spreading and energy injection, and a power-law structured jet model, all with a range of parameters. With this technique, we survey the X-ray afterglows with strong evidence for jet breaks (∼12% of our sample), and reveal cases of potential jet breaks that do not appear plainly from the light curve alone (another ∼30%), leading to insight into the missing jet break problem. Those X-ray light curves that do not show breaks or have breaks that are not consistent with one of the jet models are explored to place limits on the times of unseen jet breaks. The distribution of jet break times ranges from a few hours to a few weeks with a median of ∼1 day, similar to what was found pre-*Swift*. On average, *Swift* GRBs have lower isotropic equivalent γ-ray energies, which in turn result in lower collimation corrected γ-ray energies than those of pre-*Swift* GRBs. Finally, we explore the implications for GRB jet geometry and energetics.

Key words: gamma rays: bursts – radiation mechanisms: non-thermal – X-rays: bursts

1. INTRODUCTION

One of the most surprising puzzles to emerge from the *Swift* (Gehrels et al. 2004) mission and its dynamic study of gamma-ray bursts (GRBs) is the lack of expected jet breaks in X-ray afterglow emission. It is vital to the entire study of GRBs to understand jet geometry, because of the inferred effects on the total output energy, GRB rate, afterglow structure, interactions with environment, and jet physical mechanisms. Pre-*Swift* optical observations showed tens of cases of steepening in the light curves several days after the GRB triggers (Frail et al. 2001; Bloom et al. 2001; Zeh et al. 2006). This steepening was interpreted as evidence for the collimation of the burst ejecta with physical half-angle θ_j. The ejecta moves at relativistic velocities with a bulk Lorentz factor, Γ, and the radiation is relativistically beamed into an angle $\theta = 1/\Gamma$. As the ejecta sweeps up surrounding material, the fireball decelerates, with the beaming angle eventually exceeding the physical collimation angle, causing a sudden increase in the rate of decay of the flux (i.e., the jet break). At the same time, sideways expansion of the ejecta with relativistic speeds also causes a sudden flux decrease (Sari et al. 1999; Rhoads 1999; Zhang & Mészáros 2004). Most likely both of these effects contribute to the jet breaks, and therefore, both models must be considered. Breaks are expected to be achromatic based on the assumption that the afterglow emission regions and mechanisms are the same for various spectral regimes, and should therefore only reflect ejecta geometry. Achromaticity has indeed been confirmed in the optical/near-infrared bands in pre-*Swift* GRBs (Kulkarni et al. 1999; Harrison et al. 2001; Klose et al. 2004).

In the *Swift* era, it is X-ray afterglow light curves that provide the most homogeneous data set to study GRB afterglows. With the rapid GRB triggers provided by the *Swift*-BAT, and the autonomous prompt *Swift*-X-ray Telescope (XRT) observations that frequently begin within 1–2 minutes of the trigger, X-ray afterglows have gone from sparsely sampled single power laws (*BeppoSAX* era; de Pasquale et al. 2006) to a rich database of light curves with widely varying properties and durations. A common canonical shape of the *Swift*-XRT X-ray light curves emerged (Nousek et al. 2006; Zhang et al. 2006; Figure 1) with five components (an initial steep decay, a shallow-decay "plateau" phase, a normal decay, a jetlike decay component, and flares) that could be used to explain the overall structure of the afterglows. While elements of this canonical picture are seen in most X-ray afterglows, few afterglows contain all five components. Surprisingly, fully "canonical" jet breaks are rarely observed in the XRT light curves (Burrows & Racusin 2007; Liang et al. 2008; Evans et al. 2008).

In this work, we assume that all X-ray afterglows have inherently similar shapes (the canonical shape) with deviations in behavior due to environment, electron spectral shape, spectral regime, presence of energy injection, and jet properties. We also explore observational biases such as late beginning and early ending of observation, flares, and observing gaps that lead to missing portions of individual light curves which can produce ambiguities in the identification of segments.

We assume that the light curve segments following the initial steep decay (Figure 1, segments II–IV) are due to external forward shocks. Although we recognize that several alternative models have recently been proposed to explain the origin of the X-ray afterglows (e.g., Genet et al. 2007; Shao & Dai 2007; Ghisellini et al. 2007b; Liang et al. 2007, 2008; Uhm & Beloborodov 2007; Panaitescu 2008; Kumar et al. 2008), as discussed below (see also Liang et al. 2007, 2008), the

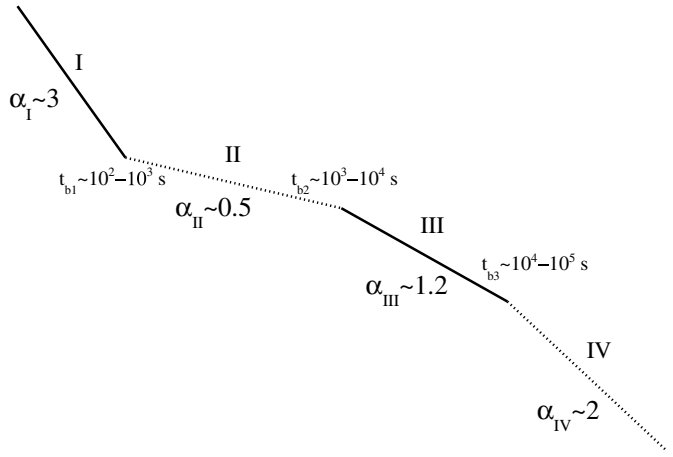

Figure 1. Canonical X-ray afterglow light curve defined by Zhang et al. (2006) and Nousek et al. (2006). Segment I is generally attributed to high latitude emission. Segment II is due to continuous energy injection by the central engine. Segment III is the normal spherical decay of the afterglow. Segment IV is the post-jet break decay. Segment V (not shown) is due to flares which can occur during any phase, in multiple, and in widely varying strengths.

X-ray data can be generally interpreted within the framework of the forward shock, so that invoking non-forward-shock models is not absolutely demanded by the data. We also focus solely on the X-ray behavior of the afterglow light curves, while acknowledging that chromatic behavior inferred from optical observations provides important clues into jet properties (Liang et al. 2008).

Based on the optical afterglow observations in the pre-*Swift* era (Frail et al. 2001; Bloom et al. 2003), we expected to find jet breaks occurring within several days after the bursts, with the light curves breaking to decay slopes of ∼2.2 (Sari et al. 1999). Several recent studies (Burrows & Racusin 2007; Liang et al. 2008; Kocevski & Butler 2008; Willingale et al. 2007; Evans et al. 2008) have searched for jet breaks in the XRT data and agree that there is a substantial deficit relative to pre-*Swift* expectations. Panaitescu (2007) suggests additional potential jet breaks in the sample, but is very broad in his jet break definition, attributing even breaks with shallower decays occurring after plateaus to jet breaks without discussion of the more global context of the light curves. This method does not follow the framework of the canonical picture observed in many afterglows, though it suggests that some jet breaks are buried in the existing measured breaks, which we explore in more detail. Previous studies of large afterglow samples have applied only the simplest afterglow models, rather than the detailed interpretations needed to explain GRBs in individual cases. For example, the end of the plateau phase is often attributed to a cessation of energy injection without considering the possibility that it might represent a jet break during energy injection (see also de Pasquale et al. 2008). Other model variations including a flat electron spectrum, different progenitor environments, and jet geometry and dynamics would slightly alter the properties of the canonical behavior. Therefore, in this study we perform a more generalized characterization of all XRT afterglows, re-examining a wide variety of closure relations to evaluate which segments of each light curve are consistent with each family of closure relations, whether there are any jet breaks that have been previously misinterpreted, and what limits can be placed on jet break statistics and energetics.

There are multiple reasons that we may not be detecting jet breaks in XRT data. We ask the following questions to explore this problem: Are jet breaks subtle and buried within our observing errors (see also Curran et al. 2008)? Do the jet breaks occur after the XRT observations end? Do observational biases that cause us to miss parts of the light curves result in ambiguous classifications? Could some of the breaks at the end of the plateau phases actually be jet breaks that are masked by continuing energy injection? Are those GRBs for which jet breaks are not detected somehow intrinsically or observationally different than those for which they are detected? The goal of this study is to attempt to answer these questions.

We describe the data sample selection, temporal analysis, and spectral analysis in Section 2, the closure relations in Section 3, the results in Section 4, discussion and implications in Section 5, and conclude in Section 6. Throughout this paper, we adopted the convention $F \propto t^{-\alpha}\nu^{-\beta}$ where α is the temporal index and β is the spectral index, F is the energy flux (with cgs units of erg cm^{-2} s^{-1}), and we use cosmological parameters $H_0 = 70$ km s^{-1} Mpc^{-1}, $\Omega_M = 0.3$, $\Omega_\Lambda = 0.7$.

2. DATA REDUCTION

The *Swift*-XRT detected 262 GRB X-ray afterglows between 2005 January and 2007 December. The majority of these (241) were discovered by *Swift*-BAT, and the other 21 bursts were discovered by *International Gamma-Ray Astrophysics Laboratory* (*INTEGRAL*), *High Energy Transient Explorer 2* (*HETE*), or the Interplanetary Network (IPN) that were followed up by the *Swift*-XRT beginning within approximately 1 day. We include only those afterglows with at least 60 background-subtracted photons, enough to construct a basic light curve and characterize temporal and spectral properties (in the methods described in Sections 2.1 and 2.2). Removing those objects for which we do not have adequate temporal and spectral information, our resulting main sample consists of 230 GRB X-ray afterglows: 15 of those afterglows were not originally discovered by *Swift*, 13 are short bursts ($T_{90} < 2$ s), and 85 have measured redshifts reported in the literature.

Level 1 data products were downloaded from the NASA/GSFC *Swift* Data Center (SDC) and processed using XRTDAS software (ver. 2.0.1). The *xrtpipeline* task was used to generate level 2 cleaned event files. Only events with Windowed Timing (WT) mode grades 0–2 and Photon Counting (PC) mode grades 0–12 and energies between 0.3 and 10.0 keV were used in subsequent temporal and spectral analysis.

2.1. Temporal Analysis

We assume that all X-ray light curves in our sample inherently follow the canonical form (Figure 1) described by Zhang et al. (2006) and Nousek et al. (2006). These four segments and additional component are as follows. I: the initial steep decay often attributed to high-latitude emission or the curvature effect (Kumar & Panaitescu 2000; Qin et al. 2004; Liang et al. 2006; Zhang et al. 2007a); II: the plateau, which is frequently attributed to continuous energy injection from the central engine (Rees & Mészáros 1998; Dai & Lu 1998; Sari & Mészáros 2000; Zhang & Mészáros 2001; Granot & Kumar 2006; Zhang et al. 2006; Liang et al. 2007); III: the normal decay due to the deceleration of an adiabatic fireball (Mészáros 2002; Zhang et al. 2006); IV: the post-jet break phase (Rhoads 1999; Sari et al. 1999; Mészáros 2002; Piran 2005); V: flares, which are seen in ∼1/3 of all *Swift* GRB X-ray afterglows during any phase (I–IV) and are believed to be caused by sporadic emission from the central engine (Burrows et al. 2005; Zhang et al. 2006; Chincarini

et al. 2007; Falcone et al. 2007). We classify the data into these segments based upon the criteria described below. Only 25 cases contain all four light curve segments, with 14 cases also containing flares.

This analysis does not address the phenomenon of X-ray flares, but rather excludes them from the spectral and temporal analysis. See Chincarini et al. (2007) and Falcone et al. (2007) for detailed studies of X-ray flares and analysis on this data set. These studies have shown that significant spectral evolution occurs throughout the flares, therefore in order to constrain the properties of the underlying afterglows, we remove the time intervals of significant flaring from subsequent temporal and spectral analysis. Flaring was determined by visual inspection of the light curves and hardness ratios. Only the most apparent flares were removed, with no attempt to constrain small-scale or micro-flaring. Large flares that overlap and significantly exceed the level of the underlying afterglow can also mask whole segments, making it impossible to determine the underlying temporal and spectral properties. The flaring in these cases usually occurs at the beginning of light curves, overwhelming segment I and leading to light curves with apparent segments II–III afterwards. Rather than guessing the properties or presence of these specific flaring segments, we remove those time intervals and proceed as if they were not part of the rest of the light curves.

For those X-ray afterglows that were also observed by *Chandra* at late times, we include those data points in our temporal but not spectral fits. These bursts include GRB 051221A (Burrows et al. 2006), GRB 050724 (Grupe et al. 2006), and GRB 060729 (D. Grupe et al. 2009).

2.1.1. Light Curve Construction

All light curves were extracted from the public XRT-team light curve repository (Evans et al. 2007, 2008). These XRT light curves were created by extracting the counts in a circular region around the afterglow with a variable source extraction radius designed to optimize the signal-to-noise ratio depending on the count rate in both the WT and PC mode data. A region clear of any serendipitous background sources was used to estimate the contribution of background counts in the source region. The number of counts per bin are chosen depending on the count rate to show sufficient detail with reasonable error bars and binning. The background-subtracted count rates are also corrected for the portion of the point-spread function (PSF) excluded by the extraction region and any proximity to bad columns and hot pixels in the XRT CCD. Where necessary, corrections for photon pile-up were also made by excluding a central portion of the extraction region.

2.1.2. Light Curve Fitting

We have developed tools to fit single power laws, broken power laws, double broken power laws, and triple broken power laws with the following functional forms to the XRT light curves: single power law:

$$F(t) = N\, t^{-\alpha_0}, \tag{1}$$

broken power law:

$$F(t) = N \begin{cases} t^{-\alpha_1} & t < t_{b_1} \\ t_{b_1}^{(\alpha_2-\alpha_1)}\, t^{-\alpha_2} & t > t_{b_1}, \end{cases} \tag{2}$$

double broken power law:

$$F(t) = N \begin{cases} t^{-\alpha_1} & t < t_{b_1} \\ t_{b_1}^{(\alpha_2-\alpha_1)}\, t^{-\alpha_2} & t_{b_1} < t < t_{b_2} \\ t_{b_1}^{(\alpha_2-\alpha_1)}\, t_{b_2}^{(\alpha_3-\alpha_2)}\, t^{-\alpha_3} & t > t_{b_2}, \end{cases} \tag{3}$$

triple broken power law:

$$F(t) = N \begin{cases} t^{-\alpha_1} & t < t_{b_1} \\ t_{b_1}^{(\alpha_2-\alpha_1)}\, t^{-\alpha_2} & t_{b_1} < t < t_{b_2} \\ t_{b_1}^{(\alpha_2-\alpha_1)}\, t_{b_2}^{(\alpha_3-\alpha_2)}\, t^{-\alpha_3} & t_{b_2} < t < t_{b_3} \\ t_{b_1}^{(\alpha_2-\alpha_1)}\, t_{b_2}^{(\alpha_3-\alpha_2)}\, t_{b_3}^{(\alpha_4-\alpha_3)}\, t^{-\alpha_4} & t > t_{b_3}, \end{cases} \tag{4}$$

where N is the normalization, t is the time since the burst trigger, $F(t)$ is the count rate over the soft X-ray band (0.3–10 keV), t_{b_1,b_2,b_3} are the times of breaks in the light curves, and $\alpha_{(0,1,2,3,4)}$ are the temporal indices of the power-law fits.

Our software, written in IDL, requires user input for initial guesses of the location and number of breaks (and therefore power-law model). Based upon visual inspection, the user first eliminates all obvious time intervals with significant flaring.[6] The user then makes initial guesses for light curve break times, and a least-squares fitting routine is used to fit each model. When the addition or removal of light curve segments from the initial model also provides an adequate fit, we perform an F-test and if the fit is improved at a 99% confidence level, then the new model is retained.

In order to accurately measure the light curve model parameter errors without overestimating them, we tested both $\Delta\chi^2$ confidence interval mapping and Monte Carlo simulation methods. In the Monte Carlo method, we created 10,000 simulated light curves for each GRB light curve jiggling the data points by an amount drawn randomly from the Poisson distributions derived from the source and background counts. Each of these light curves was fit with the same method as the real light curves. The 90% and 2σ confidence intervals were taken from the distributions of each fit parameter from the simulations. The broken power-law fits were not well behaved in $\Delta\chi^2$ contour space due to data binning, light curve gaps, and logarithmic fits, resulting in larger error estimates compared to the Monte Carlo method. The latter method is more free from assumptions and biases, therefore we chose to use the Monte Carlo light curve parameter error estimates for the following analysis.

We classify each segment of the light curves in terms of the canonical form (Figure 1) using the following criteria. If the light curve is a triple broken power law then identification of its segments is unambiguous, and it is designated as a type I–II–III–IV. If the light curve is best fit by a double broken power law, we apply the criteria that if $\alpha_1 > \alpha_2$ then it is designated as segments I–II–III or if $\alpha_1 < \alpha_2$ then it is designated as segments II–III–IV. If the light curve is best fit by a singly broken power law, we apply the criteria that if $\alpha_1 > \alpha_2$ then it is designated as segments I–II, while if $\alpha_1 < \alpha_2$ then it can be interpreted as either segments II–III or III–IV. If the light curve is best fit by a single power law then any segment (I, II, III, IV) is possible.

The distributions of these temporal fits are given in the left panel of Figure 2. Although the α distributions are broad, the different segments are clearly separated by our classification

[6] We note that broad-peaked flares, poorly sampled flares, or the sum of many flares could be misinterpreted as a single power-law decay from one of the phases.

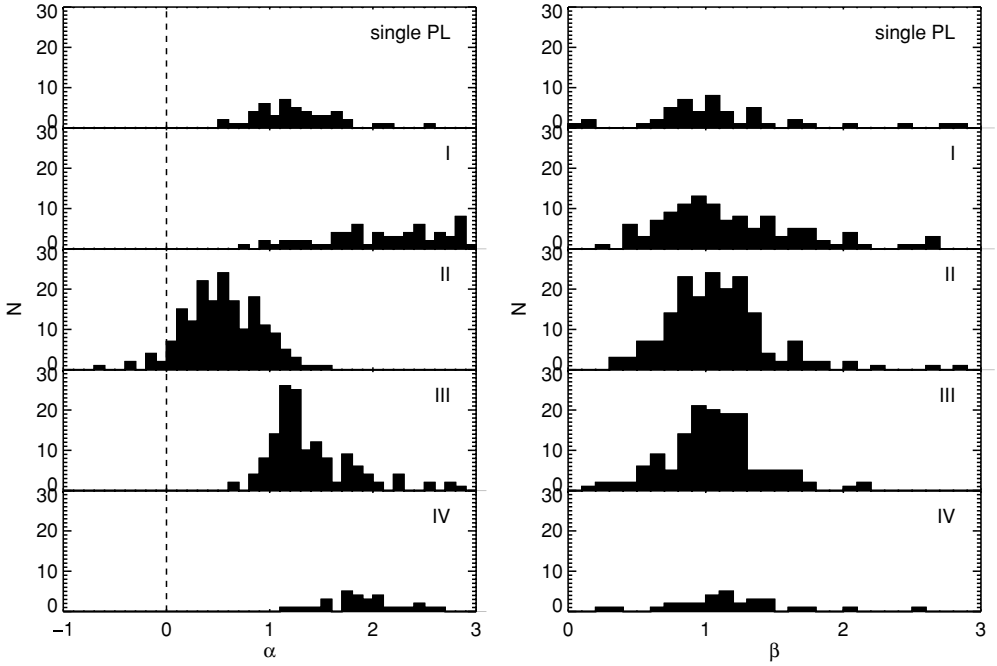

Figure 2. Distributions of light curve decay indices (α, left) and corresponding spectral indices (β, right). The top panel in each figure shows the single power-law cases, while the other panels are split into light curve segments as identified in Figure 1. Note that the overlap in the temporal distributions of segments II and III are due to contamination from ambiguous light curves as described in Section 4.3. The dashed line at $\alpha = 0$ indicates the distinction between rising and decaying light curves.

criteria described above. Kolmogorov–Smirnov (K–S) tests show that the segments I through IV are different at >99.9% level. The single power law distribution also differs from segments I, II, and IV at >99.9% level. However, the single power law and segment III distributions are more similar (4% probability of begin drawn from same inherent distribution), suggesting that some of the single power laws are segment III, with others drawn from segments I, II, and IV.

This scheme has no implicit constraints on the range of temporal indices, but does leave some ambiguity in the case of a broken power law with $\alpha_1 < \alpha_2$. This case is equivocal between segments II–III and III–IV. We generally assume that they are cases of II–III when looking at sample distributions. However, we still fit the post-jet break closure relations, allowing for the possibility of III–IV. This ambiguity and distinguishing criteria are further addressed in Section 4.3.

2.2. Spectral Analysis

We have constructed spectra for each segment of each light curve distinguished using the temporal fits defined in Section 2.1.2. These spectra were extracted using XSELECT with 20 pixel radius source extraction region, and a 40 pixel radius background region. All analysis used the version 011 (release date 2008 May 14) response matrices from the *Swift* CALDB, and Ancillary Response Files (ARFs) were made using the *xrtmkarf* task. The spectra were grouped using the *grppha* task with 20 counts per bin and were fit using χ^2 statistics unless there were fewer than 150 counts, in which case they were grouped with 10 counts per bin and were fit using Cash statistics. We fit these spectra in XSPEC to an absorbed power law with two absorption components, one fixed to the Galactic value (Kalberla et al. 2005), and another freely varying using the measured redshift if available.

The photon indices (Γ) of the spectral fits are used to measure β, the energy spectral index, where $\beta = \Gamma - 1$. The distributions of these spectral fits are shown in Figure 2. Segments II through IV are statistically similar (as tested with a K–S test). Of those light curves with segment IV, ∼90% are consistent with minimal or no spectral evolution through segments II, III, and IV (90% confidence errors). The K–S test shows that segment I differs from segments II and III at >98% level, with the distribution peaking at a slightly lower β, consistent with the possibility of a different physical origin of this phase (Zhang et al. 2006, 2007a, 2009; Liang et al. 2006). The distribution of βs for the single power-law light curves is statistically consistent with the other individual segments. These spectral properties are in agreement with the suggestion from the temporal distributions that this sample is a mixture of the other segments.

3. CLOSURE RELATIONS

The fireball model predicts the evolution of the spectral and temporal properties of GRB afterglows as the external shocks decelerate in the external environment. These effects can be characterized by relationships between the temporal and spectral indices (α and β). These so-called "closure relations" of the fireball model depend on the physical processes in the relevant portion of the afterglow light curve, the surrounding environment, electron spectral index, cooling regime, and jet geometry (Rees & Mészáros 1994; Mészáros & Rees 1997; Sari et al. 1998; Chevalier & Li 2000; Dai & Cheng 2001, see reviews by Mészáros 2002; Zhang & Mészáros 2004; Piran 2005). We apply a large set of possible models to each segment of the light curves and use them in conjunction to narrow the list of possible physical models to explain each afterglow segment, assuming that synchrotron radiation is the dominant mechanism and including only the corresponding relevant relations. We also use them to determine the presence and properties of jet breaks in our sample of X-ray light curves. All of the analytical closure relations assume a simple spectrum with sharp breaks, whereas in reality these breaks are likely smooth (Granot & Sari 2002).

Table 1
Closure Relations

			a	b	c
			No Energy Injection		Energy Injection
		β	$\alpha(\beta)$ $(p > 2)$	$\alpha(\beta)$ $(1 < p < 2)$	$\alpha(\beta)$ $(p > 2)$
			ISM, Slow Cooling		
1	$\nu_m < \nu < \nu_c$	$\frac{p-1}{2}$	$\alpha = \frac{3\beta}{2}$	$\alpha = \frac{3(2\beta+3)}{16}$	$\alpha = (q-1) + \frac{(2+q)\beta}{2}$
2	$\nu > \nu_c$	$\frac{p}{2}$	$\alpha = \frac{3\beta-1}{2}$	$\alpha = \frac{3\beta+5}{8}$	$\alpha = \frac{q-2}{2} + \frac{(2+q)\beta}{2}$
			ISM, Fast Cooling		
3	$\nu_c < \nu < \nu_m$	$\frac{1}{2}$	$\alpha = \frac{\beta}{2}$	$\alpha = \frac{\beta}{2}$	$\alpha = (q-1) + \frac{(2-q)\beta}{2}$
4	$\nu > \nu_m$	$\frac{p}{2}$	$\alpha = \frac{3\beta-1}{2}$	$\alpha = \frac{3\beta+5}{8}$	$\alpha = \frac{q-2}{2} + \frac{(2+q)\beta}{2}$
			Wind, Slow Cooling		
5	$\nu_m < \nu < \nu_c$	$\frac{p-1}{2}$	$\alpha = \frac{3\beta+1}{2}$	$\alpha = \frac{2\beta+9}{8}$	$\alpha = \frac{q}{2} + \frac{(2+q)\beta}{2}$
6	$\nu > \nu_c$	$\frac{p}{2}$	$\alpha = \frac{3\beta-1}{2}$	$\alpha = \frac{\beta+3}{4}$	$\alpha = \frac{q-2}{2} + \frac{(2+q)\beta}{2}$
			Wind, Fast Cooling		
7	$\nu_c < \nu < \nu_m$	$\frac{1}{2}$	$\alpha = \frac{1-\beta}{2}$	$\alpha = \frac{1-\beta}{2}$	$\alpha = \frac{q}{2} - \frac{(2-q)\beta}{2}$
8	$\nu > \nu_m$	$\frac{p}{2}$	$\alpha = \frac{3\beta-1}{2}$	$\alpha = \frac{\beta+3}{4}$	$\alpha = \frac{q-2}{2} + \frac{(2+q)\beta}{2}$
			Uniform Jet (spreading), Slow Cooling		
9	$\nu_m < \nu < \nu_c$	$\frac{p-1}{2}$	$\alpha = 2\beta + 1$	$\alpha = \frac{2\beta+7}{4}$	$\alpha = 2\beta + 1 - \frac{2(1-q)(\beta+2)}{3}$
10	$\nu > \nu_c$	$\frac{p}{2}$	$\alpha = 2\beta$	$\alpha = \frac{\beta+3}{2}$	$\alpha = 2\beta - \frac{2(1-q)(\beta+1)}{3}$
			ISM, Uniform Jet (nonspreading)		
11	$\nu_m < \nu < \nu_c$	$\frac{p-1}{2}$	$\alpha = \frac{6\beta+3}{4}$	$\alpha = \frac{6\beta+21}{16}$	$\alpha = \frac{6\beta+3}{4} - \frac{(1-q)(2\beta+5)}{4}$
12	$\nu > \nu_c$	$\frac{p}{2}$	$\alpha = \frac{6\beta+1}{4}$	$\alpha = \frac{3\beta+11}{8}$	$\alpha = \frac{6\beta+1}{4} - \frac{(1-q)(2\beta+3)}{4}$
			Wind, Uniform Jet (nonspreading)		
13	$\nu_m < \nu < \nu_c$	$\frac{p-1}{2}$	$\alpha = \frac{3\beta+2}{2}$	$\alpha = \frac{2\beta+13}{8}$	$\alpha = \frac{3\beta+2}{2} - \frac{(1-q)(\beta+2)}{2}$
14	$\nu > \nu_c$	$\frac{p}{2}$	$\alpha = \frac{3\beta}{2}$	$\alpha = \frac{\beta+5}{4}$	$\alpha = \frac{3\beta}{2} - \frac{(1-q)(\beta+2)}{2}$
			ISM, Structured Jet		
15	$\nu_m < \nu < \nu_c$	$\frac{p-1}{2}$	$\alpha = \frac{3k+12\beta}{8-k}$		
16	$\nu > \nu_c$	$\frac{p}{2}$	$\alpha = \frac{12\beta+2k-4}{8-k}$		
			Wind, Structured Jet		
17	$\nu_m < \nu < \nu_c$	$\frac{p-1}{2}$	$\alpha = \frac{6\beta+k\beta+2}{4-k}$		
18	$\nu > \nu_c$	$\frac{p}{2}$	$\alpha = \frac{6\beta+k-k\beta-2}{4-k}$		

Notes. Convention $F_\nu \propto t^{-\alpha}\nu^{-\beta}$ adopted throughout. Structured Jet relations require $k < \tilde{k}$ with $\tilde{k}$ defined in the text. Closure relations reference codes used in Figures 4, 6, 9–11 with references noted in subscripts. (1a) *ISMs2a*[1,2], (1b) *ISMs2b*[1,3], (1c) *ISMs2ai*[2], (2a) *ISMs3a*[1,2], (2b) *ISMs3b*[1,3], (2c) *ISMs3ai*[2], (3a) *ISMf2a*[1,2], (3b) *ISMf2b*[1], (3c) *ISMf2ai*[2], (4a) *ISMf3a*[1,2], (4b) *ISMf3b*[1], (4c) *ISMf3ai*[2], (5a) *WINDs2a*[1,2], (5b) *WINDs2b*[1,3], (5c) *WINDs2ai*[2], (6a) *WINDs3a*[1,2], (6b) *WINDs3b*[1,3], (6c) *WINDs3ai*[2], (7a) *WINDf2a*[1,2], (7b) *WINDf2b*[1], (7c) *WINDf2ai*[2], (8a) *WINDf3a*[1,2], (8b) *WINDf3b*[1], (8c) *WINDf3ai*[2], (9a) *JETs2a*[1], (9b) *JETs2b*[1,3], (9c) *JET2ai*[4], (10a) *JETs3a*[1], (10b) *JETs3b*[1,3], (10c) *JETs3ai*[4], (11a) *JETsISM2a*[5], (11b) *JETsISM2b*[5], (11c) *JETsISM2ai*[4,5], (12a) *JETsISM3a*[5], (12b) *JETsISM3b*[5], (12c) *JETsISM3ai*[4,5], (13a) *JETsWIND2a*[5], (13b) *JETsWIND2b*[5], (13c) *JETsWIND2ai*[4,5], (14a) *JETsWIND3a*[5], (14b) *JETsWIND3b*[5], (14c) *JETsWIND3ai*[4,5], (15) *JETsoISM2a*[5], (16) *JETsoISM3a*[5], (17) *JETsoWIND2a*[5], (18) *JETsoWIND3a*[5].

References. (1) Zhang & Mészáros 2004; (2) Zhang et al. 2006; (3) Dai & Cheng 2001; (4) Modified from Panaitescu et al. 2006; (5) Modified from Panaitescu 2005.

However, unfortunately even with broadband SEDs for each light curve segment, the smoothness of these spectral breaks is impossible to measure except in perhaps a few special cases. In order to learn about the global properties of X-ray afterglows in a statistical sample, we make simplifying assumptions including neglecting the smoothness of these breaks.

We present an extensive set of closure relations (Table 1) including those for constant density interstellar medium (ISM, $n(r) =$ constant) and wind ($n(r) \propto r^{-2}$) environments, electron spectral index cases of $1 < p < 2$ and $p > 2$, and slow cooling and fast cooling regimes (Sari et al. 1998). For each case, we present closure relations both with and without energy injection. These various theoretical permutations have been invoked to explain the likely physical scenarios in the general scheme and in many individual observational cases, but have never been combined on such a large sample of afterglow light curves.

Table 2
Prominent Jet Breaks

GRB	Segments	Time	α	β	t (ks)	z	log $E_{\gamma,\mathrm{iso}}$ (erg)	θ_j (deg)	log E_γ (erg)	Requirements[†]
050315	I–II–III–IV	t_b	$1.86^{+0.58}_{-0.36}$	$1.30^{+0.35}_{-0.29}$	$240.6^{+69.3}_{-76.3}$	1.95[a]	52.7	5.6	50.3	Uni ν_2 p_2
		$t_{b,\mathrm{EI}}$	$0.69^{+0.05}_{-0.05}$	$0.96^{+0.09}_{-0.09}$	$7.3^{+1.4}_{-1.1}$			1.5	49.2	**EI** ν_2 p_2
050319	I–II–III–IV	t_b	$1.58^{+0.44}_{-0.26}$	$1.37^{+0.57}_{-0.47}$	$55.3^{+19.1}_{-26.0}$	3.24[b]	52.6	2.8	49.7	Uni ν_2
		$t_{b,\mathrm{EI}}$	$0.67^{+0.15}_{-0.14}$	$0.95^{+0.15}_{-0.14}$	$4.0^{+7.6}_{-2.2}$			1.1	48.9	
050505	II–III–IV	t_b	$1.81^{+0.30}_{-0.15}$	$1.13^{+0.17}_{-0.16}$	$45.9^{+25.4}_{-11.0}$	4.28[c]	53.2	2.1	50.0	ν_2
		$t_{b,\mathrm{EI}}$	$1.12^{+0.10}_{-0.09}$	$1.07^{+0.13}_{-0.12}$	$6.5^{+2.4}_{-1.1}$			1.0	49.4	
050713B	I–II–III–IV	t_b	$2.10^{+1.91}_{-0.71}$	$1.13^{+7.87}_{-2.13}$	$381.2^{+314.9}_{-114.3}$	...	...	6.5ξ	...	Uni
		$t_{b,\mathrm{EI}}$	$1.04^{+0.13}_{-0.14}$	$0.92^{+0.20}_{-0.23}$	$32.9^{+12.2}_{-20.5}$	...	...	2.6ξ	...	
050814	I–II–III–IV	t_b	$2.25^{+0.98}_{-0.41}$	$0.71^{+0.86}_{-0.39}$	$88.7^{+22.2}_{-15.5}$	5.30[d]	53.1	2.5	50.1	Uni
		$t_{b,\mathrm{EI}}$	$0.82^{+0.13}_{-0.12}$	$0.98^{+0.19}_{-0.17}$	$7.4^{+4.6}_{-2.3}$			1.0	49.3	
050820A	I–II–III–IV	t_b	$1.74^{+1.02}_{-0.23}$	$2.57^{+3.57}_{-2.51}$	$634.7^{+1044.6}_{-267.9}$	2.62[e]	53.1	6.6	50.9	Uni
		$t_{b,\mathrm{EI}}$	$1.19^{+0.05}_{-0.05}$	$1.03^{+0.07}_{-0.07}$	$7.3^{+3.7}_{-5.7}$			1.2	49.4	**EI** p_2
051016B	I–II–III–IV	t_b	$1.74^{+1.07}_{-0.42}$	$0.37^{+1.37}_{-1.37}$	$135.0^{+82.8}_{-86.4}$	0.94[f]	...	5.4	...	
		$t_{b,\mathrm{EI}}$	$0.81^{+0.09}_{-0.12}$	$0.98^{+0.17}_{-0.17}$	$4.8^{+3.2}_{-3.4}$			1.5	...	
051109A	I–II–III–IV	t_b	$1.34^{+0.13}_{-0.09}$	$1.01^{+0.27}_{-0.20}$	$79.4^{+61.3}_{-43.9}$	2.35[g]	52.7	3.4	50.0	ν_2 p_2
		$t_{b,\mathrm{EI}}$	$1.09^{+0.05}_{-0.07}$	$1.15^{+0.11}_{-0.10}$	$3.1^{+0.6}_{-2.7}$			1.0	48.9	
051221A	I–II–III–IV	t_b	$1.86^{+1.54}_{-0.89}$	$2.04^{+5.32}_{-1.39}$	$351.6^{+293.5}_{-249.0}$	0.55[h]	51.5	11.6	49.8	Uni
		$t_{b,\mathrm{EI}}$	$1.21^{+0.21}_{-0.20}$	$0.87^{+0.28}_{-0.29}$	$32.1^{+28.6}_{-19.9}$			4.7	49.0	
060109	I–II–III–IV	t_b	$2.03^{+1.00}_{-0.44}$	$1.38^{+0.63}_{-0.52}$	$25.6^{+19.2}_{-12.5}$	...	...	2.4ξ	...	Uni
		$t_{b,\mathrm{EI}}$	$1.09^{+0.33}_{-0.32}$	$1.58^{+0.41}_{-0.36}$	$5.6^{+2.2}_{-1.1}$	...	...	1.3ξ	...	
060204B	I–II–III–IV	t_b	$1.98^{+1.81}_{-0.63}$	$1.41^{+3.48}_{-1.02}$	$84.8^{+144.1}_{-53.6}$	...	...	3.7ξ	...	
		$t_{b,\mathrm{EI}}$	$1.34^{+0.16}_{-0.17}$	$1.50^{+0.41}_{-0.36}$	$6.8^{+2.1}_{-2.0}$	...	...	1.4ξ	...	
060428A	I–II–III–IV	t_b	$2.47^{+1.77}_{-0.52}$	$1.69^{+1.21}_{-0.90}$	$846.6^{+641.6}_{-255.1}$	...	...	8.8ξ	...	Uni
		$t_{b,\mathrm{EI}}$	$1.05^{+0.19}_{-0.13}$	$1.05^{+0.27}_{-0.24}$	$47.3^{+64.9}_{-22.0}$	...	...	3.0ξ	...	
060510A	I–II–III–IV	t_b	$1.57^{+0.45}_{-0.13}$	$1.04^{+0.24}_{-0.23}$	$63.6^{+136.4}_{-23.9}$	...	...	3.3ξ	...	
060605	I–II–III–IV	t_b	$2.05^{+0.40}_{-0.27}$	$1.12^{+0.27}_{-0.23}$	$14.7^{+8.6}_{-3.9}$	3.77[i]	52.5	1.7	49.2	Uni
		$t_{b,\mathrm{EI}}$	$1.26^{+0.24}_{-0.26}$	$1.25^{+0.18}_{-0.17}$	$5.1^{+0.9}_{-0.7}$			1.2	48.8	
060614	I–II–III–IV	t_b	$2.11^{+1.81}_{-0.37}$	$0.70^{+0.24}_{-0.24}$	$125.5^{+100.6}_{-35.7}$	0.13[j]	51.2	9.5	49.4	
		$t_{b,\mathrm{EI}}$	$1.33^{+0.24}_{-0.30}$	$1.02^{+0.22}_{-0.20}$	$35.5^{+8.1}_{-6.3}$			5.9	49.0	
060707	I–II–III–IV	t_b	$2.54^{+1.71}_{-1.62}$	$1.74^{+2.09}_{-1.07}$	$1059.4^{+454.0}_{-494.5}$	3.43[k]	52.8	8.1	50.8	Uni
		$t_{b,\mathrm{EI}}$	$0.96^{+0.17}_{-0.16}$	$0.70^{+0.52}_{-0.28}$	$16.3^{+24.8}_{-12.2}$			1.7	49.4	
060729	I–II–III–IV	t_b	$1.96^{+0.67}_{-0.17}$	$0.30^{+1.45}_{-1.16}$	$2266.2^{+2990.5}_{-528.8}$	0.54[l]	51.5	23.1	50.4	Uni ν_1
		$t_{b,\mathrm{EI}}$	$1.30^{+0.05}_{-0.05}$	$1.06^{+0.06}_{-0.05}$	$76.8^{+6.4}_{-6.2}$			6.5	49.3	**EI** ν_1 p_2
060807	I–II–III–IV	t_b	$1.95^{+0.39}_{-0.23}$	$1.41^{+0.89}_{-0.63}$	$29.1^{+17.2}_{-15.0}$	...	...	2.5ξ	...	Uni
		$t_{b,\mathrm{EI}}$	$1.06^{+0.12}_{-0.16}$	$1.17^{+0.21}_{-0.19}$	$4.7^{+0.4}_{-0.9}$	...	...	1.3ξ	...	
060813	II–III–IV	t_b	$2.68^{+0.96}_{-0.50}$	$0.85^{+0.54}_{-0.29}$	$52.8^{+15.5}_{-10.9}$	...	...	3.1ξ	...	NSp Uni ISM ν_1 p_2
		$t_{b,\mathrm{EI}}$	$1.18^{+0.07}_{-0.08}$	$1.04^{+0.17}_{-0.16}$	$1.0^{+0.3}_{-0.3}$	...	...	0.7ξ	...	NSp **EI** ISM ν_1 p_2
060814	I–II–III–IV	t_b	$1.72^{+0.24}_{-0.16}$	$1.37^{+0.18}_{-0.27}$	$47.6^{+12.0}_{-12.1}$	0.84[m]	52.8	3.4	50.1	NSp Uni Wind ν_2 p_2
		$t_{b,\mathrm{EI}}$	$1.02^{+0.11}_{-0.10}$	$1.10^{+0.14}_{-0.13}$	$7.5^{+1.9}_{-4.3}$			1.7	49.5	
061019	II–III–IV	t_b	$2.33^{+1.98}_{-0.71}$	$1.09^{+0.89}_{-0.85}$	$186.3^{+136.6}_{-104.2}$	...	...	5.0ξ	...	Uni
		$t_{b,\mathrm{EI}}$	$1.11^{+0.28}_{-0.21}$	$1.00^{+0.60}_{-0.51}$	$21.0^{+22.9}_{-9.9}$	...	...	2.2ξ	...	
061021	I–II–III–IV	t_b	$1.19^{+0.21}_{-0.08}$	$0.93^{+0.18}_{-0.16}$	$143.5^{+414.1}_{-121.7}$	...	...	4.5ξ	...	ν_2 p_2
		$t_{b,\mathrm{EI}}$	$0.98^{+0.06}_{-0.18}$	$1.09^{+0.10}_{-0.09}$	$7.1^{+2.7}_{-5.9}$	...	...	1.5ξ	...	
061222A	I–II–III–IV	t_b	$1.73^{+0.10}_{-0.08}$	$1.28^{+0.14}_{-0.15}$	$66.7^{+15.3}_{-16.2}$	...	...	3.4ξ	...	NSp Uni Wind ν_2 p_2
		$t_{b,\mathrm{EI}}$	$0.98^{+0.10}_{-0.13}$	$1.09^{+0.12}_{-0.11}$	$2.8^{+1.4}_{-1.2}$	...	...	1.0ξ	...	
070129	I–II–III–IV	t_b	$1.28^{+0.34}_{-0.17}$	$1.14^{+0.49}_{-0.32}$	$120.1^{+174.0}_{-88.4}$	...	...	4.2ξ	...	p_2
		$t_{b,\mathrm{EI}}$	$0.91^{+0.13}_{-0.27}$	$1.25^{+0.22}_{-0.20}$	$11.2^{+2.0}_{-2.9}$	...	...	1.7ξ	...	
070306	I–II–III–IV	t_b	$2.07^{+0.60}_{-0.22}$	$1.11^{+0.39}_{-0.26}$	$115.3^{+154.6}_{-74.4}$	1.50[n]	52.7	4.5	50.2	
		$t_{b,\mathrm{EI}}$	$1.41^{+0.27}_{-0.67}$	$1.23^{+0.20}_{-0.18}$	$21.9^{+5.7}_{-3.8}$			2.4	49.6	

Table 2
(Continued)

GRB	Segments	Time	α	β	t (ks)	z	log $E_{\gamma,\rm iso}$ (erg)	θ_j (deg)	log E_γ (erg)	Requirements[†]
070328	I–II–III–IV	t_b	$1.48^{+0.04}_{-0.04}$	$1.04^{+0.13}_{-0.12}$	$1.8^{+2.2}_{-0.8}$	...	...	0.9ξ	...	ν_2
070419B	II–III–IV	t_b	$2.43^{+0.56}_{-0.28}$	$0.90^{+0.38}_{-0.33}$	$57.7^{+20.9}_{-16.1}$	...	...	3.2ξ	...	Uni ν_1 p_2
		$t_{b,\rm EI}$	$1.41^{+0.29}_{-0.24}$	$0.63^{+0.19}_{-0.18}$	$14.4^{+5.8}_{-7.4}$	...	...	1.9ξ	...	
070420	I–II–III–IV	t_b	$1.85^{+0.36}_{-0.22}$	$0.97^{+0.53}_{-0.28}$	$57.6^{+45.9}_{-21.0}$	...	...	3.2ξ	...	
		$t_{b,\rm EI}$	$1.23^{+0.10}_{-0.11}$	$1.04^{+0.21}_{-0.19}$	$2.8^{+0.9}_{-0.6}$	...	...	1.0ξ	...	

[†]Abbreviations for Uniform jet (Uni), Spreading jet (Sp), Nonspreading jet (NSp), $1 < p < 2$ (p_{12}), $p > 2$ (p_2), $\nu < \nu_c$ (ν_1), $\nu > \nu_c$ (ν_2).

Notes. Prominent jet breaks are those with a distinct segment IV which are consistent with the post-jet break closure relations. Alternative times for jet angle limits depend on models fit. Energy injection (EI) breaks are listed only if at least one jet-break-with-energy-injection-relation is consistent. Requirements listed are for those properties of families of closure relations that are required by consistent models. ξ is defined in Equation (13). All errors are 2σ confidence.

References. [a]Berger et al. 2005b; [b]Jakobsson et al. 2006a; [c]Berger et al. 2006b; [d]Jakobsson et al. 2006b; [e]Prochaska et al. 2007a; [f]Soderberg et al. 2005; [g]Quimby et al. 2005; [h]Soderberg et al. 2006; [i]Ferrero et al. 2008; [j]Gal-Yam et al. 2006; [k]Jakobsson et al. 2006a; [l]Thöne et al. 2006b; [m]Thöne et al. 2007a; [n]Jaunsen et al. 2008.

Table 3
Hidden Jet Breaks

GRB	Segments	Time	α	β	t (ks)	z	log $E_{\gamma,\rm iso}$ (erg)	θ_j (deg)	log E_γ (erg)	Requirements[†]
050416A	I–II–III	t_b	$0.90^{+0.04}_{-0.03}$	$0.40^{+0.10}_{-0.10}$	$1.1^{+1.0}_{-0.4}$	0.65[a]	50.8	1.6	47.4	**EI** ν_1 p_2
050802	II–IV	t_b	$1.52^{+0.13}_{-0.06}$	$0.85^{+0.07}_{-0.13}$	$6.1^{+3.1}_{-1.2}$	1.71[b]	52.4	1.6	49.0	**EI** ν_1 p_2
050815	II–IV	t_b	$2.21^{+0.51}_{-0.32}$	$0.39^{+0.65}_{-0.47}$	$4.3^{+0.7}_{-0.8}$	...	...	1.2ξ	...	ν_1
		$t_{b,\rm EI}$	$0.19^{+0.14}_{-0.17}$	$1.15^{+0.92}_{-0.51}$	< 0.09	...	...	0.3ξ	...	
050822	I–II–III	t_b	$1.04^{+0.06}_{-0.06}$	$1.26^{+0.20}_{-0.18}$	$18.1^{+4.9}_{-4.2}$	...	...	2.1ξ	...	**EI** p_2
051111	I–II–IV	t_b	$4.78^{+1.93}_{-1.49}$	$1.22^{+0.40}_{-0.37}$	$42.2^{+13.4}_{-8.7}$	1.55[c]	52.7	3.0	49.9	Sp ν_1 p_2
060210	II–III	t_b	$1.30^{+0.09}_{-0.07}$	$1.07^{+0.10}_{-0.10}$	$25.8^{+9.8}_{-6.9}$	3.91[d]	53.6	1.5	50.1	**EI** p_2
060218	I–II–IV	t_b	$1.30^{+0.34}_{-0.21}$	$4.86^{+2.59}_{-1.00}$	$71.2^{+132.1}_{-59.4}$	0.03[e]	48.7	16.4	47.3	NSp **EI** ν_2 p_2
060413	I–II–IV	t_b	$2.71^{+0.24}_{-0.18}$	$0.55^{+0.39}_{-0.51}$	$23.8^{+1.1}_{-0.7}$	...	...	2.3ξ	...	Sp ν_1 p_2
060712	I–II–III	t_b	$1.17^{+0.20}_{-0.13}$	$1.60^{+0.46}_{-0.36}$	$12.0^{+12.2}_{-5.5}$	...	...	1.8ξ	...	**EI** p_2
060719	I–II–III	t_b	$1.22^{+0.10}_{-0.10}$	$1.77^{+0.41}_{-0.34}$	$7.9^{+2.9}_{-2.2}$	...	...	1.5ξ	...	**EI** p_2
070220	I–II–IV	t_b	$2.04^{+0.34}_{-0.22}$	$0.58^{+0.40}_{-0.31}$	$13.0^{+3.4}_{-2.0}$	...	...	1.8ξ	...	ν_1
070429A	I–II–IV	t_b	$3.96^{+1.54}_{-2.04}$	$0.52^{+1.50}_{-0.70}$	$551.7^{+81.9}_{-110.5}$	...	...	7.5ξ	...	ν_1

[†]Abbreviations for Uniform jet (Uni), Spreading jet (Sp), Nonspreading jet (NSp), $1 < p < 2$ (p_{12}), $p > 2$ (p_2), $\nu < \nu_c$ (ν_1), $\nu > \nu_c$ (ν_2).

Notes. Hidden jet breaks require jet break closure relations in the last light curve segment. Other notes are the same as for Prominent Jet Breaks table.

References. [a]Soderberg et al. 2007; [b]Fynbo et al. 2005; [c]Prochaska et al. 2006a; [d]Cucchiara et al. 2006a; [e]Mirabal et al. 2006.

The constant density ISM environment, the simplest plausible model, is often well fit by observations. However, the wind environment is closer to what one would expect for the medium surrounding high-mass stars near the end of their lives (i.e., Wolf–Rayet stars). This dilemma has led to theoretical speculation of how massive star environments might appear observationally to have a constant density. van Marle et al. (2006) conducted numerical simulations of stellar wind environments where the wind exists only in a region very close to the star, and showed that the right combination of wind pressure, ISM density, progenitor rotation, and metallicity, can make a wind environment appear like an ISM environment when probed by the GRB forward shock. However, it is difficult to constrain these conditions observationally. Chevalier (2007) compares the environments and interactions of SNe Ib/c to the expectations for the GRB case, finding the main difference to be in the progenitor metallicity, ISM pressure, and possibly rotation. He also finds that GRB environments could produce a close termination shock outside of which the medium would be constant density. Both the ISM and wind environments are surely simplistic descriptions of actual GRB environments, especially when considering that local examples of Wolf–Rayet stars such as Eta Carinae show massive irregular winds that can be modeled by neither a constant density nor a r^{-2} environment. In this study, it is only feasible to test the simplest models, therefore we choose to include both ISM and wind closure relation alternatives and determine directly which model best approximates each afterglow.

The electron spectral index, p, is typically expected to be larger than 2 to avoid a divergent total integrated energy for harder distributions unless a high-energy cutoff is invoked. Numerical modeling of electron acceleration (Achterberg et al. 2001; Eichler & Waxman 2005) is also consistent with $p > 2$. However, a $p < 2$ flat electron spectrum has been adapted to explain specific observations of shallow temporal decays (Panaitescu & Kumar 2001; Bhattacharya 2001). Therefore, we

Table 4
Possible Jet Breaks

GRB	Segments	Time	α	β	t (ks)	z	log $E_{\gamma,\mathrm{iso}}$ (erg)	θ_j (deg)	log E_γ (erg)	Requirements[†]
050219A	I–II–III	t_b	$1.29^{+0.92}_{-0.28}$	$0.91^{+0.26}_{-0.24}$	$32.3^{+114.2}_{-26.0}$	...	...	2.6ξ	...	
		t_{lastdet}	$1.29^{+0.92}_{-0.28}$	$0.91^{+0.26}_{-0.24}$	>3091.94	...	...	$>14.3\xi$	...	
050318	III–IV	t_b	$2.06^{+0.58}_{-0.35}$	$1.02^{+0.22}_{-0.20}$	$20.7^{+10.2}_{-9.6}$	1.44[a]	51.9	2.9	49.1	
		t_{lastdet}	$2.06^{+0.58}_{-0.35}$	$1.02^{+0.22}_{-0.20}$	>57.83			>4.3	>49.4	
		t_{start}	$1.35^{+0.12}_{-0.16}$	$1.13^{+0.18}_{-0.16}$	<3.28			<1.5	<48.5	
050326	III–IV	t_b	$1.73^{+0.30}_{-0.21}$	$0.88^{+0.42}_{-0.24}$	$27.0^{+45.3}_{-6.1}$	...	...	2.4ξ	...	
		t_{lastdet}	$1.73^{+0.30}_{-0.21}$	$0.88^{+0.42}_{-0.24}$	>531.42	...	...	$>7.4\xi$	...	
		t_{start}	$1.51^{+0.16}_{-0.61}$	$1.11^{+0.71}_{-0.59}$	<3.26	...	...	$<1.1\xi$	...	
050408	III–IV	t_b	$1.25^{+1.04}_{-0.24}$	$0.61^{+0.25}_{-0.22}$	$136.4^{+556.8}_{-124.5}$	1.24[b]	...	5.1	...	
		t_{lastdet}	$1.25^{+1.04}_{-0.24}$	$0.61^{+0.25}_{-0.22}$	>2582.09			>15.5	...	
050525A	Single PL	t_{lastdet}	$1.52^{+0.10}_{-0.08}$	$1.63^{+0.68}_{-0.48}$	>1071.16	0.61[c]	52.4	>13.3	>50.8	p_2
		t_{start}	$1.52^{+0.10}_{-0.08}$	$1.63^{+0.68}_{-0.48}$	<5.86			<1.9	<49.1	p_2
050603	Single PL	t_{lastdet}	$1.64^{+0.11}_{-0.12}$	$0.91^{+0.15}_{-0.14}$	>1134.90	2.82[d]	53.5	>7.2	>51.4	
		t_{start}	$1.64^{+0.11}_{-0.12}$	$0.91^{+0.15}_{-0.14}$	<34.05			<1.9	<50.2	
050714B	I–II–III	t_b	$2.51^{+1.90}_{-1.12}$	$3.29^{+0.70}_{-0.60}$	$207.0^{+68.4}_{-56.0}$	...	...	5.2ξ	...	**EI** p_2
		t_{lastdet}	$2.51^{+1.90}_{-1.12}$	$3.29^{+0.70}_{-0.60}$	>954.98	...	...	$>9.2\xi$	...	**EI** p_2
050717	I–II–III	t_b	$1.71^{+0.26}_{-0.18}$	$0.66^{+0.46}_{-0.38}$	$1.6^{+2.9}_{-0.6}$	...	...	0.8ξ	...	
		t_{lastdet}	$1.71^{+0.26}_{-0.18}$	$0.66^{+0.46}_{-0.38}$	>91.38	...	...	$>3.8\xi$	...	
050726	II–IV	t_b	$1.50^{+0.15}_{-0.12}$	$1.11^{+0.29}_{-0.24}$	$3.0^{+2.1}_{-1.4}$	...	...	1.1ξ	...	
		t_{lastdet}	$1.50^{+0.15}_{-0.12}$	$1.11^{+0.29}_{-0.24}$	>669.73	...	...	$>8.1\xi$	...	
		t_{start}	$0.80^{+0.12}_{-0.23}$	$0.84^{+0.26}_{-0.16}$	<0.13	...	...	$<0.3\xi$	...	
050803	I–II–III	t_b	$1.78^{+0.18}_{-0.12}$	$1.24^{+0.22}_{-0.20}$	$18.2^{+2.7}_{-2.7}$	...	...	2.1ξ	...	p_2
		t_{lastdet}	$1.78^{+0.18}_{-0.12}$	$1.24^{+0.22}_{-0.20}$	>1372.26	...	...	$>10.6\xi$	...	p_2
050826	I–II–III	t_b	$1.71^{+1.55}_{-0.52}$	$1.50^{+0.60}_{-0.53}$	$38.6^{+33.9}_{-17.5}$	0.30[e]	...	3.9	...	
		t_{lastdet}	$1.71^{+1.55}_{-0.52}$	$1.50^{+0.60}_{-0.53}$	>190.81			>7.2	...	
050827	Single PL	t_{lastdet}	$1.63^{+0.21}_{-0.19}$	$0.92^{+0.31}_{-0.27}$	>880.94	...	...	$>9.0\xi$	...	
		t_{start}	$1.63^{+0.21}_{-0.19}$	$0.92^{+0.31}_{-0.27}$	<64.16	...	...	$<3.4\xi$	...	
050922B	I–II–III	t_b	$1.94^{+0.59}_{-0.38}$	$9.00^{+10.0}_{-10.0}$	$239.2^{+112.6}_{-76.2}$	...	...	5.5ξ	...	
		t_{lastdet}	$1.94^{+0.59}_{-0.38}$	$9.00^{+10.0}_{-10.0}$	>2251.50	...	...	$>12.7\xi$	...	
050922C	III–IV	t_b	$1.41^{+0.10}_{-0.08}$	$1.20^{+0.27}_{-0.24}$	$4.1^{+1.1}_{-2.2}$	2.20[f]	52.6	1.2	48.9	p_2
		t_{lastdet}	$1.41^{+0.10}_{-0.08}$	$1.20^{+0.27}_{-0.24}$	>97.71			>4.0	>50.0	p_2
		t_{start}	$1.05^{+0.04}_{-0.08}$	$1.01^{+0.09}_{-0.07}$	<0.12			<0.3	<47.8	
051008	III–IV	t_b	$1.96^{+0.17}_{-0.14}$	$1.14^{+0.29}_{-0.21}$	$16.7^{+3.4}_{-3.4}$	...	...	2.0ξ	...	
		t_{lastdet}	$1.96^{+0.17}_{-0.14}$	$1.14^{+0.29}_{-0.21}$	>414.39	...	...	$>6.7\xi$	...	
		t_{start}	$0.88^{+0.14}_{-0.15}$	$0.99^{+0.23}_{-0.21}$	<3.20	...	...	$<1.1\xi$	...	
051211B	III–IV	t_b	$1.78^{+1.94}_{-0.81}$	$1.63^{+1.60}_{-0.94}$	$272.5^{+163.5}_{-204.7}$	...	...	5.8ξ	...	
		t_{lastdet}	$1.78^{+1.94}_{-0.81}$	$1.63^{+1.60}_{-0.94}$	>861.98	...	...	$>8.9\xi$	...	
		t_{start}	$0.81^{+0.11}_{-0.16}$	$1.25^{+0.40}_{-0.35}$	<10.97	...	...	$<1.7\xi$	...	
051227	I–II–III	t_b	$1.48^{+0.43}_{-0.25}$	$0.88^{+0.32}_{-0.26}$	$3.8^{+6.9}_{-2.4}$	...	...	1.2ξ	...	
		t_{lastdet}	$1.48^{+0.43}_{-0.25}$	$0.88^{+0.32}_{-0.26}$	>103.10	...	...	$>4.0\xi$	...	
060105	I–II–III	t_b	$2.00^{+0.27}_{-0.21}$	$1.39^{+0.32}_{-0.14}$	$55.0^{+9.1}_{-7.2}$	...	...	3.2ξ	...	p_2
		t_{lastdet}	$2.00^{+0.27}_{-0.21}$	$1.39^{+0.32}_{-0.14}$	>573.86	...	...	$>7.6\xi$	...	p_2
060111B	I–II–III	t_b	$1.39^{+0.28}_{-0.17}$	$1.03^{+0.48}_{-0.42}$	$6.8^{+5.1}_{-1.2}$	...	...	1.4ξ	...	
		t_{lastdet}	$1.39^{+0.28}_{-0.17}$	$1.03^{+0.48}_{-0.42}$	>351.59	...	...	$>6.3\xi$	...	
060115	I–II–III	t_b	$1.18^{+0.39}_{-0.27}$	$1.37^{+0.92}_{-0.63}$	$43.9^{+19.0}_{-24.4}$	3.53[g]	52.8	2.4	49.8	
		t_{lastdet}	$1.18^{+0.39}_{-0.27}$	$1.37^{+0.92}_{-0.63}$	>468.33			>5.8	>50.5	
060124	III–IV	t_b	$1.44^{+0.07}_{-0.05}$	$0.98^{+0.10}_{-0.09}$	$59.1^{+27.9}_{-12.2}$	2.30[h]	52.1	3.8	49.4	
		t_{lastdet}	$1.44^{+0.07}_{-0.05}$	$0.98^{+0.10}_{-0.09}$	>2094.00			>14.3	>50.6	
		t_{start}	$1.04^{+0.10}_{-0.11}$	$1.04^{+0.11}_{-0.10}$	<0.11			<0.4	<47.4	

Table 4
(Continued)

GRB	Segments	Time	α	β	t (ks)	z	log $E_{\gamma,\mathrm{iso}}$ (erg)	θ_j (deg)	log E_γ (erg)	Requirements[†]
060219	I–II–III	t_b	$1.48^{+0.43}_{-0.32}$	$2.16^{+1.95}_{-0.97}$	$28.1^{+15.6}_{-16.1}$	...	...	2.5ξ	...	p_2
		t_{lastdet}	$1.48^{+0.43}_{-0.32}$	$2.16^{+1.95}_{-0.97}$	>399.42	...	...	$>6.7\xi$	...	p_2
060313	I–II–III	t_b	$1.51^{+0.17}_{-0.13}$	$1.52^{+0.41}_{-0.35}$	$6.5^{+2.1}_{-2.7}$	...	...	1.4ξ	...	**EI** p_2
		t_{lastdet}	$1.51^{+0.17}_{-0.13}$	$1.52^{+0.41}_{-0.35}$	>428.64	...	...	$>6.8\xi$	...	**EI** p_2
060418	I–II–III	t_b	$1.55^{+0.29}_{-0.11}$	$0.86^{+0.39}_{-0.31}$	$5.7^{+17.1}_{-3.8}$	4.05[i]	53.7	0.8	49.7	
		t_{lastdet}	$1.55^{+0.29}_{-0.11}$	$0.86^{+0.39}_{-0.31}$	>739.27			>5.2	>51.3	
060526	I–II–III	t_b	$1.71^{+0.31}_{-0.26}$	$0.96^{+0.65}_{-0.43}$	$23.5^{+10.3}_{-9.0}$	3.22[j]	52.6	2.1	49.4	
		t_{lastdet}	$1.71^{+0.31}_{-0.26}$	$0.96^{+0.65}_{-0.43}$	>440.34			>6.2	>50.4	
060906	I–II–III	t_b	$1.73^{+0.52}_{-0.32}$	$0.51^{+0.38}_{-0.30}$	$14.2^{+3.8}_{-2.3}$	3.69[k]	53.0	1.5	49.5	ν_1
		t_{lastdet}	$1.73^{+0.52}_{-0.32}$	$0.51^{+0.38}_{-0.30}$	>365.38			>5.0	>50.5	ν_1
060908	III–IV	t_b	$1.38^{+0.16}_{-0.11}$	$0.86^{+0.27}_{-0.24}$	$0.9^{+1.5}_{-0.3}$	2.43[l]	52.8	0.6	48.6	
		t_{lastdet}	$1.38^{+0.16}_{-0.11}$	$0.86^{+0.27}_{-0.24}$	>1087.46			>8.8	>50.9	
		t_{start}	$0.80^{+0.14}_{-0.11}$	$1.12^{+0.16}_{-0.15}$	<0.08			<0.2	<47.8	
060926	I–II–III	t_b	$1.54^{+0.41}_{-0.22}$	$0.92^{+0.79}_{-0.47}$	$4.9^{+4.3}_{-4.1}$	3.21[m]	...	1.2	...	
		t_{lastdet}	$1.54^{+0.41}_{-0.22}$	$0.92^{+0.79}_{-0.47}$	>283.79			>5.3	...	
060927	II–IV	t_b	$1.52^{+1.12}_{-0.27}$	$0.99^{+0.46}_{-0.26}$	$3.3^{+2.0}_{-2.1}$	5.47[n]	52.9	0.8	48.9	
		t_{lastdet}	$1.52^{+1.12}_{-0.27}$	$0.99^{+0.46}_{-0.26}$	>208.31			>3.7	>50.2	
		t_{start}	$0.67^{+0.13}_{-0.32}$	$0.57^{+0.59}_{-0.32}$	<0.07			<0.2	<47.6	
061007	Single PL	t_{lastdet}	$1.68^{+0.01}_{-0.01}$	$0.86^{+0.02}_{-0.02}$	>1284.22	1.26[o]	53.8	>8.2	>51.9	**EI** ν_1 p_2
		t_{start}	$1.68^{+0.01}_{-0.01}$	$0.86^{+0.02}_{-0.02}$	<0.09			<0.2	<48.7	**EI** ν_1 p_2
061201	II–IV	t_b	$1.84^{+0.25}_{-0.23}$	$0.61^{+0.71}_{-0.33}$	$2.3^{+1.2}_{-0.9}$	0.11[p]	50.1	2.9	47.2	ν_1
		t_{lastdet}	$1.84^{+0.25}_{-0.23}$	$0.61^{+0.71}_{-0.33}$	>132.49			>13.5	>48.5	ν_1
		t_{start}	$0.52^{+0.17}_{-0.17}$	$0.46^{+0.25}_{-0.23}$	<0.09			<0.9	<46.1	
061202	I–II–III	t_b	$1.66^{+0.10}_{-0.08}$	$1.41^{+0.25}_{-0.23}$	$16.9^{+1.2}_{-2.2}$	...	...	2.0ξ	...	**EI** ν_1 p_2
		t_{lastdet}	$1.66^{+0.10}_{-0.08}$	$1.41^{+0.25}_{-0.23}$	>635.56	...	...	$>7.9\xi$	...	**EI** ν_1 p_2
061210	Single PL	t_{lastdet}	$2.15^{+1.57}_{-1.16}$	$0.74^{+2.76}_{-0.78}$	>989.79	0.41[q]	50.8	>21.2	>49.7	
		t_{start}	$2.15^{+1.57}_{-1.16}$	$0.74^{+2.76}_{-0.78}$	<221.16			<12.1	<49.2	
070107	III–IV	t_b	$1.76^{+0.41}_{-0.29}$	$1.28^{+0.77}_{-0.49}$	$153.2^{+57.3}_{-62.0}$	...	...	4.6ξ	...	
		t_{lastdet}	$1.76^{+0.41}_{-0.29}$	$1.28^{+0.77}_{-0.49}$	>816.92	...	...	$>8.7\xi$	...	
		t_{start}	$1.04^{+0.05}_{-0.06}$	$1.21^{+0.18}_{-0.17}$	<0.18	...	...	$<0.4\xi$	...	
070125	II–IV	t_b	$1.85^{+0.29}_{-0.23}$	$1.24^{+0.58}_{-0.33}$	$90.9^{+30.1}_{-26.0}$	1.55[r]	...	4.2	...	
		t_{lastdet}	$1.85^{+0.29}_{-0.23}$	$1.24^{+0.58}_{-0.33}$	>972.61			>10.2	...	
		t_{start}	$0.64^{+0.54}_{-1.37}$	$0.96^{+0.47}_{-0.35}$	<46.70			<3.3	...	
070208	II–IV	t_b	$1.56^{+0.35}_{-0.21}$	$0.93^{+0.31}_{-0.27}$	$9.8^{+4.7}_{-2.6}$	1.17[s]	51.4	2.7	48.4	Uni ν_2
		t_{lastdet}	$1.56^{+0.35}_{-0.21}$	$0.93^{+0.31}_{-0.27}$	>480.38			>11.8	>49.7	Uni ν_2
		t_{start}	$0.12^{+0.15}_{-0.17}$	$8.99^{+9.99}_{-9.99}$	<0.13			<0.5	<47.0	
070318	III–IV	t_b	$1.91^{+1.87}_{-0.62}$	$9.00^{+10.0}_{-10.0}$	$308.6^{+249.0}_{-54.3}$	0.84[t]	52.0	8.9	50.1	Uni
		t_{lastdet}	$1.91^{+1.87}_{-0.62}$	$9.00^{+10.0}_{-10.0}$	>786.73			>12.7	>50.4	Uni
		t_{start}	$0.87^{+0.06}_{-0.06}$	$1.29^{+0.17}_{-0.16}$	<0.07			<0.4	<47.3	
070411	III–IV	t_b	$1.28^{+0.37}_{-0.13}$	$1.22^{+0.62}_{-0.34}$	$20.6^{+50.1}_{-9.9}$	2.95[u]	52.9	1.9	49.6	
		t_{lastdet}	$1.28^{+0.37}_{-0.13}$	$1.22^{+0.62}_{-0.34}$	>727.54			>7.1	>50.8	
		t_{start}	$0.93^{+0.12}_{-0.14}$	$1.07^{+0.39}_{-0.22}$	<0.46			<0.4	<48.4	
070412	I–II–III	t_b	$1.43^{+1.47}_{-0.23}$	$1.64^{+0.68}_{-0.48}$	$13.9^{+13.7}_{-10.3}$	...	...	1.9ξ	...	p_2
		t_{lastdet}	$1.43^{+1.47}_{-0.23}$	$1.64^{+0.68}_{-0.48}$	>682.84	...	...	$>8.1\xi$	...	p_2
070521	II–IV	t_b	$1.81^{+0.17}_{-0.14}$	$1.07^{+0.25}_{-0.21}$	$7.2^{+1.0}_{-1.1}$	...	...	1.5ξ	...	
		t_{lastdet}	$1.81^{+0.17}_{-0.14}$	$1.07^{+0.25}_{-0.21}$	>161.32	...	...	$>4.7\xi$	...	
		t_{start}	$0.49^{+0.05}_{-0.07}$	$0.99^{+0.22}_{-0.21}$	<0.11	...	...	$<0.3\xi$	...	
070611	I–II–III	t_b	$3.04^{+1.98}_{-1.32}$	$1.79^{+2.79}_{-2.01}$	$97.2^{+33.7}_{-45.6}$	2.04[v]	51.8	5.0	49.4	
		t_{lastdet}	$3.04^{+1.98}_{-1.32}$	$1.79^{+2.79}_{-2.01}$	>433.72			>8.8	>49.9	

Table 4
(Continued)

GRB	Segments	Time	α	β	t (ks)	z	log $E_{\gamma,\mathrm{iso}}$ (erg)	θ_j (deg)	log E_γ (erg)	Requirements[†]
070616	III–IV	t_b	$2.26^{+1.69}_{-0.58}$	$1.58^{+0.45}_{-0.31}$	$48.9^{+31.4}_{-23.4}$	...	...	3.0ξ	...	p_2
		t_{lastdet}	$2.26^{+1.69}_{-0.58}$	$1.58^{+0.45}_{-0.31}$	>371.12	...	...	$>6.5\xi$	...	p_2
		t_{start}	$1.25^{+0.11}_{-0.13}$	$1.51^{+0.72}_{-0.62}$	<0.14	...	...	$<0.3\xi$	...	
070714B	I–II–III	t_b	$1.58^{+0.13}_{-0.11}$	$0.88^{+0.37}_{-0.22}$	$0.9^{+0.2}_{-0.2}$	0.92[w]	52.0	1.0	48.2	
		t_{lastdet}	$1.58^{+0.13}_{-0.11}$	$0.88^{+0.37}_{-0.22}$	>133.69			>6.4	>49.8	
070721B	I–II–III	t_b	$2.21^{+0.39}_{-0.24}$	$0.88^{+0.26}_{-0.24}$	$9.2^{+1.2}_{-1.3}$	3.63[x]	53.3	1.2	49.6	$\nu_1\ p_2$
		t_{lastdet}	$2.21^{+0.39}_{-0.24}$	$0.88^{+0.26}_{-0.24}$	>93.25			>2.8	>50.3	$\nu_1\ p_2$
070810A	II–IV	t_b	$1.53^{+0.47}_{-0.32}$	$1.28^{+0.51}_{-0.41}$	$7.6^{+3.2}_{-5.3}$	2.17[y]	51.3	2.2	48.2	
		t_{lastdet}	$1.53^{+0.47}_{-0.32}$	$1.28^{+0.51}_{-0.41}$	>39.64			>4.1	>48.7	
		t_{start}	$0.83^{+0.07}_{-0.17}$	$1.14^{+0.26}_{-0.23}$	<0.10			<0.4	<46.8	
070911	Single PL	t_{lastdet}	$1.79^{+0.24}_{-0.23}$	$0.84^{+0.20}_{-0.18}$	>1515.59	...	...	$>11.0\xi$	...	
		t_{start}	$1.79^{+0.24}_{-0.23}$	$0.84^{+0.20}_{-0.18}$	<144.01	...	...	$<4.5\xi$	...	
071003	III–IV	t_b	$1.74^{+0.15}_{-0.14}$	$1.22^{+0.32}_{-0.26}$	$35.8^{+5.7}_{-7.4}$	1.60[z]	52.2	3.3	49.4	
		t_{lastdet}	$1.74^{+0.15}_{-0.14}$	$1.22^{+0.32}_{-0.26}$	>863.21			>10.8	>50.5	
		t_{start}	$0.88^{+0.30}_{-0.62}$	$0.95^{+0.26}_{-0.23}$	<22.34			<2.7	<49.3	
071010A	II–IV	t_b	$1.68^{+0.44}_{-0.36}$	$1.11^{+0.81}_{-0.56}$	$70.2^{+19.3}_{-17.4}$	0.98[aa]	50.2	8.2	48.2	
		t_{lastdet}	$1.68^{+0.44}_{-0.36}$	$1.11^{+0.81}_{-0.56}$	>468.48			>16.7	>48.9	
		t_{start}	$-0.62^{+0.77}_{-1.36}$	$1.63^{+0.96}_{-0.70}$	<34.07			<6.3	<48.0	
071011	I–II–III	t_b	$2.90^{+1.14}_{-0.78}$	$0.49^{+2.99}_{-1.37}$	$474.1^{+71.3}_{-89.3}$	...	...	7.1ξ	...	
		t_{lastdet}	$2.90^{+1.14}_{-0.78}$	$0.49^{+2.99}_{-1.37}$	>1404.74	...	...	$>10.7\xi$	...	
071025	I–II–III	t_b	$1.90^{+0.11}_{-0.10}$	$1.22^{+0.19}_{-0.17}$	$3.6^{+0.7}_{-0.7}$	...	...	1.1ξ	...	
		t_{lastdet}	$1.90^{+0.11}_{-0.10}$	$1.22^{+0.19}_{-0.17}$	>497.60	...	...	$>7.2\xi$	...	
071028	I–II–III	t_b	$2.80^{+1.97}_{-1.24}$	$0.95^{+0.49}_{-0.32}$	$31.8^{+8.2}_{-13.3}$	...	...	2.6ξ	...	
		t_{lastdet}	$2.80^{+1.97}_{-1.24}$	$0.95^{+0.49}_{-0.32}$	>87.33	...	...	$>3.8\xi$	...	
071031	I–II–III	t_b	$1.80^{+1.12}_{-0.58}$	$0.70^{+0.58}_{-0.58}$	$61.2^{+30.2}_{-43.5}$	2.69[ab]	...	3.2	...	
		t_{lastdet}	$1.80^{+1.12}_{-0.58}$	$0.70^{+0.58}_{-0.58}$	>590.79			>7.4	...	
071118	I–II–III	t_b	$1.85^{+1.92}_{-0.46}$	$0.92^{+0.66}_{-0.58}$	$12.7^{+2.9}_{-3.5}$	...	...	1.8ξ	...	ν_1
		t_{lastdet}	$1.85^{+1.92}_{-0.46}$	$0.92^{+0.66}_{-0.58}$	>121.79	...	...	$>4.3\xi$	...	ν_1

[†]Abbreviations for Uniform jet (Uni), Spreading jet (Sp), Nonspreading jet (NSp), $1 < p < 2$ (p_{12}), $p > 2$ (p_2), $\nu < \nu_c$ (ν_1), $\nu > \nu_c$ (ν_2).

Notes. Possible jet breaks are consistent with both pre- and post-jet break closure relations. They have pre- and post-break slopes similar to the segments III–IV or II–IV of the Prominent sample, or are single power laws with steep slopes either and late starts or long coverage, and are therefore more likely to be jet breaks than the Unlikely sample. The requirements are the result of another iteration of the internal consistency after excluding the remaining pre-jet break closure relations in final segments. t_{start} and t_{lastdet} times and opening angle limits are only listed if they are feasible within the canonical framework. Other notes are the same as for Prominent Jet Breaks table.

References. [a]Berger et al. 2005b; [b]Berger et al. 2005b; [c]Della Valle et al. 2006; [d]Berger & Becker 2005; [e]Mirabal et al. 2007; [f]Jakobsson et al. 2006a; [g]Piranomonte et al. 2006a; [h]Mirabal & Halpern 2006; [i]Prochaska et al. 2007a; [j]Jakobsson et al. 2006a; [k]Jakobsson et al. 2006a; [l]Rol et al. 2006; [m]Piranomonte et al. 2006b; [n]Ruiz-Velasco et al. 2007; [o]Osip et al. 2006; [p]Stratta et al. 2007; [q]Berger et al. 2007b; [r]Cenko et al. 2008; [s]Cucchiara et al. 2007c; [t]Jaunsen et al. 2007a; [u]Jakobsson et al. 2007d; [v]Thöne et al. 2007c; [w]Graham et al. 2008; [x]Malesani et al. 2007; [y]Thöne et al. 2007d; [z]Perley et al. 2008; [aa]Prochaska et al. 2007b; [ab]Ledoux et al. 2007.

choose to include all plausible alternatives. When evaluating the closure relations for $1 < p < 2$, we adopt the treatment described by Dai & Cheng (2001).

We evaluate sets of closure relations whose form is

$$\alpha = f(\beta) \tag{5}$$

by defining a new parameter, Ψ, such that

$$\Psi \equiv \alpha_{\mathrm{obs}} - f(\beta_{\mathrm{obs}}). \tag{6}$$

Using the measured values of α_{obs} and β_{obs}, we compare the output (Ψ) to the expectation of zero. A relation is deemed valid if the output value is consistent within the error found by propagating the $2\sigma = 95.4\%$ confidence measurement errors on α and β.

In the case of energy injection, the closure relations give $\alpha = f(\beta, q)$, where q is the luminosity index defined as $L(t) = L_0(t/t_b)^{-q}$, which is physically valid for $q < 1$ (Zhang et al. 2006; Zhang & Mészáros 2001). The energy injection closure relations in Table 1 reduce to the normal isotropic relations when $q = 1$. We solve for $q = g(\alpha, \beta)$ using the observed values to determine q, as

$$q_{\mathrm{obs}} = \begin{cases} g(\alpha_{\mathrm{obs}}, \beta_{\mathrm{obs}}) & (g < 1) \\ 1 & (g \geqslant 1). \end{cases} \tag{7}$$

Table 5
Unlikely Jet Breaks

GRB	Segments	Time	α	β	t (ks)	z	log $E_{\gamma,\mathrm{iso}}$ (erg)	θ_j (deg)	log E_γ (erg)	Requirements[†]
050124	Single PL	t_{lastdet}	$1.50^{+0.21}_{-0.16}$	$0.83^{+0.30}_{-0.18}$	>4967.45	···	···	$>17.1\xi$	···	
		t_{start}	$1.50^{+0.21}_{-0.16}$	$0.83^{+0.30}_{-0.18}$	<11.13	···	···	$<1.7\xi$	···	
050128	II–III	t_b	$1.30^{+0.08}_{-0.07}$	$0.96^{+0.17}_{-0.16}$	$2.9^{+3.9}_{-1.0}$	···	···	1.0ξ	···	
		t_{lastdet}	$1.30^{+0.08}_{-0.07}$	$0.96^{+0.17}_{-0.16}$	>99.44	···	···	$>4.0\xi$	···	
		t_{start}	$0.70^{+0.16}_{-0.20}$	$0.77^{+0.24}_{-0.17}$	<0.24	···	···	$<0.4\xi$	···	
050215B	Single PL	t_{lastdet}	$0.93^{+0.21}_{-0.17}$	$0.66^{+0.63}_{-0.49}$	>3011.04	···	···	$>14.2\xi$	···	
		t_{start}	$0.93^{+0.21}_{-0.17}$	$0.66^{+0.63}_{-0.49}$	<5.81	···	···	$<1.4\xi$	···	
050219B	Single PL	t_{lastdet}	$1.21^{+0.05}_{-0.05}$	$1.11^{+0.19}_{-0.17}$	>120.17	···	···	$>4.2\xi$	···	
		t_{start}	$1.21^{+0.05}_{-0.05}$	$1.11^{+0.19}_{-0.17}$	<3.18	···	···	$<1.1\xi$	···	
050223	Single PL	t_{lastdet}	$0.92^{+0.26}_{-0.24}$	$2.42^{+6.58}_{-3.42}$	>72.71	0.58[a]	50.9	>7.4	>48.9	
		t_{start}	$0.92^{+0.26}_{-0.24}$	$2.42^{+6.58}_{-3.42}$	<2.88			<2.2	<47.8	
050401	II–III	t_b	$1.44^{+0.10}_{-0.09}$	$0.84^{+0.18}_{-0.13}$	$5.0^{+0.9}_{-0.8}$	2.90[b]	53.5	0.9	49.6	
		t_{lastdet}	$1.44^{+0.10}_{-0.09}$	$0.84^{+0.18}_{-0.13}$	>776.68			>6.2	>51.2	
050410	II–III	t_b	$1.19^{+0.44}_{-0.20}$	$0.28^{+0.84}_{-0.72}$	$18.4^{+19.7}_{-11.1}$	···	···	2.1ξ	···	
		t_{lastdet}	$1.19^{+0.44}_{-0.20}$	$0.28^{+0.84}_{-0.72}$	>864.12	···	···	$>8.9\xi$	···	
		t_{start}	$0.62^{+0.18}_{-0.29}$	$1.22^{+1.88}_{-1.15}$	<1.91	···	···	$<0.9\xi$	···	
050412	Single PL	t_{lastdet}	$1.64^{+0.25}_{-0.24}$	$0.54^{+0.20}_{-0.20}$	>0.63	···	···	$>0.6\xi$	···	
		t_{start}	$1.64^{+0.25}_{-0.24}$	$0.54^{+0.20}_{-0.20}$	<0.10	···	···	$<0.3\xi$	···	
050502B	Single PL	t_{lastdet}	$0.75^{+0.23}_{-0.23}$	$1.72^{+2.12}_{-0.95}$	>290.03	···	···	$>5.9\xi$	···	
		t_{start}	$0.75^{+0.23}_{-0.23}$	$1.72^{+2.12}_{-0.95}$	<0.07	···	···	$<0.3\xi$	···	
050509A	Single PL	t_{lastdet}	$1.12^{+0.13}_{-0.12}$	$2.09^{+1.79}_{-1.19}$	>1098.92	···	···	$>9.7\xi$	···	
		t_{start}	$1.12^{+0.13}_{-0.12}$	$2.09^{+1.79}_{-1.19}$	<3.68	···	···	$<1.1\xi$	···	
050520	Single PL	t_{lastdet}	$1.55^{+0.73}_{-0.60}$	$0.10^{+1.96}_{-1.42}$	>222.82	···	···	$>5.3\xi$	···	
		t_{start}	$1.55^{+0.73}_{-0.60}$	$0.10^{+1.96}_{-1.42}$	<7.69	···	···	$<1.5\xi$	···	
050607	II–III	t_b	$1.24^{+0.48}_{-0.22}$	$1.66^{+1.17}_{-0.72}$	$14.0^{+18.4}_{-7.2}$	···	···	1.9ξ	···	
		t_{lastdet}	$1.24^{+0.48}_{-0.22}$	$1.66^{+1.17}_{-0.72}$	>874.03	···	···	$>8.9\xi$	···	
		t_{start}	$0.60^{+0.15}_{-0.17}$	$0.91^{+0.48}_{-0.31}$	<0.10	···	···	$<0.3\xi$	···	
050701	Single PL	t_{lastdet}	$1.18^{+0.25}_{-0.22}$	$1.61^{+1.56}_{-1.31}$	>164.14	···	···	$>4.8\xi$	···	
		t_{start}	$1.18^{+0.25}_{-0.22}$	$1.61^{+1.56}_{-1.31}$	<6.21	···	···	$<1.4\xi$	···	
050712	II–III	t_b	$1.23^{+0.31}_{-0.18}$	$0.83^{+0.52}_{-0.40}$	$48.0^{+37.1}_{-29.9}$	···	···	3.0ξ	···	
		t_{lastdet}	$1.23^{+0.31}_{-0.18}$	$0.83^{+0.52}_{-0.40}$	>1833.39	···	···	$>11.8\xi$	···	
		t_{start}	$0.66^{+0.14}_{-0.18}$	$1.16^{+0.33}_{-0.29}$	<0.17	···	···	$<0.4\xi$	···	
050713A	I–II–III	t_b	$1.17^{+0.07}_{-0.06}$	$1.27^{+0.18}_{-0.19}$	$7.4^{+2.8}_{-3.4}$	···	···	1.5ξ	···	
		t_{lastdet}	$1.17^{+0.07}_{-0.06}$	$1.27^{+0.18}_{-0.19}$	>1711.35	···	···	$>11.5\xi$	···	
050716	Single PL	t_{lastdet}	$1.02^{+0.09}_{-0.08}$	$1.13^{+0.12}_{-0.24}$	>1759.19	···	···	$>11.6\xi$	···	
		t_{start}	$1.02^{+0.09}_{-0.08}$	$1.13^{+0.12}_{-0.24}$	<0.10	···	···	$<0.3\xi$	···	
050724	Single PL	t_{lastdet}	$0.96^{+0.22}_{-0.20}$	$1.05^{+0.96}_{-0.65}$	>1910.50	0.26[c]	50.2	>33.6	>49.5	
		t_{start}	$0.96^{+0.22}_{-0.20}$	$1.05^{+0.96}_{-0.65}$	<0.08			<0.8	<46.2	
050730	II–III	t_b	$2.58^{+0.10}_{-0.09}$	$0.71^{+0.06}_{-0.06}$	$9.1^{+0.4}_{-0.4}$	3.97[d]	53.1	1.2	49.4	none
		t_{lastdet}	$2.58^{+0.10}_{-0.09}$	$0.71^{+0.06}_{-0.06}$	>492.43			>5.3	>50.7	none
050801	II–III	t_b	$1.17^{+0.06}_{-0.07}$	$0.98^{+0.36}_{-0.32}$	$0.2^{+0.0}_{-0.1}$	···	···	0.4ξ	···	
		t_{lastdet}	$1.17^{+0.06}_{-0.07}$	$0.98^{+0.36}_{-0.32}$	>624.37	···	···	$>7.9\xi$	···	
		t_{start}	$-0.36^{+0.64}_{-1.08}$	$1.12^{+0.85}_{-0.56}$	<0.09	···	···	$<0.3\xi$	···	
050824	II–III	t_b	$0.93^{+0.23}_{-0.13}$	$1.39^{+0.40}_{-0.32}$	$70.2^{+64.6}_{-29.4}$	0.83[e]	···	4.3	···	
		t_{lastdet}	$0.93^{+0.23}_{-0.13}$	$1.39^{+0.40}_{-0.32}$	>2070.91			>15.4	···	
050915A	I–II–III	t_b	$1.15^{+0.14}_{-0.13}$	$0.97^{+0.49}_{-0.41}$	$1.4^{+4.1}_{-0.8}$	···	···	0.8ξ	···	
		t_{lastdet}	$1.15^{+0.14}_{-0.13}$	$0.97^{+0.49}_{-0.41}$	>474.97	···	···	$>7.1\xi$	···	
050915B	I–II–III	t_b	$1.01^{+0.68}_{-0.29}$	$1.04^{+2.42}_{-0.68}$	$35.8^{+70.8}_{-23.0}$	···	···	2.7ξ	···	
		t_{lastdet}	$1.01^{+0.68}_{-0.29}$	$1.04^{+2.42}_{-0.68}$	>613.98	···	···	$>7.8\xi$	···	

Table 5
(Continued)

GRB	Segments	Time	α	β	t (ks)	z	log $E_{\gamma,\mathrm{iso}}$ (erg)	θ_j (deg)	log E_γ (erg)	Requirements[†]
051006	Single PL	t_{lastdet}	$1.59^{+0.13}_{-0.11}$	$0.83^{+0.55}_{-0.49}$	>16.19	...	...	>2.0ξ	...	
		t_{start}	$1.59^{+0.13}_{-0.11}$	$0.83^{+0.55}_{-0.49}$	<0.11	...	...	<0.3ξ	...	
051016A	I–II–III	t_b	$1.04^{+0.24}_{-0.16}$	$1.45^{+0.65}_{-0.51}$	$2.8^{+8.2}_{-2.1}$	...	...	1.0ξ	...	
		t_{lastdet}	$1.04^{+0.24}_{-0.16}$	$1.45^{+0.65}_{-0.51}$	>930.89	...	...	>9.1ξ	...	
051021A	Single PL	t_{lastdet}	$1.00^{+0.10}_{-0.08}$	$1.23^{+0.42}_{-0.34}$	>1430.45	...	...	>10.7ξ	...	
		t_{start}	$1.00^{+0.10}_{-0.08}$	$1.23^{+0.42}_{-0.34}$	<11.25	...	...	<1.7ξ	...	
051022	II–III	t_b	$2.29^{+0.68}_{-0.40}$	$0.74^{+0.38}_{-0.30}$	$234.7^{+37.3}_{-81.8}$	...	...	5.5ξ	...	none
		t_{lastdet}	$2.29^{+0.68}_{-0.40}$	$0.74^{+0.38}_{-0.30}$	>1263.29	...	...	>10.2ξ	...	none
051028	Single PL	t_{lastdet}	$1.19^{+0.26}_{-0.18}$	$1.01^{+0.52}_{-0.43}$	>847.05	...	...	>8.8ξ	...	
		t_{start}	$1.19^{+0.26}_{-0.18}$	$1.01^{+0.52}_{-0.43}$	<25.79	...	...	<2.4ξ	...	
051109B	I–II–III	t_b	$0.97^{+0.22}_{-0.14}$	$1.02^{+0.68}_{-0.35}$	$2.2^{+2.0}_{-1.2}$	0.08[f]	48.7	4.3	46.2	
		t_{lastdet}	$0.97^{+0.22}_{-0.14}$	$1.02^{+0.68}_{-0.35}$	>145.62			>21.0	>47.5	
051117A	II–III	t_b	$1.11^{+0.17}_{-0.12}$	$2.02^{+0.32}_{-0.26}$	$65.7^{+40.6}_{-32.6}$	...	...	3.4ξ	...	
		t_{lastdet}	$1.11^{+0.17}_{-0.12}$	$2.02^{+0.32}_{-0.26}$	>1886.19	...	...	>11.9ξ	...	
060108	I–II–III	t_b	$1.20^{+0.21}_{-0.15}$	$1.14^{+0.45}_{-0.35}$	$20.9^{+9.7}_{-7.6}$	...	...	2.2ξ	...	
		t_{lastdet}	$1.20^{+0.21}_{-0.15}$	$1.14^{+0.45}_{-0.35}$	>427.37	...	...	>6.8ξ	...	
060110	Single PL	t_{lastdet}	$1.18^{+1.58}_{-1.39}$	$2.77^{+6.23}_{-3.77}$	>492.92	...	...	>7.2ξ	...	
		t_{start}	$1.18^{+1.58}_{-1.39}$	$2.77^{+6.23}_{-3.77}$	<242.21	...	...	<5.5ξ	...	
060111A	Single PL	t_{lastdet}	$0.85^{+0.07}_{-0.06}$	$1.32^{+0.26}_{-0.23}$	>761.73	...	...	>8.5ξ	...	
		t_{start}	$0.85^{+0.07}_{-0.06}$	$1.32^{+0.26}_{-0.23}$	<0.07	...	...	<0.3ξ	...	
060121	Single PL	t_{lastdet}	$1.21^{+0.08}_{-0.08}$	$1.41^{+0.27}_{-0.28}$	>1042.08	...	...	>9.5ξ	...	
		t_{start}	$1.21^{+0.08}_{-0.08}$	$1.41^{+0.27}_{-0.28}$	<10.60	...	...	<1.7ξ	...	
060123	Single PL	t_{lastdet}	$1.21^{+0.18}_{-0.16}$	$0.74^{+0.33}_{-0.27}$	>1042.63	...	...	>9.5ξ	...	
		t_{start}	$1.21^{+0.18}_{-0.16}$	$0.74^{+0.33}_{-0.27}$	<75.10	...	...	<3.6ξ	...	
060203	II–III	t_b	$1.23^{+0.24}_{-0.17}$	$1.19^{+0.48}_{-0.31}$	$11.1^{+9.3}_{-2.1}$	...	...	1.7ξ	...	
		t_{lastdet}	$1.23^{+0.24}_{-0.17}$	$1.19^{+0.48}_{-0.31}$	>304.87	...	...	>6.0ξ	...	
		t_{start}	$0.55^{+0.23}_{-0.27}$	$1.33^{+0.48}_{-0.41}$	<3.00	...	...	<1.1ξ	...	
060206	II–III	t_b	$1.24^{+0.05}_{-0.04}$	$1.31^{+0.18}_{-0.16}$	$5.9^{+1.2}_{-5.1}$	4.05[g]	52.6	1.2	48.9	
		t_{lastdet}	$1.24^{+0.05}_{-0.04}$	$1.31^{+0.18}_{-0.16}$	>3697.33			>13.0	>51.0	
060223A	II–III	t_b	$1.27^{+0.14}_{-0.12}$	$1.65^{+0.66}_{-0.52}$	$0.3^{+0.1}_{-0.1}$	4.41[h]	52.6	0.4	47.9	
		t_{lastdet}	$1.27^{+0.14}_{-0.12}$	$1.65^{+0.66}_{-0.52}$	>28.57			>2.1	>49.4	
060306	I–II–III	t_b	$1.06^{+0.10}_{-0.07}$	$1.14^{+0.23}_{-0.21}$	$8.2^{+5.7}_{-5.0}$	...	...	1.6ξ	...	
		t_{lastdet}	$1.06^{+0.10}_{-0.07}$	$1.14^{+0.23}_{-0.21}$	>382.21	...	...	>6.5ξ	...	
060312	I–II–III	t_b	$1.17^{+0.39}_{-0.27}$	$0.62^{+0.45}_{-0.26}$	$10.3^{+6.4}_{-7.7}$	...	...	1.7ξ	...	
		t_{lastdet}	$1.17^{+0.39}_{-0.27}$	$0.62^{+0.45}_{-0.26}$	>172.44	...	...	>4.9ξ	...	
060319	II–III	t_b	$1.18^{+0.08}_{-0.07}$	$1.15^{+0.27}_{-0.23}$	$18.3^{+10.}_{-4.2}$	...	...	2.1ξ	...	
		t_{lastdet}	$1.18^{+0.08}_{-0.07}$	$1.15^{+0.27}_{-0.23}$	>3737.78	...	...	>15.4ξ	...	
060323	II–III	t_b	$1.22^{+0.22}_{-0.13}$	$1.07^{+0.37}_{-0.43}$	$0.8^{+0.7}_{-0.2}$	...	...	0.7ξ	...	
		t_{lastdet}	$1.22^{+0.22}_{-0.13}$	$1.07^{+0.37}_{-0.43}$	>91.51	...	...	>3.8ξ	...	
		t_{start}	$0.10^{+0.46}_{-0.54}$	$0.89^{+0.42}_{-0.26}$	<0.29	...	...	<0.4ξ	...	
060421	II–III	t_b	$1.30^{+0.27}_{-0.18}$	$0.31^{+0.80}_{-0.55}$	$0.8^{+6.8}_{-0.4}$	...	...	0.6ξ	...	
		t_{lastdet}	$1.30^{+0.27}_{-0.18}$	$0.31^{+0.80}_{-0.55}$	>116.06	...	...	>4.2ξ	...	
		t_{start}	$0.54^{+0.50}_{-0.80}$	$0.50^{+0.40}_{-0.40}$	<0.11	...	...	<0.3ξ	...	
060502A	I–II–III	t_b	$1.12^{+0.13}_{-0.09}$	$0.88^{+0.21}_{-0.19}$	$28.8^{+29.7}_{-12.7}$	1.51[i]	52.4	2.9	49.5	
		t_{lastdet}	$1.12^{+0.13}_{-0.09}$	$0.88^{+0.21}_{-0.19}$	>1601.07			>13.0	>50.8	
060505	Single PL	t_{lastdet}	$1.33^{+0.42}_{-0.31}$	$1.40^{+0.91}_{-0.97}$	>1428.69	0.09[j]	49.6	>38.2	>48.9	
		t_{start}	$1.33^{+0.42}_{-0.31}$	$1.40^{+0.91}_{-0.97}$	<51.76			<11.0	<47.9	
060507	II–III	t_b	$1.14^{+0.16}_{-0.12}$	$1.14^{+0.31}_{-0.26}$	$11.0^{+9.5}_{-2.3}$	...	...	1.7ξ	...	
		t_{lastdet}	$1.14^{+0.16}_{-0.12}$	$1.14^{+0.31}_{-0.26}$	>893.39	...	...	>9.0ξ	...	

Table 5
(Continued)

GRB	Segments	Time	α	β	t (ks)	z	log $E_{\gamma,\mathrm{iso}}$ (erg)	θ_j (deg)	log E_γ (erg)	Requirements[†]
060512	I–II–III	t_b	$1.21^{+0.29}_{-0.16}$	$1.14^{+0.51}_{-0.32}$	$6.1^{+31.8}_{-1.5}$	0.44[k]	...	1.9	...	
		t_{lastdet}	$1.21^{+0.29}_{-0.16}$	$1.14^{+0.51}_{-0.32}$	>323.03			>8.4	...	
060522	I–II–III	t_b	$1.41^{+0.42}_{-0.28}$	$1.33^{+1.06}_{-0.68}$	$7.6^{+5.8}_{-3.1}$	5.11[l]	52.9	1.1	49.2	
		t_{lastdet}	$1.41^{+0.42}_{-0.28}$	$1.33^{+1.06}_{-0.68}$	>144.80			>3.3	>50.1	
060602A	Single PL	t_{lastdet}	$1.06^{+0.99}_{-1.21}$	$2.83^{+1.38}_{-1.12}$	>799.63	...	...	>8.6ξ	...	
		t_{start}	$1.06^{+0.99}_{-1.21}$	$2.83^{+1.38}_{-1.12}$	<158.18	...	...	<4.7ξ	...	
060602B	Single PL	t_{lastdet}	$1.12^{+0.11}_{-0.09}$	$1.04^{+1.27}_{-0.46}$	>653.62	...	...	>8.0ξ	...	
		t_{start}	$1.12^{+0.11}_{-0.09}$	$1.04^{+1.27}_{-0.46}$	<0.10	...	...	<0.3ξ	...	
060604	I–II–III	t_b	$1.21^{+0.11}_{-0.09}$	$1.07^{+0.24}_{-0.20}$	$25.7^{+16.4}_{-6.0}$	2.68[m]	52.0	2.7	49.0	
		t_{lastdet}	$1.21^{+0.11}_{-0.09}$	$1.07^{+0.24}_{-0.20}$	>1920.57			>13.6	>50.4	
060607A	I–II–III	t_b	$3.41^{+0.18}_{-0.17}$	$0.56^{+0.13}_{-0.12}$	$12.8^{+0.4}_{-0.5}$	3.08[n]	53.0	1.5	49.5	none
		t_{lastdet}	$3.41^{+0.18}_{-0.17}$	$0.56^{+0.13}_{-0.12}$	>208.38			>4.3	>50.4	none
060708	I–II–III	t_b	$1.27^{+0.12}_{-0.11}$	$1.02^{+0.20}_{-0.19}$	$12.6^{+4.6}_{-7.0}$	...	...	1.8ξ	...	
		t_{lastdet}	$1.27^{+0.12}_{-0.11}$	$1.02^{+0.20}_{-0.19}$	>1202.58	...	...	>10.1ξ	...	
060714	I–II–III	t_b	$1.22^{+0.08}_{-0.06}$	$1.18^{+0.24}_{-0.21}$	$3.9^{+2.2}_{-1.3}$	2.71[o]	52.9	1.0	49.1	
		t_{lastdet}	$1.22^{+0.08}_{-0.06}$	$1.18^{+0.24}_{-0.21}$	>1215.93			>8.9	>50.9	
060717	Single PL	t_{lastdet}	$0.85^{+0.21}_{-0.25}$	$1.14^{+0.62}_{-0.57}$	>39.53	...	...	>2.8ξ	...	
		t_{start}	$0.85^{+0.21}_{-0.25}$	$1.14^{+0.62}_{-0.57}$	<0.23	...	...	<0.4ξ	...	
060804	II–III	t_b	$1.25^{+0.14}_{-0.13}$	$1.26^{+0.43}_{-0.28}$	$1.1^{+2.3}_{-0.4}$	...	...	0.7ξ	...	
		t_{lastdet}	$1.25^{+0.14}_{-0.13}$	$1.26^{+0.43}_{-0.28}$	>248.86	...	...	>5.6ξ	...	
		t_{start}	$-0.18^{+0.59}_{-0.59}$	$0.83^{+0.85}_{-0.43}$	<0.13	...	...	<0.3ξ	...	
060805A	II–III	t_b	$1.38^{+0.26}_{-0.20}$	$1.48^{+0.92}_{-0.67}$	$2.9^{+1.6}_{-1.5}$	...	...	1.1ξ	...	
		t_{lastdet}	$1.38^{+0.26}_{-0.20}$	$1.48^{+0.92}_{-0.67}$	>294.57	...	...	>5.9ξ	...	
		t_{start}	$0.13^{+0.26}_{-0.49}$	$1.33^{+1.24}_{-0.73}$	<0.11	...	...	<0.3ξ	...	
060805B	Single PL	t_{lastdet}	$1.00^{+0.46}_{-0.41}$	$0.79^{+0.52}_{-0.22}$	>377.43	...	...	>6.5ξ	...	
		t_{start}	$1.00^{+0.46}_{-0.41}$	$0.79^{+0.52}_{-0.22}$	<126.50	...	...	<4.3ξ	...	
060825	Single PL	t_{lastdet}	$0.92^{+0.06}_{-0.07}$	$0.89^{+0.66}_{-0.54}$	>357.94	...	...	>6.4ξ	...	
		t_{start}	$0.92^{+0.06}_{-0.07}$	$0.89^{+0.66}_{-0.54}$	<0.08	...	...	<0.3ξ	...	
060901	Single PL	t_{lastdet}	$1.39^{+0.53}_{-0.38}$	$0.70^{+0.83}_{-0.35}$	>115.88	...	...	>4.2ξ	...	
		t_{start}	$1.39^{+0.53}_{-0.38}$	$0.70^{+0.83}_{-0.35}$	<13.82	...	...	<1.9ξ	...	
060904A	I–II–III	t_b	$1.29^{+0.21}_{-0.18}$	$2.19^{+1.02}_{-0.59}$	$4.2^{+4.9}_{-2.4}$	...	...	1.2ξ	...	
		t_{lastdet}	$1.29^{+0.21}_{-0.18}$	$2.19^{+1.02}_{-0.59}$	>1025.42	...	...	>9.5ξ	...	
060904B	II–III	t_b	$1.42^{+0.15}_{-0.12}$	$1.21^{+0.27}_{-0.26}$	$6.9^{+2.5}_{-2.7}$	0.70[p]	51.6	2.5	48.5	
		t_{lastdet}	$1.42^{+0.15}_{-0.12}$	$1.21^{+0.27}_{-0.26}$	>674.98			>13.9	>50.0	
		t_{start}	$0.76^{+0.06}_{-0.08}$	$1.20^{+0.49}_{-0.43}$	<0.08			<0.5	<47.1	
060912A	II–III	t_b	$1.11^{+0.10}_{-0.07}$	$1.10^{+0.28}_{-0.25}$	$0.9^{+1.0}_{-0.4}$	...	...	0.7ξ	...	
		t_{lastdet}	$1.11^{+0.10}_{-0.07}$	$1.10^{+0.28}_{-0.25}$	>868.42	...	...	>8.9ξ	...	
060919	II–III	t_b	$1.02^{+0.29}_{-0.18}$	$0.81^{+1.18}_{-0.89}$	$0.5^{+0.6}_{-0.3}$	...	...	0.6ξ	...	
		t_{lastdet}	$1.02^{+0.29}_{-0.18}$	$0.81^{+1.18}_{-0.89}$	>306.94	...	...	>6.0ξ	...	
		t_{start}	$0.75^{+0.53}_{-0.97}$	$0.49^{+0.58}_{-0.57}$	<0.10	...	...	<0.3ξ	...	
060923A	I–II–III	t_b	$1.15^{+0.08}_{-0.07}$	$1.07^{+0.36}_{-0.26}$	$4.1^{+1.9}_{-1.3}$	...	...	1.2ξ	...	
		t_{lastdet}	$1.15^{+0.08}_{-0.07}$	$1.07^{+0.36}_{-0.26}$	>930.68	...	...	>9.1ξ	...	
060923B	Single PL	t_{lastdet}	$0.54^{+0.10}_{-0.09}$	$1.33^{+0.72}_{-0.60}$	>5.98	...	...	>1.4ξ	...	
		t_{start}	$0.54^{+0.10}_{-0.09}$	$1.33^{+0.72}_{-0.60}$	<0.12	...	...	<0.3ξ	...	
060923C	I–II–III	t_b	$1.24^{+1.26}_{-0.48}$	$1.43^{+1.63}_{-0.90}$	$103.1^{+234.8}_{-91.5}$	...	...	4.0ξ	...	
		t_{lastdet}	$1.24^{+1.26}_{-0.48}$	$1.43^{+1.63}_{-0.90}$	>1358.96	...	...	>10.5ξ	...	
060929	II–III	t_b	$1.06^{+0.27}_{-0.12}$	$0.53^{+0.38}_{-0.35}$	$1.3^{+6.6}_{-0.9}$	...	...	0.8ξ	...	
		t_{lastdet}	$1.06^{+0.27}_{-0.12}$	$0.53^{+0.38}_{-0.35}$	>613.90	...	...	>7.8ξ	...	
		t_{start}	$0.47^{+0.24}_{-1.56}$	$0.89^{+2.49}_{-0.94}$	<0.10	...	...	<0.3ξ	...	

Table 5
(Continued)

GRB	Segments	Time	α	β	t (ks)	z	log $E_{\gamma,\mathrm{iso}}$ (erg)	θ_j (deg)	log E_γ (erg)	Requirements[†]
061004	I–II–III	t_b	$1.22^{+0.18}_{-0.15}$	$1.23^{+0.50}_{-0.24}$	$2.4^{+1.7}_{-0.7}$	···	···	1.0ξ	···	
		t_{lastdet}	$1.22^{+0.18}_{-0.15}$	$1.23^{+0.50}_{-0.24}$	>134.39	···	···	$>4.4\xi$	···	
061025	Single PL	t_{lastdet}	$1.48^{+0.46}_{-0.44}$	$0.84^{+0.40}_{-0.39}$	>74.91	···	···	$>3.6\xi$	···	
		t_{start}	$1.48^{+0.46}_{-0.44}$	$0.84^{+0.40}_{-0.39}$	<8.95	···	···	$<1.6\xi$	···	
061110A	I–II–III	t_b	$1.11^{+0.76}_{-0.38}$	$0.81^{+0.64}_{-0.55}$	$97.8^{+262.6}_{-86.1}$	0.76[q]	51.4	6.9	49.3	
		t_{lastdet}	$1.11^{+0.76}_{-0.38}$	$0.81^{+0.64}_{-0.55}$	>903.10			>15.9	>50.0	
061110B	Single PL	t_{lastdet}	$1.42^{+0.40}_{-0.37}$	$1.05^{+0.52}_{-0.42}$	>21.11	3.44[r]	···	>2.0	···	
		t_{start}	$1.42^{+0.40}_{-0.37}$	$1.05^{+0.52}_{-0.42}$	<3.14			<1.0	···	
061121	I–II–III–IV	t_b	$1.55^{+0.08}_{-0.06}$	$0.80^{+0.12}_{-0.11}$	$29.2^{+15.2}_{-6.9}$	1.31[s]	53.4	2.3	50.3	none
		t_{lastdet}	$1.55^{+0.08}_{-0.06}$	$0.80^{+0.12}_{-0.11}$	>2100.85			>11.2	>51.7	none
061122	Single PL	t_{lastdet}	$1.24^{+0.10}_{-0.09}$	$1.08^{+0.16}_{-0.17}$	>1267.39	···	···	$>10.3\xi$	···	
		t_{start}	$1.24^{+0.10}_{-0.09}$	$1.08^{+0.16}_{-0.17}$	<24.47	···	···	$<2.3\xi$	···	
061126	Single PL	t_{lastdet}	$1.29^{+0.02}_{-0.02}$	$0.96^{+0.12}_{-0.12}$	>2819.49	···	···	$>13.8\xi$	···	
		t_{start}	$1.29^{+0.02}_{-0.02}$	$0.96^{+0.12}_{-0.12}$	<1.60	···	···	$<0.8\xi$	···	
070103	II–III	t_b	$1.42^{+0.17}_{-0.16}$	$0.98^{+0.44}_{-0.44}$	$4.8^{+0.4}_{-3.6}$	···	···	1.3ξ	···	
		t_{lastdet}	$1.42^{+0.17}_{-0.16}$	$0.98^{+0.44}_{-0.44}$	>179.87	···	···	$>4.9\xi$	···	
		t_{start}	$0.37^{+0.13}_{-0.88}$	$1.21^{+1.50}_{-0.75}$	<0.09	···	···	$<0.3\xi$	···	
070219	I–II–III	t_b	$1.14^{+0.52}_{-0.26}$	$0.69^{+0.94}_{-0.41}$	$7.0^{+13.3}_{-2.6}$	···	···	1.5ξ	···	
		t_{lastdet}	$1.14^{+0.52}_{-0.26}$	$0.69^{+0.94}_{-0.41}$	>219.86	···	···	$>5.3\xi$	···	
070224	I–II–III	t_b	$0.87^{+0.70}_{-0.22}$	$0.13^{+0.73}_{-0.82}$	$28.9^{+189.2}_{-21.4}$	···	···	2.5ξ	···	
		t_{lastdet}	$0.87^{+0.70}_{-0.22}$	$0.13^{+0.73}_{-0.82}$	>1388.35	···	···	$>10.6\xi$	···	
070227	Single PL	t_{lastdet}	$1.13^{+0.19}_{-0.19}$	$1.37^{+0.59}_{-0.45}$	>906.39	···	···	$>9.0\xi$	···	
		t_{start}	$1.13^{+0.19}_{-0.19}$	$1.37^{+0.59}_{-0.45}$	<55.92	···	···	$<3.2\xi$	···	
070311	I–II–III	t_b	$4.08^{+1.96}_{-0.96}$	$0.68^{+1.40}_{-0.68}$	$208.8^{+33.5}_{-69.1}$	···	···	5.2ξ	···	none
		t_{lastdet}	$4.08^{+1.96}_{-0.96}$	$0.68^{+1.40}_{-0.68}$	>556.74	···	···	$>7.5\xi$	···	none
070330	I–II–III	t_b	$1.02^{+0.25}_{-0.20}$	$0.94^{+0.47}_{-0.35}$	$10.8^{+10.1}_{-5.4}$	···	···	1.7ξ	···	
		t_{lastdet}	$1.02^{+0.25}_{-0.20}$	$0.94^{+0.47}_{-0.35}$	>317.48	···	···	$>6.1\xi$	···	
070506	Single PL	t_{lastdet}	$0.52^{+0.15}_{-0.16}$	$1.08^{+0.39}_{-0.37}$	>8.12	2.31[t]	51.6	>2.0	>48.4	
		t_{start}	$0.52^{+0.15}_{-0.16}$	$1.08^{+0.39}_{-0.37}$	<0.43			<0.7	<47.5	
070508	II–III–IV	t_b	$1.76^{+0.47}_{-0.21}$	$1.47^{+0.68}_{-0.44}$	$49.7^{+80.1}_{-43.4}$	0.82[u]	52.9	3.5	50.2	none
		t_{lastdet}	$1.76^{+0.47}_{-0.21}$	$1.47^{+0.68}_{-0.44}$	>758.84			>9.7	>51.0	none
070509	Single PL	t_{lastdet}	$0.99^{+0.15}_{-0.14}$	$0.91^{+0.81}_{-0.73}$	>46.65	···	···	$>3.0\xi$	···	
		t_{start}	$0.99^{+0.15}_{-0.14}$	$0.91^{+0.81}_{-0.73}$	<0.08	···	···	$<0.3\xi$	···	
070517	II–III	t_b	$1.18^{+0.18}_{-0.16}$	$1.11^{+0.48}_{-0.28}$	$2.9^{+2.4}_{-1.0}$	···	···	1.0ξ	···	
		t_{lastdet}	$1.18^{+0.18}_{-0.16}$	$1.11^{+0.48}_{-0.28}$	>389.19	···	···	$>6.6\xi$	···	
		t_{start}	$-0.02^{+0.30}_{-0.43}$	$0.96^{+0.63}_{-0.36}$	<0.11	···	···	$<0.3\xi$	···	
070518	I–II–III	t_b	$1.11^{+1.63}_{-0.29}$	$1.48^{+0.82}_{-0.49}$	$75.9^{+292.1}_{-49.4}$	···	···	3.6ξ	···	
		t_{lastdet}	$1.11^{+1.63}_{-0.29}$	$1.48^{+0.82}_{-0.49}$	>1672.71	···	···	$>11.4\xi$	···	
070520A	I–II–III	t_b	$0.94^{+0.49}_{-0.27}$	$1.27^{+1.13}_{-0.63}$	$16.3^{+50.0}_{-10.6}$	···	···	2.0ξ	···	
		t_{lastdet}	$0.94^{+0.49}_{-0.27}$	$1.27^{+1.13}_{-0.63}$	>293.19	···	···	$>5.9\xi$	···	
070529	I–II–III	t_b	$1.31^{+0.12}_{-0.10}$	$1.13^{+0.39}_{-0.31}$	$2.4^{+2.8}_{-1.2}$	2.50[v]	52.9	0.9	48.9	
		t_{lastdet}	$1.31^{+0.12}_{-0.10}$	$1.13^{+0.39}_{-0.31}$	>561.33			>6.8	>50.7	
070531	Single PL	t_{lastdet}	$1.33^{+0.26}_{-0.23}$	$0.06^{+0.68}_{-0.44}$	>0.98	···	···	$>0.7\xi$	···	
		t_{start}	$1.33^{+0.26}_{-0.23}$	$0.06^{+0.68}_{-0.44}$	<0.14	···	···	$<0.3\xi$	···	
070612B	Single PL	t_{lastdet}	$1.76^{+1.37}_{-0.40}$	$0.74^{+1.09}_{-0.77}$	>408.97	···	···	$>6.7\xi$	···	
		t_{start}	$1.76^{+1.37}_{-0.40}$	$0.74^{+1.09}_{-0.77}$	<3.36	···	···	$<1.1\xi$	···	
070628	I–II–III	t_b	$1.17^{+0.07}_{-0.07}$	$1.21^{+0.16}_{-0.15}$	$6.2^{+0.6}_{-1.0}$	···	···	1.4ξ	···	
		t_{lastdet}	$1.17^{+0.07}_{-0.07}$	$1.21^{+0.16}_{-0.15}$	>83.14	···	···	$>3.7\xi$	···	

Table 5
(Continued)

GRB	Segments	Time	α	β	t (ks)	z	log $E_{\gamma,\mathrm{iso}}$ (erg)	θ_j (deg)	log E_γ (erg)	Requirements[†]
070714A	Single PL	t_{lastdet}	$0.80^{+0.14}_{-0.10}$	$1.34^{+0.72}_{-0.62}$	>175.18	...	...	>4.9ξ	...	
		t_{start}	$0.80^{+0.14}_{-0.10}$	$1.34^{+0.72}_{-0.62}$	<0.08	...	...	<0.3ξ	...	
070724B	Single PL	t_{lastdet}	$1.18^{+0.29}_{-0.25}$	$1.09^{+1.06}_{-0.78}$	>718.59	...	...	>8.3ξ	...	
		t_{start}	$1.18^{+0.29}_{-0.25}$	$1.09^{+1.06}_{-0.78}$	<68.95	...	...	<3.4ξ	...	
070802	I–II–III	t_b	$1.07^{+0.16}_{-0.13}$	$1.12^{+0.68}_{-0.49}$	$4.9^{+3.6}_{-3.6}$	2.45[w]	50.7	2.1	47.6	
		t_{lastdet}	$1.07^{+0.16}_{-0.13}$	$1.12^{+0.68}_{-0.49}$	>341.41			>10.4	>49.0	
070809	I–II–III	t_b	$1.16^{+0.98}_{-0.51}$	$0.28^{+0.77}_{-0.51}$	$8.7^{+4.7}_{-6.6}$	...	...	1.6ξ	...	
		t_{lastdet}	$1.16^{+0.98}_{-0.51}$	$0.28^{+0.77}_{-0.51}$	>71.37	...	...	>3.5ξ	...	
071010B	Single PL	t_{lastdet}	$0.64^{+0.09}_{-0.09}$	$1.08^{+0.29}_{-0.26}$	>156.13	0.95[x]	51.2	>8.4	>49.3	
		t_{start}	$0.64^{+0.09}_{-0.09}$	$1.08^{+0.29}_{-0.26}$	<6.24			<2.5	<48.2	
071020	II–III	t_b	$1.14^{+0.03}_{-0.02}$	$0.73^{+0.09}_{-0.09}$	$0.2^{+0.1}_{-0.0}$	2.15[y]	52.4	0.4	47.7	
		t_{lastdet}	$1.14^{+0.03}_{-0.02}$	$0.73^{+0.09}_{-0.09}$	>1480.55			>11.7	>50.7	
071021	I–II–III	t_b	$1.21^{+0.44}_{-0.24}$	$0.95^{+0.38}_{-0.36}$	$34.0^{+38.7}_{-19.2}$	...	...	2.6ξ	...	
		t_{lastdet}	$1.21^{+0.44}_{-0.24}$	$0.95^{+0.38}_{-0.36}$	>994.91	...	...	>9.4ξ	...	
071112C	Single PL	t_{lastdet}	$1.36^{+0.03}_{-0.03}$	$0.73^{+0.07}_{-0.06}$	>578.37	0.82[z]	...	>9.6	...	
		t_{start}	$1.36^{+0.03}_{-0.03}$	$0.73^{+0.07}_{-0.06}$	<0.09			<0.4	...	
071117	Single PL	t_{lastdet}	$0.86^{+0.12}_{-0.11}$	$1.15^{+0.29}_{-0.26}$	>62.82	1.33[aa]	52.1	>4.4	>49.5	
		t_{start}	$0.86^{+0.12}_{-0.11}$	$1.15^{+0.29}_{-0.26}$	<2.88			<1.4	<48.5	
071122	Single PL	t_{lastdet}	$2.51^{+0.14}_{-0.13}$	$0.87^{+0.17}_{-0.12}$	>1.51	1.14[ab]	50.1	>2.0	>46.9	ν_1 p_2
		t_{start}	$2.51^{+0.14}_{-0.13}$	$0.87^{+0.17}_{-0.12}$	<0.15			<0.8	<46.1	ν_1 p_2

[†]Abbreviations for Uniform jet (Uni), Spreading jet (Sp), Nonspreading jet (NSp), $1 < p < 2$ (p_{12}), $p > 2$ (p_2), $\nu < \nu_c$ (ν_1), $\nu > \nu_c$ (ν_2).

Notes. Unlikely jet breaks are consistent with both pre- and post-jet break closure relations in their last light curve segment, and their temporal decays and decay transitions either resemble segments II–III of the Prominent sample or are fit by single power laws. The Unlikely jet break sample also contains six afterglows that are not consistent with any closure relations after internal consistency checks but have temporal behavior consistent with post-jet break decays, and are denoted with the requirements of "none." t_{start} and t_{lastdet} times and opening angle limits are only listed if they are feasible within the canonical framework. Other notes are the same as for Prominent Jet Breaks table.

References. [a]Pellizza et al. 2006; [b]Watson et al. 2006; [c]Prochaska et al. 2006b; [d]Chen et al. 2005; [e]Sollerman et al. 2007; [f]Perley et al. 2006; [g]Fynbo et al. 2006b; [h]Berger et al. 2006a; [i]Cucchiara et al. 2006b; [j]Fynbo et al. 2006c; [k]Bloom et al. 2006b; [l]Cenko et al. 2006; [m]Castro-Tirado et al. 2006; [n]Ledoux et al. 2006; [o]Jakobsson et al. 2006a; [p]Fugazza et al. 2006; [q]Thöne et al. 2006a; [r]Fynbo et al. 2006a; [s]Bloom et al. 2006a; [t]Thöne et al. 2007b; [u]Jakobsson et al. 2007a; [v]Berger et al. 2007a; [w]Elíasdóttir et al. 2008; [x]Cenko et al. 2007a; [y]Jakobsson et al. 2007e; [z]Jakobsson et al. 2007c; [aa]Jakobsson et al. 2007b; [ab]Cucchiara et al. 2007a.

We then calculate Ψ, as $\Psi = \alpha_{\mathrm{obs}} - f(\beta_{\mathrm{obs}}, q_{\mathrm{obs}})$. Consequently, when $q_{\mathrm{obs}} < 1$, by the criteria set in Equation (7), $\Psi = 0$.

3.1. Segment I

The steep decline of segment I in the canonical X-ray light curve is probably due to the tail end of the prompt emission and is governed by the curvature effect, for which emission from different viewing angles reaches the observer with different delays due to light propagation effects (Kumar & Panaitescu 2000; Zhang et al. 2006). The relationship between the temporal and spectral slopes of the high latitude emission is

$$\alpha = 2 + \beta \tag{8}$$

or in our formulation

$$\Psi = \alpha - 2 - \beta \tag{9}$$

and is independent of any of the environmental or other parameters that affect the closure relations for the external shock. Therefore, we only use this relation to help discriminate segment I from other segments and we do not use this relation to constrain any of the burst properties explored throughout the rest of this paper. We find that ~41% of the segment I in our sample are consistent with this relation, with the remainder either steeper (~26%) or shallower (~34%) than this relation.

Zhang et al. (2007a, 2009) explore steep declines in the XRT afterglow data set and discuss several physical explanations, finding that steep decays with and without significant spectral evolution can be explained by the curvature effect. They explore the subset with distinct spectral evolution and no clear and obvious contaminating flaring to conclude that the data are best characterized by an apparent evolution of a cutoff power-law (CPL) spectrum. Those that are contaminated with flaring mix spectral evolution during the flares with possible spectral evolution of the underlying afterglow, leading to difficulty in characterizing the mean spectral and temporal properties. Zhang et al. (2009) can interpret the apparent spectral evolution during the steep decay phase using a curvature effect model that invokes a non-power-law spectrum at the end of the prompt emission phase. Those afterglows with α steeper than $2 + \beta$ could also be caused by only seeing the tail of a flare and interpreting it as the steep decay. This is further complicated by the choice of t_0 for determining the slope of the temporal decay that affects segment I much more strongly than the other segments (Zhang et al. 2006; Liang et al. 2006). Zhang et al. (2007a) fit t_0 in their

Table 6
Nonjet Breaks

GRB	Segments	Time	α	β	t (ks)	z	log $E_{\gamma,\rm iso}$ (erg)	θ_j (deg)	log E_γ (erg)	Requirements[†]
050126	I–II	$t_{\rm lastdet}$	$0.93^{+0.23}_{-0.43}$	$0.85^{+0.74}_{-0.52}$	>70.49	1.29[a]	51.9	>0.7	>47.8	
050406	I–II	$t_{\rm lastdet}$	$0.61^{+0.24}_{-0.25}$	$1.32^{+0.83}_{-0.52}$	>1000.88	2.44[b]	51.2	>1.3	>47.6	
050421	II–III	$t_{\rm lastdet}$	$3.42^{+0.28}_{-0.25}$	$0.63^{+0.58}_{-0.47}$	>1.34	···	···	>0.3ξ	···	none
050422	I–II	$t_{\rm lastdet}$	$0.83^{+0.24}_{-0.39}$	$2.03^{+5.26}_{-1.51}$	>1324.00	···	···	>0.5ξ	···	
050721	I–II	$t_{\rm lastdet}$	$1.17^{+0.09}_{-0.23}$	$1.04^{+0.23}_{-0.31}$	>3385.42	···	···	>0.6ξ	···	
050819	I–II	$t_{\rm lastdet}$	$0.40^{+0.19}_{-0.16}$	$1.46^{+0.82}_{-0.59}$	>410.41	···	···	>0.6ξ	···	
050904	Single PL	$t_{\rm lastdet}$	$2.07^{+0.11}_{-0.09}$	$0.19^{+0.06}_{-0.06}$	>313.51	6.30[c]	53.7	>3.3	>50.9	
050908	I–II	$t_{\rm lastdet}$	$1.08^{+0.11}_{-0.11}$	$1.21^{+0.45}_{-0.43}$	>121.71	3.34[d]	52.2	>0.4	>47.6	
050916	I–II	$t_{\rm lastdet}$	$0.67^{+0.13}_{-0.29}$	$0.70^{+0.93}_{-0.50}$	>35.90	···	···	>0.5ξ	···	
051001	I–II	$t_{\rm lastdet}$	$1.03^{+0.07}_{-0.10}$	$0.86^{+0.13}_{-0.13}$	>550.41	···	···	>0.7ξ	···	
051021B	I–II	$t_{\rm lastdet}$	$0.57^{+0.65}_{-0.79}$	$0.73^{+7.88}_{-1.27}$	>58.24	···	···	>1.1ξ	···	
051117B	I–II	$t_{\rm lastdet}$	$0.95^{+0.20}_{-0.30}$	$0.77^{+1.35}_{-0.93}$	>174.16	···	···	>0.7ξ	···	
051210	II–III	$t_{\rm lastdet}$	$3.55^{+1.63}_{-0.79}$	$0.92^{+1.22}_{-0.57}$	>0.94	···	···	>0.4ξ	···	Sp ν_1 p_2
060116	I–II	$t_{\rm lastdet}$	$1.03^{+0.06}_{-0.06}$	$0.41^{+0.33}_{-0.25}$	>745.56	···	···	>0.4ξ	···	
060202	I–II	$t_{\rm lastdet}$	$0.86^{+0.05}_{-0.04}$	$2.21^{+0.23}_{-0.21}$	>2735.50	···	···	>0.8ξ	···	
060211A	I–II	$t_{\rm lastdet}$	$0.51^{+0.10}_{-0.10}$	$1.47^{+0.65}_{-0.42}$	>793.72	···	···	>0.8ξ	···	
060211B	I–II	$t_{\rm lastdet}$	$0.54^{+0.24}_{-0.20}$	$0.75^{+0.47}_{-0.45}$	>186.62	···	···	>0.7ξ	···	
060403	I–II	$t_{\rm lastdet}$	$1.03^{+0.24}_{-0.35}$	$0.89^{+1.16}_{-0.61}$	>208.40	···	···	>0.9ξ	···	
060427	I–II	$t_{\rm lastdet}$	$1.19^{+0.10}_{-0.09}$	$1.33^{+0.41}_{-0.35}$	>97.86	···	···	>0.5ξ	···	
060428B	I–II	$t_{\rm lastdet}$	$0.95^{+0.07}_{-0.06}$	$0.81^{+0.44}_{-0.27}$	>901.80	···	···	>0.6ξ	···	
060510B	I–II	$t_{\rm lastdet}$	$0.90^{+0.16}_{-0.12}$	$1.32^{+0.64}_{-0.41}$	>728.31	4.94[e]	53.4	>0.5	>49.0	
060801	II–III	$t_{\rm lastdet}$	$3.74^{+1.68}_{-0.53}$	$1.18^{+1.01}_{-0.60}$	>1.33	···	···	>0.4ξ	···	ν_1 p_2
061002	I–II	$t_{\rm lastdet}$	$0.95^{+0.17}_{-0.28}$	$1.42^{+0.37}_{-0.36}$	>45.69	···	···	>0.5ξ	···	
061006	I–II	$t_{\rm lastdet}$	$0.73^{+0.10}_{-0.11}$	$1.00^{+0.59}_{-0.38}$	>105.22	···	···	>0.5ξ	···	
061102	I–II	$t_{\rm lastdet}$	$0.47^{+0.32}_{-0.32}$	$-0.91^{+9.91}_{-0.09}$	>130.84	···	···	>0.6ξ	···	
061222B	I–II	$t_{\rm lastdet}$	$1.28^{+0.14}_{-0.11}$	$0.73^{+0.67}_{-0.36}$	>416.55	3.36[f]	52.9	>0.4	>48.3	
070110	I–II	$t_{\rm lastdet}$	$0.82^{+0.13}_{-0.08}$	$1.13^{+0.28}_{-0.18}$	>2179.74	2.35[g]	52.5	>0.6	>48.3	
070223	I–II	$t_{\rm lastdet}$	$0.95^{+0.11}_{-0.13}$	$0.90^{+1.20}_{-0.73}$	>826.56	···	···	>1.2ξ	···	
070419A	I–II	$t_{\rm lastdet}$	$0.67^{+0.50}_{-0.41}$	$2.83^{+6.17}_{-3.83}$	>798.80	0.97[h]	···	>1.2	···	
070520B	I–II	$t_{\rm lastdet}$	$1.13^{+0.52}_{-0.66}$	$1.09^{+1.07}_{-0.88}$	>12.00	···	···	>0.8ξ	···	
070621	I–II	$t_{\rm lastdet}$	$0.99^{+0.05}_{-0.04}$	$1.70^{+0.39}_{-0.34}$	>856.13	···	···	>0.5ξ	···	
070704	I–II	$t_{\rm lastdet}$	$0.98^{+0.13}_{-0.14}$	$0.66^{+0.36}_{-0.23}$	>294.69	···	···	>0.5ξ	···	
070721A	I–II	$t_{\rm lastdet}$	$0.75^{+0.07}_{-0.07}$	$1.65^{+0.63}_{-0.48}$	>654.69	···	···	>0.4ξ	···	
070724A	I–II	$t_{\rm lastdet}$	$0.84^{+0.10}_{-0.22}$	$0.67^{+0.50}_{-0.26}$	>86.67	0.46[i]	49.3	>1.8	>46.0	
070808	I–II	$t_{\rm lastdet}$	$0.95^{+0.12}_{-0.10}$	$1.40^{+0.66}_{-0.71}$	>179.99	···	···	>0.4ξ	···	
071001	I–II	$t_{\rm lastdet}$	$0.53^{+0.15}_{-0.19}$	$1.23^{+0.98}_{-0.40}$	>4.78	···	···	>0.4ξ	···	
071227	I–II	$t_{\rm lastdet}$	$1.14^{+0.17}_{-0.17}$	$1.74^{+0.60}_{-0.27}$	>145.34	0.38[j]	49.8	>1.5	>46.3	

[†] Abbreviations for Uniform jet (Uni), Spreading jet (Sp), Nonspreading jet (NSp), $1 < p < 2$ (p_{12}), $p > 2$ (p_2), $\nu < \nu_c$ (ν_1), $\nu > \nu_c$ (ν_2).

Notes. Nonjet breaks are the remaining GRBs not in the other categories that are with inconsistent with previous criteria, only contain segments I–II, are naked GRBs (0–I), or were ruled out by internal consistency checks. $t_{\rm lastdet}$ times and opening angle limits are only listed if they are feasible within the canonical framework. Other notes are the same as for Prominent Jet Breaks table.

References. [a]Berger et al. 2005a; [b]Schady et al. 2006; [c]Kawai et al. 2006; [d]Fugazza et al. 2005; [e]Price et al. 2007; [f]Berger 2006; [g]Jaunsen et al. 2007b; [h]Cenko et al. 2007b; [i]Cucchiara et al. 2007b; [j]D'Avanzo et al. 2009.

multicomponent spectral evolution models to best characterize the temporal decay, rather than using the BAT trigger time. This method could help explain some of the deviations. However, these efforts are beyond the scope of this study and have little consequence for the analysis of segments II–IV and the study of jet breaks, so are not repeated here.

3.2. Segments II–III

The closure relations governing external shocks depend on the local environment, range of electron spectral index, cooling regime, energy injection, peak frequency and cooling frequency. The pre-jet break "isotropic" relations and the post-jet break

relations are given in Table 1. The framework for the closure relations for the slow and fast cooling cases is explored by Sari et al. (1998) and expanded upon for the collimated case by Sari et al. (1999). Dai & Cheng (2001) include the $1 < p < 2$ cases, with additional cases given in Zhang & Mészáros (2004). The addition of the energy injection mechanism to explain the plateau portion of X-ray light curves brought additional parallel closure relation sets for $p > 2$ given in Zhang et al. (2006). We extract the additional jet break relations from information provided in Panaitescu (2005) and Panaitescu et al. (2006). We choose not to include the cases of energy injection for $1 < p < 2$ because this scenario is unduly complicated, unlikely, and often not analytically solvable.

In segments II–III, the relationship between the electron slope (p) and the measured X-ray spectral slope (Γ) is derived in (Sari et al. 1998) as

$$\Gamma - 1 \equiv \beta = \begin{cases} 1/2 & \nu_c < \nu < \nu_m \\ (p-1)/2 & \nu_m < \nu < \nu_c \\ p/2 & \nu_m, \nu_c < \nu, \end{cases} \quad (10)$$

where ν_m and ν_c are the synchrotron and cooling frequencies, respectively.

3.3. Segment IV

Other large-scale studies (Liang et al. 2008; Panaitescu 2007; Evans et al. 2008) of jet break closure relations address only the simplest cases of the uniform jet (Zhang & Mészáros 2004). We also include the nonspreading uniform jet with energy injection, the laterally spreading uniform jet with and without energy injection and the simplest form of structured jets with power-law angular distribution of energy outflow from Panaitescu et al. (2006). We apply all of these cases for both ISM and wind environments. We choose not to apply any of the $1 < p < 2$ closure relations that include energy injection and occur post-jet break, as well as anything more complex than the most simple $p > 2$ structured jet relations due to their complexity and impracticability. Closure relations for all jet models are listed in Table 1. All of these relations are for on-beam geometry. In particular, the power-law structured jet model requires that the line of sight is within the central cone beam.

The power-law structured jet relations are valid for a particular α and β provided the index, k, of the angular energy distribution is less than $\tilde{k}$, where

$$\tilde{k} = \begin{cases} \dfrac{8}{2\beta+5} \text{ (ISM } \nu < \nu_c) \\ \dfrac{8}{2\beta+3} \text{ (ISM } \nu > \nu_c) \\ \dfrac{8}{2\beta+4} \text{ (Wind).} \end{cases} \quad (11)$$

The case of $k > \tilde{k}$ reduces to the nonspreading uniform jet relations because the core is dominant (Panaitescu 2005).

3.4. Internal Consistency Checks

The models in Table 1 can be used in succession throughout an individual X-ray afterglow light curve, however several models often fit equally well for any given light curve segment. After fitting each closure relation to each set of α and β, we combine them to form a coherent physical model for each afterglow. While we often cannot distinguish a unique set of closure relations, we can use information from one segment to exclude inconsistent relations from other segments. We assume there is no perceptible change in the circum-GRB environment probed throughout an individual afterglow, and therefore if either an ISM or Wind environment can be excluded in any segment, we exclude it for the other segments. We do not allow transitions from slow cooling to fast cooling within any light curve. Since we do not see evidence of a change of spectral index between segments in most individual afterglows, we require the spectral regime to remain constant throughout a light curve (i.e., either $\nu < \nu_c$ or $\nu > \nu_c$ for slow cooling, or $\nu_c < \nu < \nu_m$ or $\nu > \nu_m$ for fast cooling), therefore excluding light curve breaks due to transitions of the cooling frequency through the X-ray band. Theoretically, we do not expect the electron spectral index, p, to change during an afterglow light curve. However, because we do not include the full suite of $1 < p < 2$ relations with energy injection, we are careful not to exclude a $1 < p < 2$ model just because only $p > 2$ models are available to fit other segments. We eliminate models only on the the basis of their p values being inconsistent between segments, which is especially important for those segments with $p \sim 2$ and large error bars. We require a segment consistent with a particular isotropic model to also be consistent with a corresponding jet model in the following segment, and conversely a jet model must be consistent with a corresponding previous isotropic model in terms of environment and spectral frequency regime. Similarly, any energy injection model in segment II must be consistent with the models for the following segment (if present) in terms of environment and frequency regime. When a post-jet break relation with energy injection is applied, we require q to be consistent between pre- and post-jet break segments. We also only allow jet breaks to directly precede potential segments III or IV. Ambiguous single power laws have no restrictions on available sets of closure relations.

Using these criteria, we eliminate some models to better constrain a coherent picture for each afterglow. Unfortunately, a unique set of models is often still unattainable, as several equally likely relations remain. In an attempt to extract any available information from the remaining closure relations, we look at constraints from families of closure relations to determine specific properties. For example, if several closure relations are consistent with a particular segment or whole afterglow but they are all ISM relations, then we can conclude that this afterglow is consistent with the expectations of an ISM environment. This also works for families of relations with a common spectral frequency regime, environment, and pre/post-jet break regime.

3.5. Classification

Our sample is broken up into four groups (as described in Section 2.1.2) based on their temporal properties. These groups include the I–II–III–IV/II–III–IV sample which have distinct segment IV, segments I–II–III, ambiguous segments II–III/III–IV, and single power laws. The latter three samples may contain jet breaks and still fit within the canonical light curve picture. The presence of observing biases can explain the missing contextual clues that would make jet break distinctions more clear. In order to avoid imposing biases on the results, we have not attempted to distinguish jet breaks based on a priori assumptions for decay indices or break times.

The fact that segments II–III/III–IV light curves do not look like the canonical light curve is likely a result of two different observing biases: a late start or early end. The behavior prior to segment II was either not observed at all due to a late

observation start, or was complicated by flaring behavior making the underlying afterglow shape unclear, both leading to an unknown initial steep decline. If the observations began even later, segment I and II would be missed, leaving only segments III–IV. Similarly, an early observation end would also lead to the observer missing the jet break. This end could be due to either a manual end of the observations because of observing constraints, or the afterglow becoming too faint for XRT detection. These two-segment ambiguous light curves may contain jet breaks as either the observed break, or with the inclusion of energy injection, the jet break would have occurred sometime prior to the start of the first segment. In this latter case, the actual jet break time is impossible to determine because there were no observations prior to the start of the apparent segment II. Considering the wide range of decay indices, observing times, and redshifts, these limitations are likely to have influenced the data.

Apparent segments I–II–III show some suggestions of deviation from the canonical form, which can also be explained by observing biases. In some cases, the temporal decay of these segments III is substantially steeper than typical segments III, as if they transitioned directly from segment II to segment IV. Alternatively, it is possible that the segment III is simply missing or buried in the data due to a short duration, large error bars, or gaps in the light curve with segment IV appearing to follow directly after segment II. Willingale et al. (2007) proposed an empirical form of the canonical light curve that is made up of two falling exponential plus power-law functions that can explain the structure of most X-ray afterglow light curves. They suggest that missing phases, like that seen in the apparent II–IV transitions, are a result of one of the two components being particularly bright, weak, or short lived.

Other types of light curves exist in the sample for which we do not observe jet breaks, and would not expect them to be hidden or ambiguous. These include light curves showing only segments I–II, where the later segments presumably occurred after observations ended. Another type and possible jet break sample contaminant is the so-called "naked bursts" which show only the initial steep decline from the prompt emission without the subsequent segments (II–IV) attributed to the afterglow. This is thought to occur because the surrounding medium is not dense enough to produce the external shocks that power GRB afterglows (Kumar & Panaitescu 2000). These GRBs can appear as either single power-law decays or broken power laws where the prompt emission and high latitude emission masquerade as segment II–III light curves in the absence of comparison to the γ-ray prompt emission. Three examples of possible naked GRBs that have been investigated extensively are the long GRBs 050421 (Godet et al. 2006) and 050412 (Mineo et al. 2007), and the short hard burst GRB 051210 (La Parola et al. 2006). To filter out these bursts we search for any light curves that appear to be segments II–III, have break times < 1000 s, and are consistent with the high latitude closure relation (Equation (8)); these should not be considered candidates for jet breaks. Using these criteria, we identify GRB 060801 as another possible naked burst in addition those identified in the literature that is also a short hard GRB. There may be more naked bursts in the single power-law sample like that of GRB 050412, but we have no clean way of distinguishing them, therefore we leave them for later discrimination. It is possible that additional naked bursts are present in the 29 GRBs excluded from the final sample due to their faintness and limited observations which made temporal and spectral analysis not possible.

In order to learn more about these ambiguous afterglows and distinguish jet breaks, we apply the closure relations. The following section describes how we use the closure relations and the temporal behavior to identify additional jet break candidates.

4. JET BREAKS

Using the above criteria and consistency checks, we define sub-samples of X-ray afterglows that potentially contain jet breaks. Large errors on α and β sometimes make definitive determination of afterglow properties via closure relations unfeasible. The cases where many (pre- and post-jet break) closure relations are consistent are evaluated using additional criteria and classified into categories based on their likelihood of containing real jet breaks. These additional criteria are based upon their resemblance to those afterglows with clear canonical jet breaks. We distinguish between those afterglows which are consistent with *only* post-jet break closure relations, those that are *only* consistent with pre-jet break closure relations, and those that are consistent with both. We divide our sample of potential jet breaks into 4 categories. The categories are the Prominent jet breaks, Hidden jet breaks, Possible jet breaks, and Unlikely jet breaks. The details of their categorical definitions follow.

4.1. Prominent Jet Break Class

We define the Prominent jet break class as those light curves for which we can clearly distinguish a break between segments III and IV, with segment IV being consistent with post-jet break closure relations, consistent with the canonical morphology (Figure 3). This conservative classification criterion requires that the light curve is composed of either segments I–II–III–IV or II–III–IV, and the final segment is consistent with post-jet break closure relations. We find 30 such afterglows, 28 of which are consistent within 2σ of at least one post-jet break closure relation in their segment IV after internal consistency checks.

In the two inconsistent cases (GRBs 061121 and 070508), all models were eliminated in the process of internal consistency checks with the 2σ criteria. The unusually bright GRB 061121 (Page et al. 2007) was triggered by a precursor, causing the choice of T_0 to affect the slopes, which may account for some of the deviations from the models. Page et al. (2007) also suggest the presence of a Comptonized component. Therefore, these outlier cases may not be well represented by the canonical form, have breaks due to other mechanisms such as the cooling frequency moving through the X-ray band, or are not valid with the suite of closure relations used here, and are ignored in the following analysis.

Based on the canonical light curve form, we assume that segment IV is post-jet break. Therefore, the post-jet break closure relations are the only models allowed in segment IV. In contrast, many closure relations are allowed by the canonical form for segments II and III. Figure 4 shows an example of a burst in the Prominent jet break category with its light curve and the closure relations that are consistent with the data. All four segments of this burst can be adequately characterized by the closure relations: segment I is consistent with the high latitude relation; segment II requires $p > 2$ and energy injection, but is consistent with either slow or fast cooling and either ISM or wind environment; segment III is consistent with either isotropic or jet-with-energy-injection relations; and segment IV is consistent with either a spreading or nonspreading jet with an ISM or wind environment. The resulting fits imply that the jet break time cannot be unambiguously established; if the II–III break is due to the

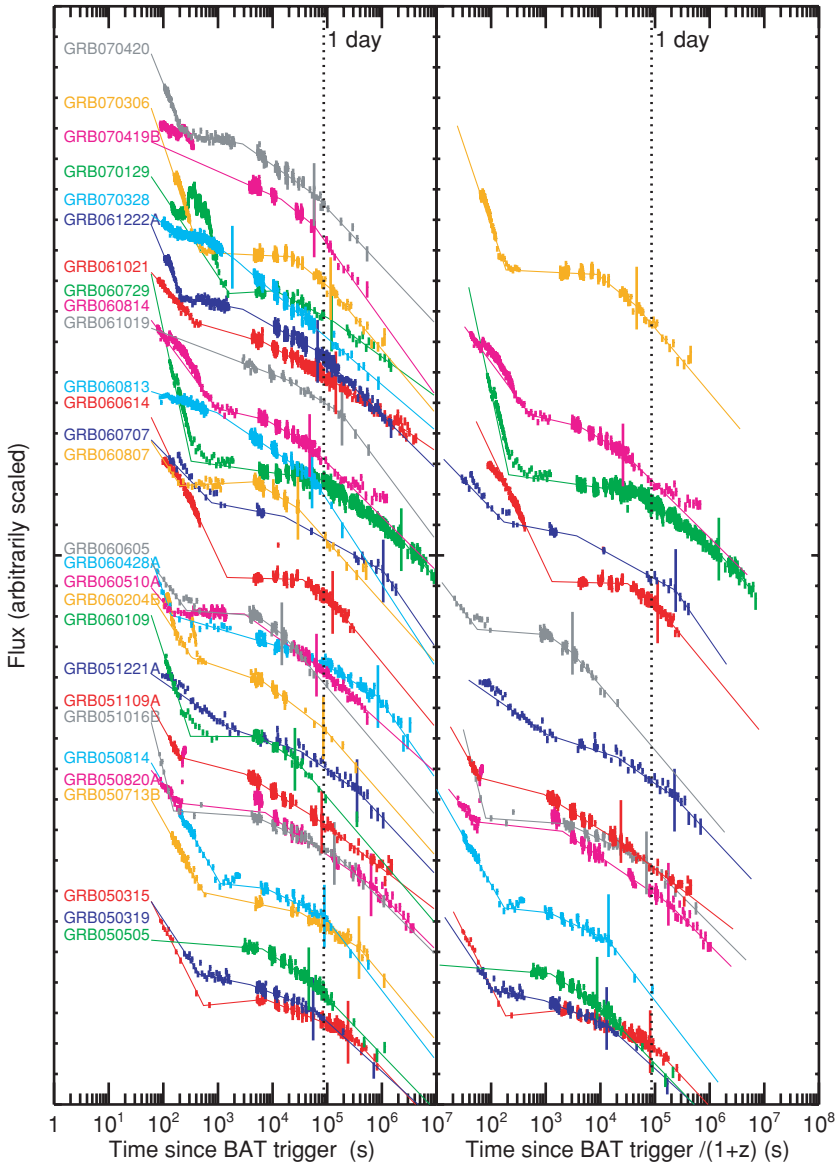

Figure 3. Arbitrarily scaled light curves and temporal fits for all Prominent jet breaks in the observed frame (left) and rest frame (right, where available). The final light curve break is indicated by the vertical line in the same color as the light curve and fit.

cessation of energy injection then the III–IV break is a jet break, but it is also possible that the II–III break is the jet break and the III–IV break is due to the end of energy injection (see also Ferrero et al. 2008 for a similar analysis of this GRB). We list the properties of the Prominent jet break bursts in Table 2. The distributions of these properties will be discussed in Section 4.4.

We wish to assess the deficit of jet breaks in the XRT afterglow sample, therefore we must make a reasonable estimate of the fraction of our sample with jet breaks, accounting for a variety of observing biases. Due to various observing constraints and light curve profiles, not all burst observations began with an immediate slew nor were they all observed out to a time at which the jet break is expected to have occurred. Therefore, to calculate an accurate jet break fraction, we reduce our sample to only those GRBs for which the observations span a time frame where we would expect a jet break. Previous studies of optical jet breaks (Frail et al. 2001; Bloom et al. 2003; Zeh et al. 2006) showed them to occur several days after the GRB trigger. Instead of making a priori assumptions about achromaticity or assuming similar behavior, we determine the time frame during which we would expect a jet break by studying the Prominent jet break sample.

The Prominent jet break sample consists of 28 X-ray afterglows with $t_{\rm start}$ ranging from a few minutes for those light curves that start with segment I to an hour for those that start during segment II, and $t_{\rm stop}$ ranging between 2 days and five months (excluding late-time *Chandra* observations). The important measurement from the Prominent sample is the jet break time (t_b) which ranges between 0.02 and 26.2 days (excluding earlier breaks that suggest post-jet-breaks-with-energy-injection). Excluding the extremely late jet break case of GRB 060729, and the extremely early jet break case of GRB070328, the latest light curve break in the whole sample is ∼12 days, with 90% occurring within 10 days. Therefore, we define our "complete" sample (those GRBs for which observations sufficiently cover a time range where a jet break could have been measured), to begin before 0.1 days and end after 10 days. Of the 230 GRBs in our sample, 82 fit these completeness criteria. The distributions of observation start, stop, break, last detection, and the jet break lower limit (described in Section 5) are shown in Figure 5.

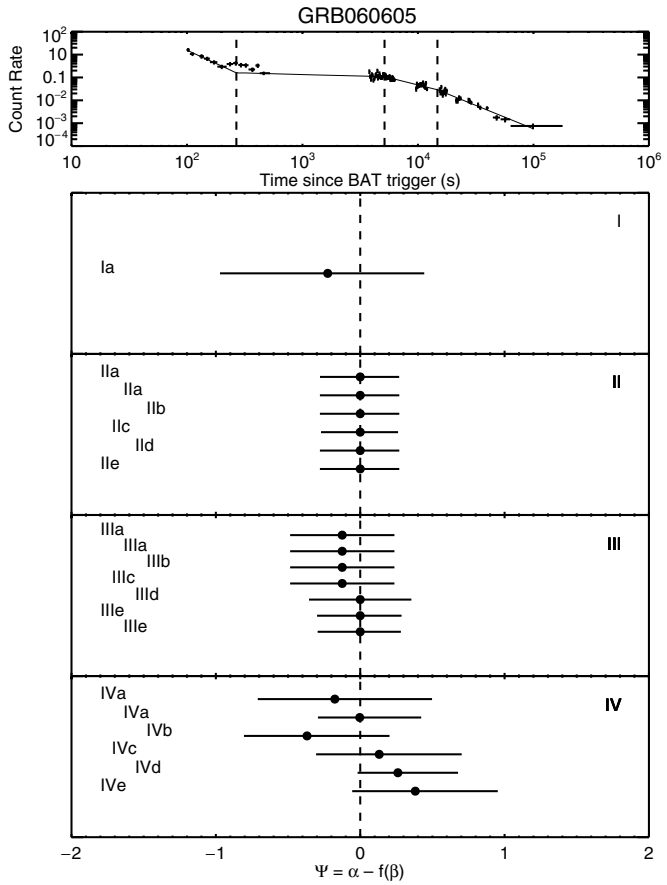

Figure 4. Top panel shows the light curve in (0.3–10.0 keV counts s^{-1}) and fits for GRB 060605, an example of a Prominent Jet Break. The four lower panels show the fits to the closure relations for the cases that are consistent with the data at the 2σ confidence level. An x-axis value consistent with $\Psi = 0$ (dashed line) is valid. The relations that involve energy injection require the q parameter to be consistent with $q < 1$, which is evaluated by the Ψ parameter (Equation (6)). Ia—*HighLat*; IIa—*ISMs2ai* ($p = 3.20^{+0.44}_{-0.43}, q = 0.02^{+0.17}_{-0.18}$); IIb—*ISMs3ai* ($p = 2.20^{+0.44}_{-0.43}, q = 0.03^{+0.26}_{-0.27}$); IIc—*WINDs3ai* ($p = 2.20^{+0.44}_{-0.43}, q = 0.03^{+0.26}_{-0.27}$); IId—*ISMf2ai* ($q = 0.07^{+0.58}_{-0.60}$); IIe—*ISMf3ai* ($p = 2.20^{+0.44}_{-0.43}, q = 0.03^{+0.26}_{-0.27}$); IIf—*WINDf3ai* ($p = 2.20^{+0.44}_{-0.43}, q = 0.03^{+0.26}_{-0.27}$); IIIa—*ISMs3a* ($p = 2.51^{+0.36}_{-0.33}$); IIIb—*WINDs3a* ($p = 2.51^{+0.36}_{-0.33}$); IIIc—*ISMf3a* ($p = 2.51^{+0.36}_{-0.33}$); IIId—*WINDf3a* ($p = 2.51^{+0.36}_{-0.33}$); IIIe—*JETs3ai* ($p = 2.51^{+0.36}_{-0.33}, q = 0.17^{+0.24}_{-0.24}$); IIIf—*JETsISM2ai* ($p = 3.51^{+0.36}_{-0.33}, q = 0.27^{+0.17}_{-0.17}$); IIIg—*JETsISM3ai* ($p = 2.51^{+0.36}_{-0.33}, q = 0.36^{+0.23}_{-0.24}$); IVa—*JETs3a* ($p = 2.23^{+0.54}_{-0.46}$); IVb—*JETs3b* ($p = 2.23^{+0.54}_{-0.46}$); IVc—*JETsISM2a* ($p = 3.23^{+0.54}_{-0.46}$); IVd—*JETsISM3a* ($p = 2.23^{+0.54}_{-0.46}$); IVe—*JETsISM3b* ($p = 2.23^{+0.54}_{-0.46}$); IVf—*JETsWIND3a* ($p = 2.23^{+0.54}_{-0.46}$).

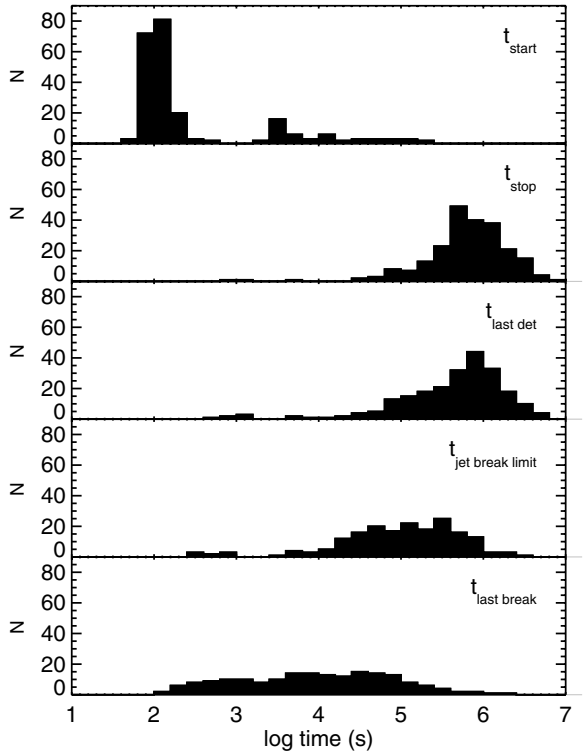

Figure 5. Distributions of observation start times, stop times, time of last detection, jet break lower limit, and time of last measured breaks.

4.2. Hidden Jet Break Class

The Prominent jet break category constitutes only ∼12% of the total sample. We examined the remaining light curves for evidence of "hidden" jet breaks, identified by their closure relations rather than the light curve morphology. Our Hidden jet break category includes those light curves with ambiguous final segments. We consider three ambiguous cases. As noted in Section 2.1.2, broken power laws with $\alpha_2 > \alpha_1$ cannot be distinguished a priori between segments II–III and III–IV. If the final segment is only consistent with post-jet break closure relations, then we designate it as a III–IV case with a Hidden jet break. The second ambiguous case involves three segment light curves initially classified as I–II–III in which the final segment is steeper than typical segment III and consequently only consistent with post-jet break closure relations. Therefore, this type appears more like a I–II–IV or a jet-break-with-energy-injection. The third ambiguous case involves single power-law light curves which are only consistent with post-jet break closure relations even though the jet break itself is not observed.

We find an additional 12 light curves that fit these criteria, of which three are from the two-segment ambiguous sample, nine are segment III from the I–II–III sample, and none are single power laws. Figure 6 shows an example that was classified as an ambiguous II–III/III–IV until we found that its final segment is only consistent with post-jet break closure relations. We list the properties of the Hidden jet breaks in Table 3.

Our classification of XRF 060218 as a Hidden jet break illustrates one limitation of our methodology. Using the closure relations in Table 1, we find a post-jet break decay to be the only possible outcome. In doing so we assume that the emission is due to a purely forward shock origin. Individual studies on XRF/GRB 060218 (Campana et al. 2006; Ghisellini et al. 2007a) show a strong early thermal component related to the associated SN 2006aj and the observed shock break out, followed by a possible Compton component. Our analysis reveals an unusually steep late-time spectral slope, which may suggest that our models are not applicable in this individual case. Therefore, this break may not be due to a jet break at all. We choose to treat all GRBs in our sample in the same way, and our methodology did not account for possible non-power-law spectral components. As a result, a small fraction of the sample could be misclassified. We note that only ∼1% of GRB afterglows show evidence for thermal spectral components.

4.3. Possible and Unlikely Jet Break Classes

We now examine the remaining light curves to search for additional jet breaks in the data set that have not been previously

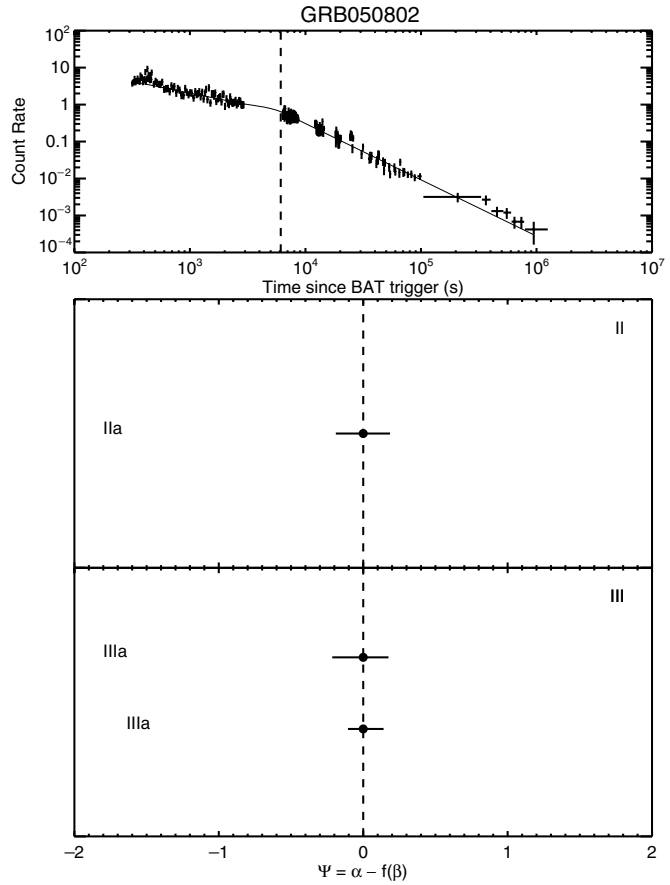

Figure 6. Same as Figure 4, except for GRB 050802, which is an example of the Hidden Jet Break category. IIa—*ISMs2ai* ($p = 2.73^{+0.25}_{-0.24}, q = 0.53^{+0.13}_{-0.13}$); IIIa—*JETs2ai* ($p = 2.71^{+0.14}_{-0.26}, q = 0.38^{+0.09}_{-0.11}$); IIIb—*JETsISM2ai* ($p = 2.71^{+0.14}_{-0.26}, q = 0.70^{+0.10}_{-0.11}$).

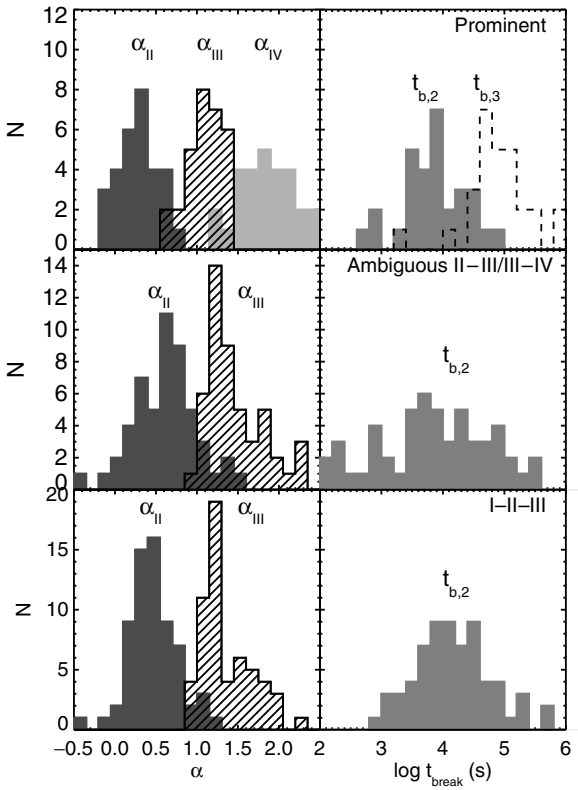

Figure 7. Histograms of temporal decay indices (left) comparing segments II–III of Prominent jet break sample to those of the ambiguous II–III/III–IV sample and the segments I–II–III sample. The distributions of break times (right) between segments II and III ($t_{b,2}$, gray) for all three samples are plotted with the break times between segments III and IV ($t_{b,3}$, dashed line) shown for comparison. These distributions are similar with an excess at larger break times in the ambiguous segments II–III/III–IV and segments I–II–III samples.

identified as Prominent or Hidden. Of the remaining 190 light curves, there are 36 that are consistent with only pre-jet break relations in their last segment, and therefore classified as nonjet breaks. The 3 naked bursts are also classified as nonjet breaks, and 6 light curves that are inconsistent with all closure relations after consistency checks are discussed below. The remaining 145 light curves are ambiguous because they are consistent with both pre- and post-jet break closure relations. This sample includes those ambiguous segments II–III/III–IV, single power laws, and segments I–II–III in which segment III is potentially post-jet break. We use the properties of the Prominent jet break sample to identify possible jet breaks in the ambiguous sample.

The samples of ambiguous segments II–III/III–IV, segments I–II–III, and the Prominent sample have the common feature of apparent segments II–III with a break in between, which is a shared distinct component that can be used to compare them. We use the Prominent jet break sample as a "control group" for comparisons with the other categories. Figure 7 shows the distributions of temporal decay indices and break times for segments II and III for all three groups. The temporal indices split relatively cleanly into several distinct distributions, especially in the Prominent sample. There is a small amount of overlap between segments III and IV in the Prominent jet break sample, but this is not surprising considering the multitude of possible model scenarios employed to explain these light curves. The distributions for the ambiguous segments II–III/III–IV are plotted assuming that they are all segments II–III. The broader and steeper distributions in this sample are consistent with some contamination by actual segments III–IV. The steeper than expected segments II and III from the sample of segments I–II–III are also consistent with the hypothesis of segment III confusion and post-jet-break-with-energy-injection. The break times between segments II and III, as plotted in the right-hand side of Figure 7, are also suggestive of these findings. The distributions are not nearly as narrow as those suggested by the canonical light curve form (Nousek et al. 2006; Zhang et al. 2006), but do suggest a spread to larger break times in the contaminated ambiguous II–III/III–IV sample and the segments I–II–III sample. The break times are also dispersed due to redshift effects whose amplitude is unknown for ∼60% of the GRBs. When looking only at those GRBs with known redshifts, these same distributions are narrower and more cleanly separated.

To further distinguish those potential jet breaks that are in this contaminated ambiguous group, we look at the correlations between the temporal decay slopes from different segments in the same light curves. In the left side of Figure 8 we plot $\alpha_{\rm III}$ versus $\alpha_{\rm II}$, $\alpha_{\rm IV}$ versus $\alpha_{\rm III}$, and $\alpha_{\rm IV}$ versus $\alpha_{\rm II}$ for the Prominent sample as our "control group" and see a reasonably clean distinction between the light curve transitions in this α–α parameter space, which can be used to classify the remaining ambiguous segments. We use the "control group" to determine the area of α–α space for each cluster of specific segment combinations. The mean values for each cluster from the control group are indicated by the black crosses. For each ambiguous

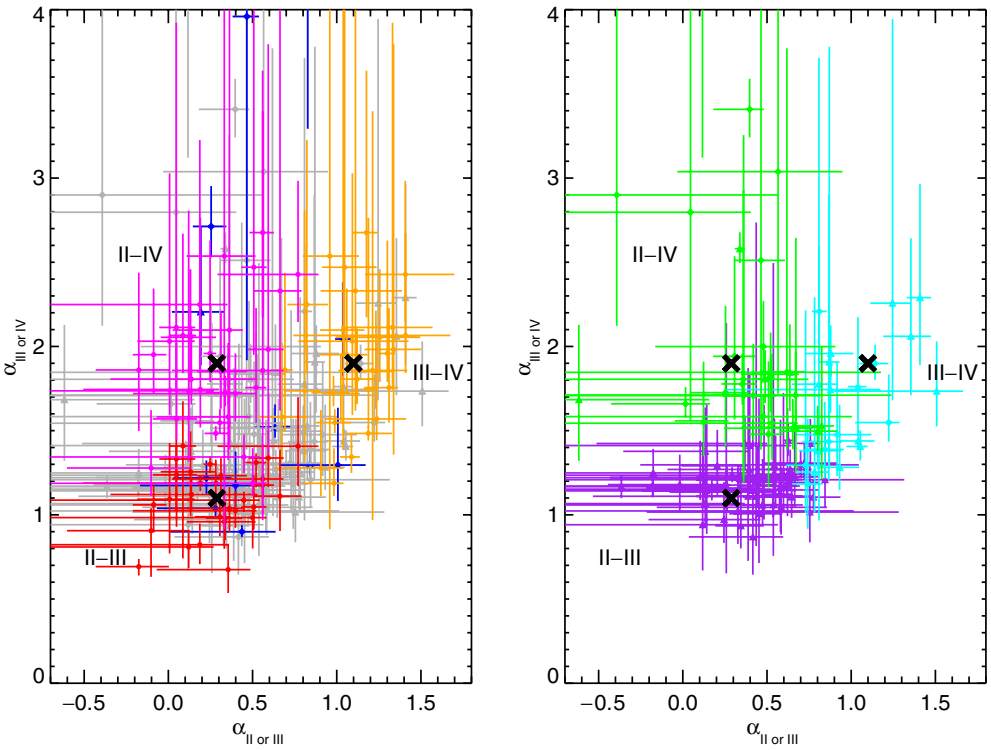

Figure 8. Correlation between temporal decays of Prominent jet break sample (left) segments II, III, and IV showing parameter space of segment transitions II–III (red), III–IV (orange), and II–IV (magenta) used to classify the ambiguous transitions of the Hidden jet break sample (blue) and distinguish the Possible and Unlikely jet break samples (gray). The black crosses mark the means of each potential transition group. The resulting classified transitions (right) are based upon their scaled proximity to the mean from the Prominent jet break sample with the newly classified segments II–III (purple), III–IV (cyan), and II–IV (green). Parameter errors are plotted with 2σ confidence intervals.

light curve, we calculate the distance in α–α space to each cluster mean weighted by σ_α, and categorize the ambiguous segment transitions based upon their proximity to these mean values (right side, Figure 8).

Applying this technique to the 98 light curves with segments II–III/III–IV or segments I–II–III from the remaining 145 ambiguous light curves, we identify 21 bursts that are similar in alpha–alpha space to the Prominent jet break sample for the segments II–IV transition, and 26 bursts that are similar to the segments II–IV. Their consistency with post-jet break closure relations and temporal slopes suggest that there are indications of jet breaks in those light curves. These are categorized as Possible jet breaks (Table 4). The remaining 51 ambiguous light curve transitions appear to be segments II–III and therefore probably pre-jet break. However, they could possibly be segment II with a post-jet-break-with-energy-injection segment III. We are unable to distinguish these cases, therefore we put these remaining afterglows into a new category called Unlikely jet breaks. (These light curves are called Unlikely jet breaks because their slopes are too shallow compared to the Prominent jet break αs to be post-jet break.) We show example light curves for each of these newly segregated groups in Figures 9–11.

Finally, we examine single power laws that are consistent with both pre- and post-jet break closure relations. The remaining ambiguous light curves consist of 47 single power-laws. These single power-law light curves do not easily fit into the canonical picture unless they are either a short snapshot of one segment or are the post-jet break component and therefore relevant to this study. Often these light curves are plagued by a low signal-to-noise ratio and few counts, which leads to minimal information to be extracted. Other light curves in this group are dominated by large flaring during part or all of their light curves, which therefore makes determination of the underlying afterglow shape impossible during that time interval. We fit only the portion of the light curves that clearly returns to the underlying nonflaring level. However, there are a few examples of outliers that do not have flares and do have strong counting statistics. The most notable and best sampled X-ray afterglow in this outlier group is that of GRB 061007 which displayed a very bright exceptionally smooth single power law. Schady et al. (2007) showed that this must be either due to a very late-time jet break requiring enormous kinetic energy or an exceptionally early jet break ($t_b < 80$ s) with highly collimated outflow from a jet that includes continuous energy injection throughout. We do not exclude these isotropic models with extreme energy requirements from our global study, but these extreme energy requirements are a valid concern addressed in Section 4.5.

We attempt to filter the single power laws that are a result of a short pre-jet break segment from those that represent a post-jet break decay. In the context of the canonical X-ray afterglow, we should be able to look at the relationship between observation start and stop times, and the temporal decay to distinguish pre- and post-jet break. Figure 12 shows the relationship between the time that the observations begin and the time of last detection as a function of α. Unfortunately, there are only 13 redshifts measured of the 47 total GRBs in this category that are consistent with at least one post-jet break closure relation. Therefore, to include as many potential jet breaks as possible, the times used in the following distinctions are in the observed frame and not the rest frame. There appears to be a general trend that suggests

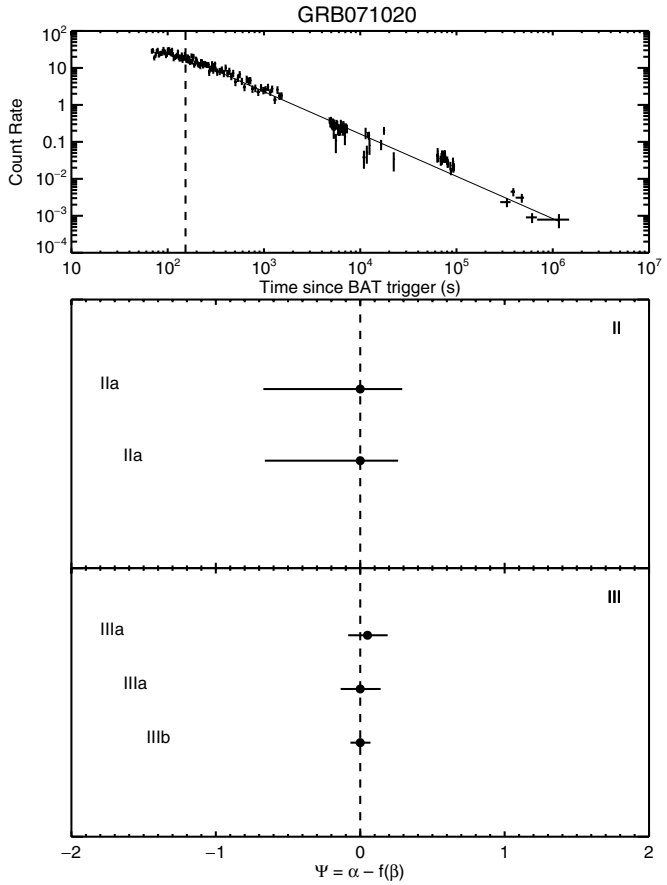

Figure 9. Same as Figure 4, except that GRB 071020 is an example of those that were classified based upon the α–α parameter space criteria into an Unlikely jet break because it showed an apparent segment II–III transition. IIa—*ISMs2ai* ($p = 2.79^{+0.24}_{-0.22}$, $q = 0.36^{+0.20}_{-0.46}$); IIb—*ISMf2ai* ($q = 0.94^{+0.47}_{-1.19}$); IIIa—*ISMs2a* ($p = 2.46^{+0.18}_{-0.18}$); IIIb—*JETs2ai* ($p = 2.46^{+0.18}_{-0.18}$, $q = 0.28^{+0.08}_{-0.07}$); IIIc—*JETsISM2ai* ($p = 2.46^{+0.18}_{-0.18}$, $q = 0.57^{+0.07}_{-0.07}$).

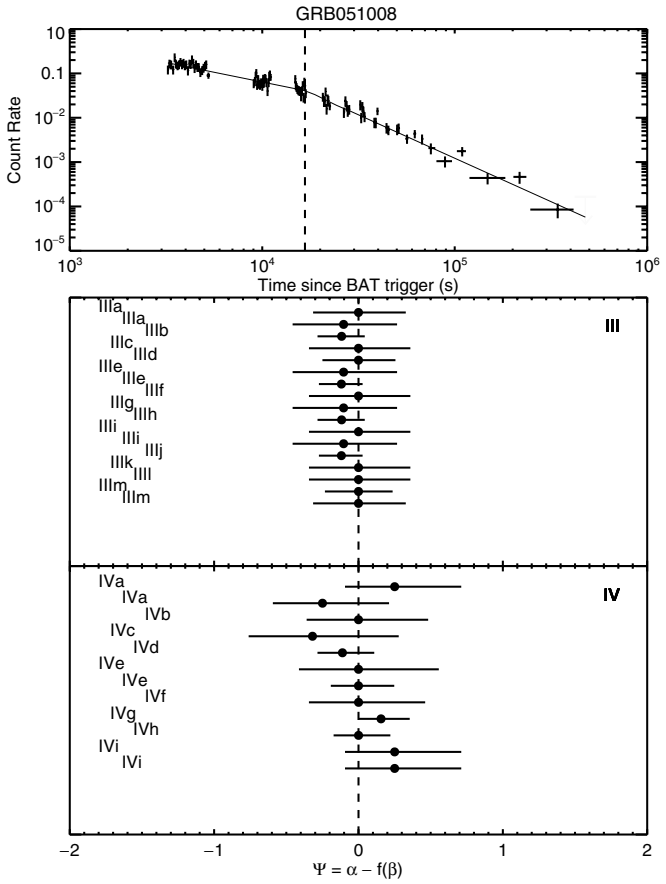

Figure 10. Same as Figure 4, except that GRB 051008 is an example of those that were classified based upon the α–α parameter space criteria into a Possible jet break with an apparent segment III–IV transition. IIIa—*ISMs2ai* ($p = 2.98^{+0.46}_{-0.43}$, $q = 0.60^{+0.22}_{-0.21}$); IIIb—*ISMs3a* ($p = 1.98^{+0.46}_{-0.43}$); IIIc—*ISMs3b* ($p = 1.98^{+0.46}_{-0.43}$); IIId—*ISMs3ai* ($p = 1.98^{+0.46}_{-0.43}$, $q = 0.90^{+0.36}_{-0.35}$); IIIe—*WINDs2ai* ($p = 2.98^{+0.46}_{-0.43}$, $q = -0.11^{+0.26}_{-0.25}$); IIIf—*WINDs3a* ($p = 1.98^{+0.46}_{-0.43}$); IIIg—*WINDs3b* ($p = 1.98^{+0.46}_{-0.43}$); IIIh—*WINDs3ai* ($p = 1.98^{+0.46}_{-0.43}$, $q = 0.90^{+0.36}_{-0.35}$); IIIi—*ISMf3a* ($p = 1.98^{+0.46}_{-0.43}$); IIIj—*ISMf3b* ($p = 1.98^{+0.46}_{-0.43}$); IIIk—*ISMf3ai* ($p = 1.98^{+0.46}_{-0.43}$, $q = 0.90^{+0.36}_{-0.35}$); IIIl—*WINDf3a* ($p = 1.98^{+0.46}_{-0.43}$); IIIm—*WINDf3b* ($p = 1.98^{+0.46}_{-0.43}$); IIIn—*WINDf3ai* ($p = 1.98^{+0.46}_{-0.43}$, $q = 0.90^{+0.36}_{-0.35}$); IIIo—*JETs3ai* ($p = 1.98^{+0.46}_{-0.43}$, $q = 0.17^{+0.27}_{-0.26}$); IIIp—*JETsISM3ai* ($p = 1.98^{+0.46}_{-0.43}$, $q = 0.31^{+0.24}_{-0.23}$); IIIq—*JETsWIND3ai* ($p = 1.98^{+0.46}_{-0.43}$, $q = 0.60^{+0.22}_{-0.21}$); IVa—*ISMs2a* ($p = 3.28^{+0.57}_{-0.42}$); IVb—*WINDs2a* ($p = 3.28^{+0.57}_{-0.42}$); IVc—*JETs2ai* ($p = 3.28^{+0.57}_{-0.42}$, $q = 0.37^{+0.23}_{-0.17}$); IVd—*JETs3a* ($p = 2.28^{+0.57}_{-0.42}$); IVe—*JETs3b* ($p = 2.28^{+0.57}_{-0.42}$); IVf—*JETs3ai* ($p = 2.28^{+0.57}_{-0.42}$, $q = 0.78^{+0.39}_{-0.29}$); IVg—*JETsISM2ai* ($p = 3.28^{+0.57}_{-0.42}$, $q = 0.73^{+0.23}_{-0.17}$); IVh—*JETsISM3a* ($p = 2.28^{+0.57}_{-0.42}$); IVi—*JETsISM3b* ($p = 2.28^{+0.57}_{-0.42}$); IVj—*JETsISM3ai* ($p = 2.28^{+0.57}_{-0.42}$, $q = 1.00^{+0.35}_{-0.26}$); IVk—*JETsWIND3a* ($p = 2.28^{+0.57}_{-0.42}$); IVl—*JETsWIND3ai* ($p = 2.28^{+0.57}_{-0.42}$, $q = 1.16^{+0.31}_{-0.23}$).

that those single power laws for which observations began late (greater than 10^4 s) tend to be steeper ($\alpha > 1.2$) than those that start early and continue for a long observation. We make a cut in this parameter space and deem those afterglows that start within or traverse the time frame for which we would expect jet breaks (from the Prominent sample) and have steep ($\alpha > 1.5$) decays as Possible jet breaks and add them to that sample. These six bursts are indicated in Figure 12. The remaining single power-law afterglows that appear to be pre-jet break are put into the Unlikely jet break category.

We present the complete sample of Possible jet breaks in Table 4. The probable jet break time for each light curve is identified as t_b. However, some ambiguity still remains of whether this is the time of the jet break. Therefore, we also list the $t_{\rm start}$ and $t_{\rm lastdet}$ (the time of last detection, if relevant) because they provide limits on the jet break time if the jet break is not t_b. Using the completeness criteria described in Section 4.1, we find that at least 23% of the Possible jet breaks and 35% of the Unlikely jet breaks were observed sufficiently long enough that we would expect to have seen a jet break during their observations.

The six afterglows that are inconsistent with all closure relations after internal consistency checks, but have temporal behavior of their final segments similar to Prominent segments III–IV or II–IV are also included in the Unlikely jet break sample. The breaks in these cases may be due to origins other than those in the canonical model such as transition of the cooling frequency through the X-ray band or Compton processes. They may also be contaminated by small-scale flaring that is not removed by our methods. They are denoted in Table 4 by "none" in the requirements field.

The complete sample of Unlikely jet breaks are listed in Table 5, and the secure Nonjet breaks are listed in Table 6. The criteria, inputs, and final memberships of the Prominent, Hidden, Possible, Unlikely, and Nonjet break categories are summarized in Table 7. The nonjet break category includes all remaining bursts, most of which are segment I–II transitions.

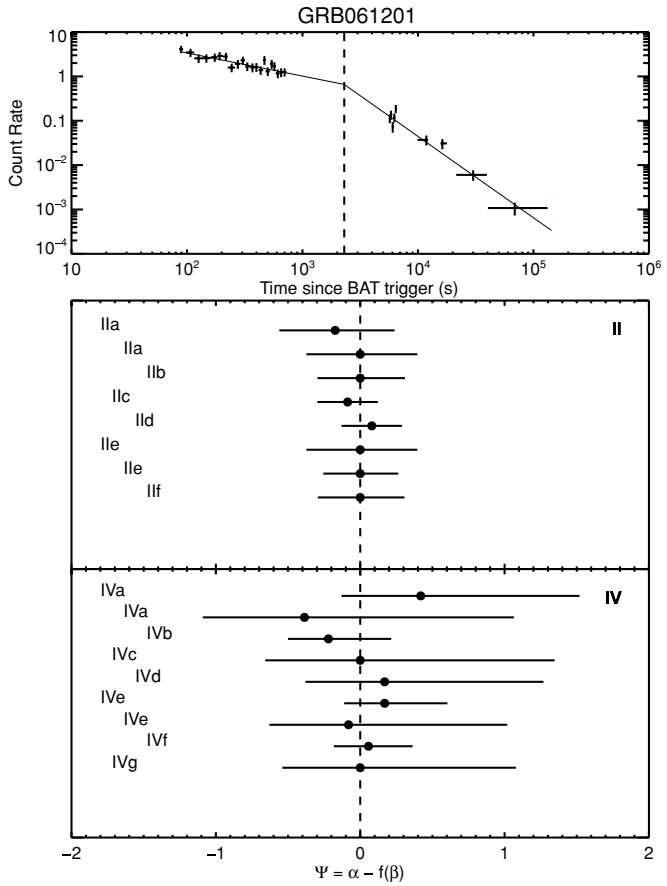

Figure 11. Same as Figure 4, except that GRB 061201 is an example of those that were classified based upon the α–α parameter space criteria into a Possible jet break with an apparent segment II–IV transition. IIa—*ISMs2a* ($p = 1.93^{+0.50}_{-0.46}$); IIb—*ISMs2ai* ($p = 1.93^{+0.50}_{-0.46}, q = 0.86^{+0.32}_{-0.30}$); IIc—*WINDs2ai* ($p = 1.93^{+0.50}_{-0.46}, q = 0.08^{+0.42}_{-0.41}$); IId—*ISMf2ai* ($q = 1.38^{+0.24}_{-0.25}$); IIe—*WINDf2ai* ($q = 1.35^{+0.26}_{-0.26}$); IIf—*JETs2ai* ($p = 1.93^{+0.50}_{-0.46}, q = 0.14^{+0.24}_{-0.23}$); IIg—*JETsISM2ai* ($p = 1.93^{+0.50}_{-0.46}, q = 0.38^{+0.23}_{-0.22}$); IIh—*JETsWIND2ai* ($p = 1.93^{+0.50}_{-0.46}, q = 0.05^{+0.25}_{-0.24}$); IVa—*WINDs2a* ($p = 2.22^{+1.43}_{-0.67}$); IVb—*JETs2a* ($p = 2.22^{+1.43}_{-0.67}$); IVc—*JETs2b* ($p = 2.22^{+1.43}_{-0.67}$); IVd—*JETs2ai* ($p = 2.22^{+1.43}_{-0.67}, q = 0.78^{+0.77}_{-0.38}$); IVe—*JETsISM2a* ($p = 2.22^{+1.43}_{-0.67}$); IVf—*JETsISM2ai* ($p = 2.22^{+1.43}_{-0.67}, q = 1.11^{+0.73}_{-0.36}$); IVg—*JETsWIND2a* ($p = 2.22^{+1.43}_{-0.67}$); IVh—*JETsWIND2b* ($p = 2.22^{+1.43}_{-0.67}$); IVi—*JETsWIND2ai* ($p = 2.22^{+1.43}_{-0.67}, q = 0.94^{+0.83}_{-0.41}$).

4.4. Significance of Closure Relation Distinctions

We evaluated the statistical significance of the jet breaks identified by closure relation distinctions by running a series of Monte Carlo simulations. These specific samples include those GRBs for which we have a distinct segment IV, ambiguous segment II–III, segment I–II–III with no segment IV, and single power laws. We generated 1000 mock sets of $\alpha, \beta, \sigma_\alpha$, and σ_β for each segment in each simulation by drawing random numbers from the Gaussian distribution of each of these parameters from the real data. These 1000 sets of light curve parameters for each sample are fit with the closure relations as we did with the real data including the application of the internal consistency checks.

The Monte Carlo simulations are used to determine how many Hidden jet breaks might result from random variations in αs and βs due to measurement errors. The fraction of Hidden jet breaks in this randomized sample indicates to us how many false Hidden jet breaks we would expect to see in the real sample. Based on the simulations, we would have expected 6.0±0.6 final segments only consistent with post-jet break closure relations, compared to the 12 found in the real data. Therefore, at least half of these Hidden jet breaks appear to be real.

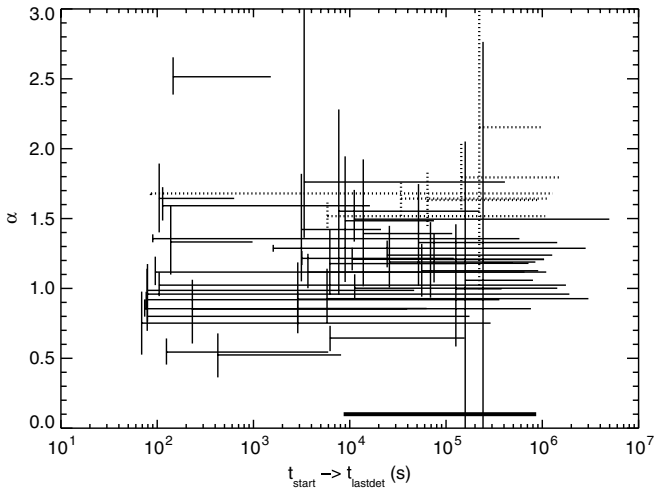

Figure 12. Representation of those light curves that are best fit by single power laws and their duration from the start of observations to their last detection and the slope of the temporal decay. Note that these times exclude segments of flaring prior to or after the single power-law observations for which the shape of the underlying afterglow cannot be determined. The data suggest that the majority of light curves with shallower temporal decays begin early and end early and steeper decays begin later and end later. Note that these times are in the observed frame due to a lack of available redshifts for this sample. The thick reference line indicates the time interval during which jet breaks occur in the Prominent sample. Those bursts whose $t_{\rm start}$ begins during the jet break time interval and whose $\alpha > 1.5$ are suspected to be jet breaks and indicated by the dotted lines.

4.5. Jet Opening Angles and Energetics

We measure jet opening angles using the methodology of Burrows & Racusin (2007), originally derived from Sari et al. (1999) and Frail et al. (2001) where the opening angle of a uniform jet is defined as

$$\theta_j = 0.057\,\xi\,t_j^{3/8} \tag{12}$$

$$\xi \equiv \left(\frac{3.5}{1+z}\right)^{3/8}\left(\frac{\eta_\gamma}{0.1}\right)^{1/8}\left(\frac{n}{E_{\gamma,\rm iso,53}}\right)^{1/8}, \tag{13}$$

where θ_j is the inferred jet half-opening angle, t_j is the jet break time in days, z is the redshift, η_γ is the assumed radiative efficiency, n is the ambient number density in cm^{-3}, and $E_{\gamma,\rm iso,53}$ is the rest frame isotropic equivalent energy radiated in gamma rays between 1 keV and 10 MeV in units of 10^{53} erg. We assume $n \sim 1$ cm^{-3} in all cases. The dependence on n is only 1/8, and therefore has only a small effect on θ_j.

Equations (12) and (13) are only valid for a constant density (ISM) medium. For the sake of comparison with pre-*Swift* values, and because we find no afterglows that are solely consistent with Wind medium models, we use only these ISM relations for determining the jet opening angle.

Zhang et al. (2007b) measured GRB efficiencies from the X-ray afterglow kinetic energies and found that GRBs have a distribution of η_γ, with most showing $\eta_\gamma < 0.1$. Therefore, we choose to use a universal value of $\eta_\gamma = 0.1$ and make comparisons with the values of E_γ listed in the literature (Bloom et al. 2003; Frail et al. 2001) for pre-*Swift* bursts. The

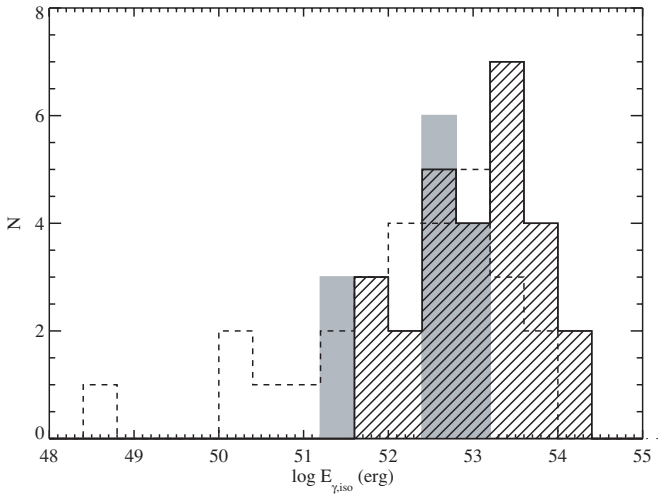

Figure 13. Distribution of our estimated $E_{\gamma,\rm iso}$s for GRBs with measured redshifts in the Prominent jet break sample (gray solid), and the Hidden and Possible jet break samples (dashed lines), compared with the pre-*Swift* measurements (filled hatched histogram) from Bloom et al. (2003) with measured redshifts. Note that the nine SHBs for which we were able to estimate $E_{\gamma,\rm iso}$ dominate the low-energy end of this distribution.

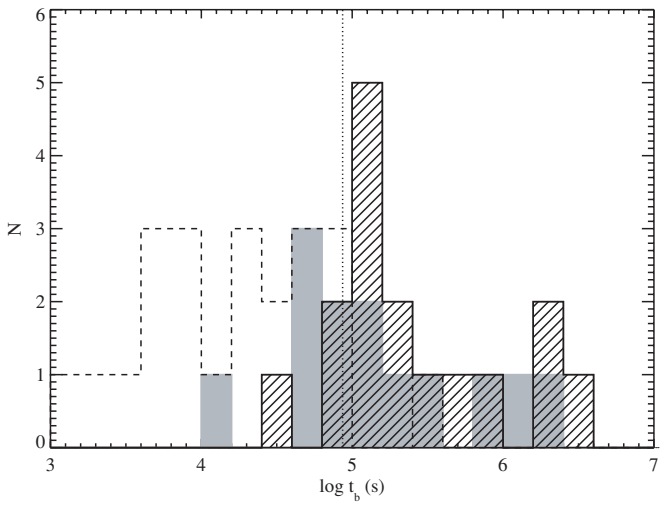

Figure 14. Distribution of our estimated break times for GRBs with measured redshifts in the Prominent jet break sample (gray solid), and the Hidden and Possible jet break samples (dashed lines), compared with the pre-*Swift* measurements (filled hatched histogram) from Bloom et al. (2003).

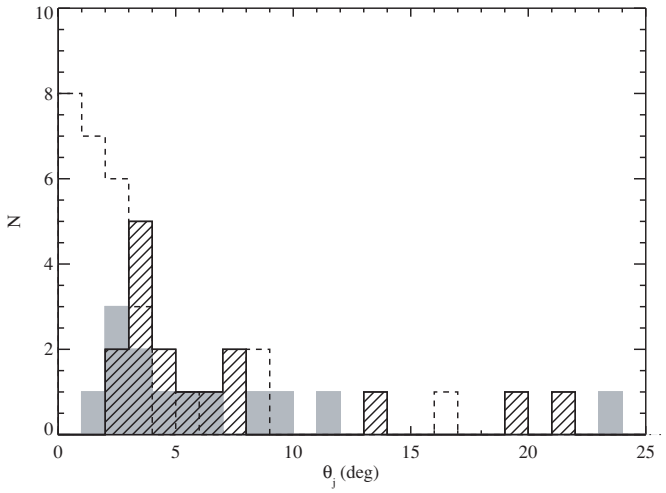

Figure 15. Distribution of our estimated jet half-opening angles (θ_j) for the GRBs with measured redshifts in the Prominent jet break sample (gray solid), and the Hidden and Possible jet break samples (dashed lines), compared with the pre-*Swift* measurements (filled hatched histogram) from Bloom et al. (2003). Note that we recalculate θ_j for the pre-*Swift* sample so that the formalism and density estimates are comparable.

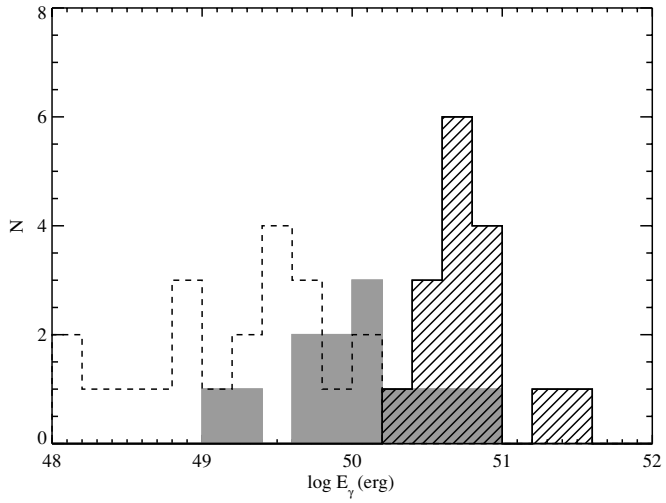

Figure 16. Distribution of our estimated collimation corrected γ-ray energy (E_γ) for GRBs with measured redshifts in the Prominent jet break sample (gray solid), and the Hidden and Possible jet break samples (dashed lines), compared with the pre-*Swift* measurements (filled hatched histogram) from Bloom et al. (2003). Note that we recalculate E_γ for the pre-*Swift* sample using the values of θ_j shown in Figure 15.

dependence on η_γ is to the 1/8 power, therefore it has only a weak effect on the θ_j estimates.

Unfortunately, $E_{\gamma,\rm iso}$ is often not a well-constrained quantity. To properly measure the bolometric fluence (approximated as the fluence between 1 keV and 10 MeV), coverage to harder energies beyond the hard X-ray band of the BAT (15–350 keV) is needed. In a handful of cases, simultaneous high-energy spectral information is available in the literature from Konus-Wind or Suzaku that can properly characterize the spectra. We describe our calculations of $E_{\gamma,\rm iso}$ in Appendix A. Many assumptions whose error contributions to $E_{\gamma,\rm iso}$ are unknown go into these calculations. Therefore, these determinations of $E_{\gamma,\rm iso}$ are to be taken with caution. The dependence on $E_{\gamma,\rm iso}$ in the jet opening angle calculations (Equations (12) and (13)) is only to the 1/8 power, consequently having minimal impact on that quantity, but substantial impact on the estimate of the total collimated energy output (E_γ). The distribution of $E_{\gamma,\rm iso}$ for our sample is shown in Figure 13 with the pre-*Swift* values (Bloom et al. 2003) for comparison. The *Swift* $E_{\gamma,\rm iso}$ distribution peaks at and extends to lower energies than that of the pre-*Swift* era. This is probably an effect of the lower thresholds and softer energy response of the BAT.

We plot our break times in Figure 14. For each burst, using the measured t_b and redshift, and estimated $E_{\gamma,\rm iso}$, we can determine the jet half-opening angle from Equation (12). Our estimated values of θ_j and the resulting E_γ (Equation (14)) are listed in Tables 2–4 and plotted in Figures 15 and 16, along with the pre-*Swift* values. The Prominent jet break distribution (with measured redshift) has a mean (median) $\theta_j = 6.^\circ5$ ($5.^\circ4$), slightly smaller than the pre-*Swift* measurements. The other categories of jet breaks have even narrower opening angles corresponding to even earlier potential jet breaks. These earlier breaks may be largely due to post-jet-breaks-with-energy-

Table 7
Jet Break Summary

Classification	GRBs	Segment Types	Definition
Prominent jet break	28	I–II–III–IV, II–III–IV	Has distinct segment IV
Hidden jet break	12	Single power law, Ambiguous II–III/III–IV, I–II–III	Last segment requires post-jet break closure relation
Possible jet break	53	Ambiguous II–III/III–IV, I–II–III, Single power law	Resembles III–IV or II–IV transition in α–α space
Unlikely jet break	100	Single power law, Ambiguous II–III/III–IV, I–II–III	Consistent with both pre- and post-jet break closure relations, but resembles II–III in α–α space, or no closure relations but temporally consistent
Nonjet break	37	I–II, Single power law, II–III, 0–I	Does not fit any jet break criteria

Table 8
GRBs Spectral Properties from the Literature

GRB	α_B	β_B	$\alpha_{\rm CPL}$	E_p (keV)	Source
050318				49 ± 7	Still et al. (2005)
050406				24	Zhang et al. (2007b)
050416A				$15.6^{+2.3}_{-2.7}$	Sakamoto et al. (2006)
050525A				82^{+4}_{-3}	Sakamoto et al. (2008)
050603	-0.79 ± 0.06	-2.15 ± 0.09		349 ± 28	Golenetskii et al. (2005a)
051109A				161^{+224}_{-58}	Golenetskii et al. (2005b)
051221A*			$-1.08^{+0.13}_{-0.14}$	402^{+93}_{-72}	Golenetskii et al. (2005c)
060115				63^{+36}_{-11}	Sakamoto et al. (2008)
060124				193^{+38}_{-39}	Romano et al. (2006)
060206				78^{+38}_{-13}	Sakamoto et al. (2008)
060418				230	Golenetskii et al. (2006f)
060614*			$-1.57^{+0.12}_{-0.14}$	302^{+214}_{-85}	Golenetskii et al. (2006b)
060707				63^{+21}_{-10}	Sakamoto et al. (2008)
060814				257^{+122}_{-58}	Golenetskii et al. (2006c)
060908				151^{+184}_{-41}	Sakamoto et al. (2008)
060927				72^{+25}_{-11}	Sakamoto et al. (2008)
061007	-0.7 ± 0.04	$-2.61^{+0.15}_{-0.21}$		399^{+19}_{-18}	Golenetskii et al. (2006d)
061121	$-0.83^{+0.24}_{-0.19}$	$-2.00^{+0.18}_{-0.32}$		455 ± 115	Golenetskii et al. (2006a)
061201*			$-0.36^{+0.40}_{-0.65}$	873^{+458}_{-284}	Golenetskii et al. (2006e)
070125	$-1.1^{+0.10}_{-0.09}$	$-2.08^{+0.10}_{-0.15}$		367^{+67}_{-51}	Bellm et al. (2008)
070508				188 ± 8	Golenetskii et al. (2007d)
070714B*			-0.86 ± 0.10	1120^{+780}_{-380}	Ohno et al. (2007)
071003			-0.97 ± 0.07	799^{+124}_{-100}	Golenetskii et al. (2007a)
071010B	$-1.25^{+0.74}_{-0.49}$	$-2.65^{+0.29}_{-0.49}$		52^{+14}_{-10}	Golenetskii et al. (2007b)
071020			$-0.65^{+0.27}_{-0.32}$	322^{+80}_{-53}	Golenetskii et al. (2007c)
071117			$-1.53^{+0.15}_{-0.16}$	278^{+236}_{-79}	Golenetskii et al. (2007e)

*Short hard GRB.
Notes. GRBs with measured redshifts and γ-ray spectral properties from the literature used to calculated $E_{\gamma,\rm iso}$. CPL provided from either Band function fit or CPL fit, but $\alpha_{\rm CPL}$ used only for SHBs.

injection or contamination by light curve breaks that are not jet breaks at all.

Only 85 of our total 230 GRBs have measured redshifts. For candidate jet breaks without measured redshifts (indicated by dashes in Tables 2–4), we assume $z = 2.3$ or $z = 0.4$, and $E_{\gamma,\rm iso} = 3.7 \times 10^{52}$ erg to get an estimate (or limit) on θ_j ($\xi \sim 1.2$; Equation (13)). The redshift value of $z = 2.3$ or $z = 0.4$ that we assumed for GRBs without measured redshifts is the mean redshift of *Swift* long and short GRBs, respectively, for our sample. These values are similar to those discussed in the literature (Jakobsson et al. 2006b; Bagoly et al. 2006; Fiore et al. 2007). However, the measurements in the literature were based on the first two years to the *Swift* mission when the mean redshift was slightly higher. More recent estimates suggest that the redshift in the third year of the *Swift* mission is lower. This difference in redshift has only a small impact on the derived opening angles. We use the median value of the $E_{\gamma,\rm iso}$ distribution from those long GRBs with measured redshifts to estimate θ_j and E_γ for those GRBs without measured redshifts.

For those X-ray afterglows where the last light curve break is consistent with one of the post-jet break closure relations, we list the jet half-opening angle (θ_j), model requirements, and input parameters in Tables 2–4, whether we have measured or assumed the required relevant parameters. We show the distributions of measured t_b, θ_j, and E_γ for all of those light

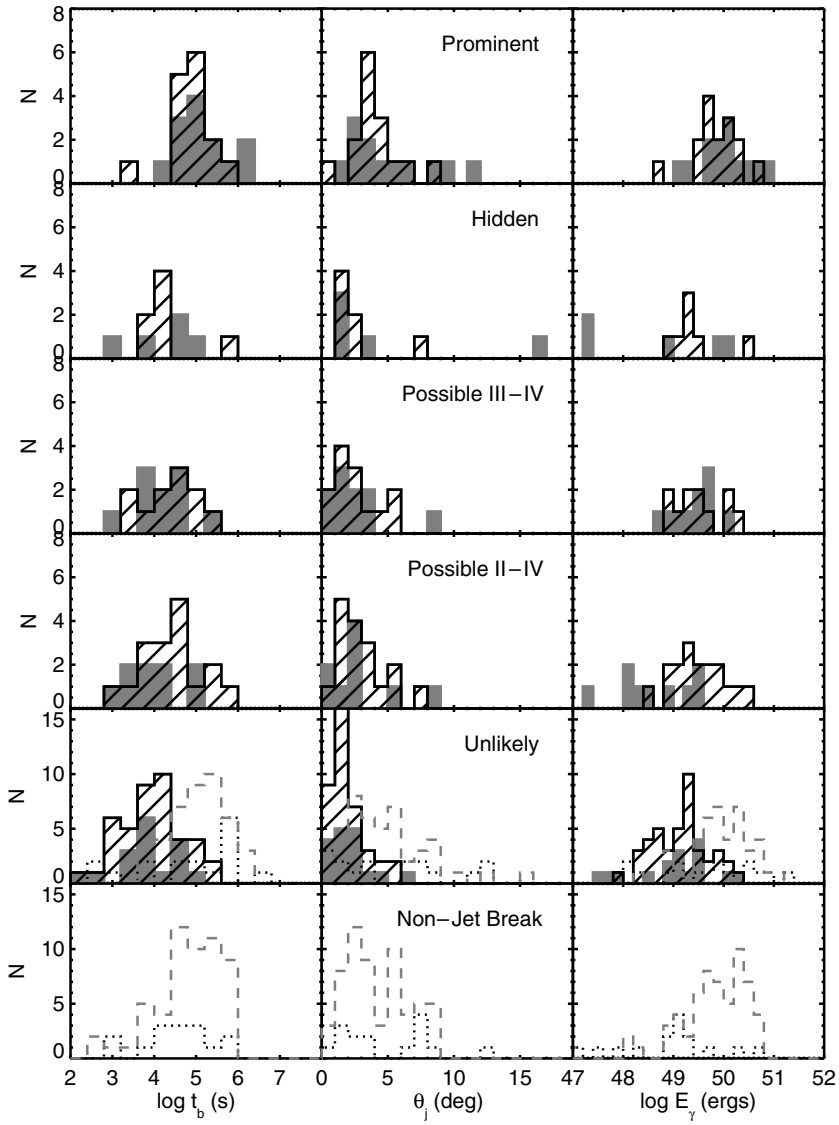

Figure 17. Distribution of t_b (left) for all potential jet breaks with measured redshifts (dark gray), those without measured redshifts (hatched lines). The jet break lower limit for Unlikely and Nonjet breaks are also shown with (dashed line) and without redshifts (dotted line). Distributions of θ_j (center), and the collimated energy output, E_γ (right), are presented for the same samples. Those GRBs without measured redshifts are assumed the average values of $z = 2.3$ for long bursts or $z = 0.4$ for short bursts.

curves in the Prominent, Hidden, Possible, Unlikely, and nonjet break samples in Figure 17, and compare the distributions for those with redshifts and measured $E_{\gamma,\rm iso}$ and those for which we had to assume average values. There is no significant difference between the distributions with and without measured redshifts.

We can now characterize the energy budget of these GRBs. Using our measurements of θ_j and $E_{\gamma,\rm iso}$ from the sources described above, we calculate E_γ, the collimated GRB energies, as

$$E_\gamma = E_{\gamma,\rm iso}(1 - \cos\theta_j). \quad (14)$$

These values and limits are listed in Tables 2–6. The distribution of E_γ is plotted in the right panels of Figure 17. Compared to pre-*Swift* optical jet break measurements which tightly cluster around $E_\gamma \sim 10^{51}$ erg (Bloom et al. 2003), our sample is less energetic, with a median value for the long bursts with estimated $E_{\gamma,\rm iso}$ in Prominent jet break sample of $\sim 9.8 \times 10^{49}$ erg. This measurement is in agreement with that obtained by Kocevski & Butler (2008).

5. DISCUSSION

There are several different observational categories of potential jet breaks that do not look like the conventional jet breaks that strictly follow the canonical form on which previous studies have focused. These categories include post-jet break segments with energy injection in segment III where the normal isotropic models do not fit, apparent segment II–III light curves in which the latter segment requires a post-jet break model suggesting they are actually segments III–IV, apparent segments II–III that have temporal decays suggestive of a III–IV or even a II–IV transition, other segments III that require a post-jet break model and cannot be fit by any of the isotropic models, and single power laws that are apparently post-jet break. Those classifications for which we are at least somewhat confident are included in the Prominent (12%), Hidden (5%), and Possible (23%) jet break categories. Those that have some characteristics suggestive of the post-jet break decay, but have temporal decays similar to pre-jet break decays are placed in the Unlikely jet break category (43%), and the remaining light

curves with clear pre-jet break behavior are included in the nonjet break category (16%).

Perhaps the most unexpected of these categories is the post-jet-break-with-energy-injection scenario which has been suggested as an alternative option to explain specific GRB afterglows (Panaitescu et al. 2006; Oates et al. 2007; Schady et al. 2007; de Pasquale et al. 2008). The idea of energy injection continuing after the jet break has intriguing implications for jet break studies. Energy injection would have the effect of making the temporal decay shallower than the underlying jet break until the energy injection ends, which would then manifest as another break in the light curve. This implies that sometimes the break between segments II and III is not caused by the cessation of energy injection in the isotropic model but rather by continuation of energy injection through the jet break with the break to segment IV occurring only after energy injection ceases. We find four examples in the Prominent jet break category and seven in the Hidden jet break category which require this scenario to explain our model fits, in addition to many other segments III that are consistent with post-jet-break-with-energy-injection models. This is significantly larger than the 7.4 ± 1.0 that we would have expected from our Monte Carlo simulations. These specific bursts are indicated in Tables 2 and 3 with the alternative jet opening angle and jet break time listed for all of those for which at least one post-jet-break-with-energy-injection model is consistent.

Many single power-law light curves can be explained within the context of the canonical light curve formalism by observing biases (e.g., late start times, early stop times). However, there are several exceptions. Some simply have large errors in α due to light curves with few bins. A few well-constrained outliers remain, the most notable being GRB 061007, whose light curve extends from 80 s to nearly one million seconds after the trigger, with a continuous, well-constrained, steep, smooth temporal decay. If we assume that these afterglows behave like the canonical light curve, these results imply that the steeper single power laws are post-jet break decays where the preceding light curve segments were either missed due to a late start or masked by flaring activity.

In order to gauge the likelihood of these exceptions being pre- or post-jet break, we calculate the expected collimated energy outputs limits (E_γ) in the method described in Section 4.5 for these bursts if the jet breaks were prior to the start of the observations or after the end of the observations (Figure 18). Those bursts for which the observations extend beyond the time frame for which we would expect a jet break based on the behavior of the Prominent jet break category require enormous collimated energy outputs ($\gg 10^{51}$ erg), suggesting that the jet break was prior to the observation start. These early jet breaks are difficult to explain in terms of the canonical form (Liang et al. 2009). There are 10 of these single power-law afterglows that persist through the entire expected jet break time window, 3 of which have very well sampled light curves (GRB 050716, GRB 061007, GRB 061126). The two other than GRB 061007 have relatively shallow decays ($\alpha \sim 1$), suggesting they are pre-jet break. Perley et al. (2008) and Gomboc et al. (2008) demonstrate inconsistencies between the optical and X-ray properties of GRB 061126 suggesting an additional component is needed to explain the X-rays which is outside of the standard model. These bursts remain enigmatic and are difficult to understand in the context of the majority of *Swift* burst. They may have exceptionally late jet breaks, or perhaps do not break at all, implying a large jet opening angle or perhaps isotropic outflow.

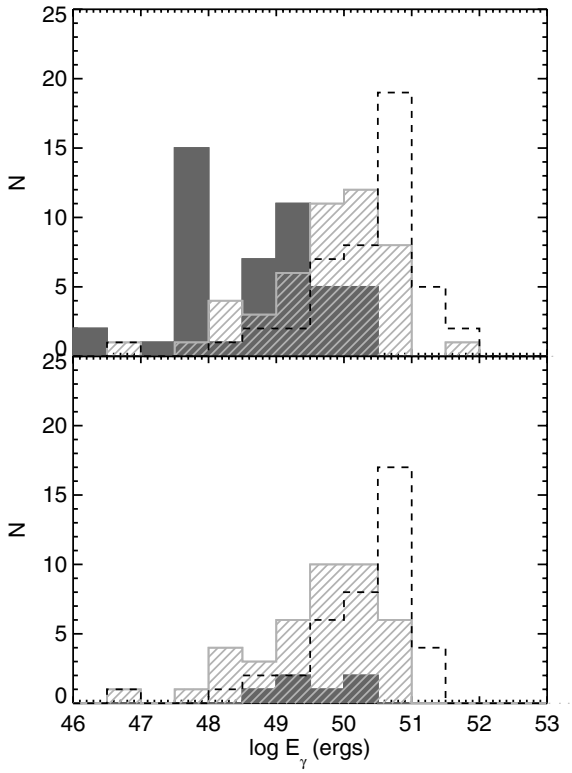

Figure 18. Distributions of collimated γ-ray energy output limits (top) for single power-law light curves using jet opening angles estimated by using $t_{\rm start}$ (solid histogram), $t_{\rm jblim}$ (hatched histogram), and $t_{\rm stop}$ (dashed line). The bottom panel also shows the distributions of E_γ assuming jet break after $t_{\rm jblim}$ or $t_{\rm stop}$ for post-jet break candidates from Figure 12 and assumes pre-jet break limit for remaining single power-law light curves. When no redshifts are available, we assume $E_{\gamma,\rm iso} = 10^{53}$ erg and $z = 2.3$ for long bursts or $z = 0.4$ for short bursts.

Another variation on the unusual noncanonical light curve categories are those with segments I–II where segment II has a slope of $\sim$1 and is consistent with the normal spherical decay closure relations as well as the normal decay with energy injection relations. There are 19 light curves in our sample that fit these criteria. This deviation from the canonical behavior implies either that these GRBs did not experience the energy injection phase, or that segment I was misidentified due to flaring behavior. These objects may be similar to the shallow single power-law light curves except that their steep decay was observed first. In fact, five of these light curves fit our completeness criteria like those exceptional single power-law cases, implying that they are unusually long lived for segments II or III. Perhaps the lack of energy injection or cause of this phase differs somehow from that of the canonical afterglows. It is interesting to note that these X-ray light curves (after segment I) would have been considered normal in the pre-*Swift* era.

We have unearthed many additional jet break candidates in the data, but the fundamental question remains: why do more afterglows not have obvious jet breaks? The most straightforward and plausible explanation for the lack of conventional jet breaks in XRT light curves is simply that the observations end before the jet breaks occur. The more fundamental question is what makes these afterglows for which we do not observe jet breaks different from those for which we do observe jet breaks?

We have some cases of jet breaks at very late times (greater than 10^6 s). At these times, the fluxes are low, and uncertainties on the data points are large, making it difficult to detect jet

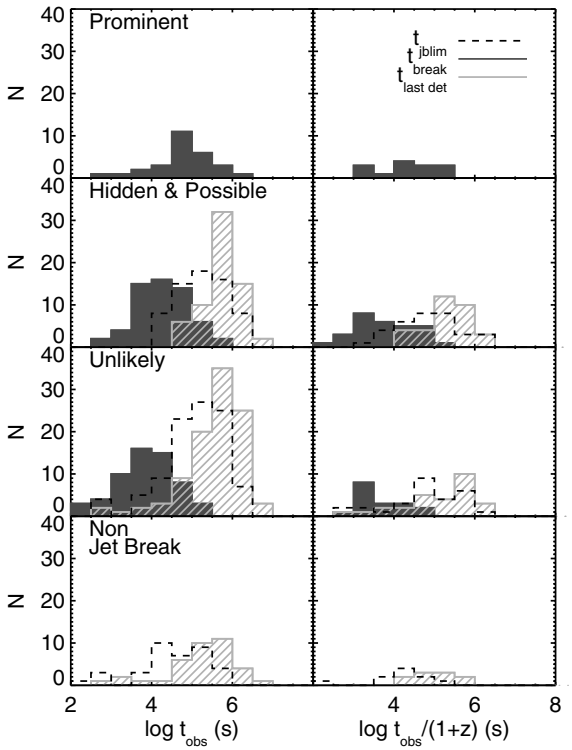

Figure 19. Distributions of times of the last detection, jet break lower limit, and time of potential jet breaks for the different categories of jet break in both the observed frame (left) and rest frame (right).

breaks. In fact, many light curves end before this time frame, in which case we could be missing the jet breaks completely. Curran et al. (2008) simulated GRB afterglow light curves based on real XRT data and showed that hidden jet breaks could be present in even well sampled XRT light curves. We evaluate the probability that such a bias exists within our data set by doing a similar exercise, calculating the last time at which a jet break could occur without being detectable. This time is determined by forcing an additional break into the light curve with a slope equal to $\alpha_f + 1$, where α_f is the measured slope of the last light curve segment. We then find the earliest break time that increases the overall χ^2 by 2.7 (corresponding to 90% confidence for one parameter of interest). We refer to this time as the jet break lower limit ($t_{\rm jblim}$). We excluded light curves with segment IV from this analysis because an additional break does not fit within the context of the canonical structure. In 8% of the total sample, the fits using this additional break did not converge, therefore in these cases, the jet break limit is the time of the last detection.

The distributions of times of last detections, jet break lower limits, and times of potential jet breaks in both the observed frame and rest-frame are shown in Figure 19. The distributions of jet break times for the Prominent, Hidden, and Possible jet break categories overlap, with the latter sample peaking at an earlier time. This might be due to contamination in the Possible jet break sample by breaks that are not jet breaks. These other breaks may be from the segment II–III transition, or the previously mentioned jet-breaks-with-energy-injection (between segments II and III) which tend to occur earlier than other (segment III–IV) jet breaks. The important thing to extract from Figure 19 is that the majority of the bursts in the Unlikely jet break and nonjet break categories have last detection and jet break lower limits consistent with the range of Prominent jet break times. It is probable that these light curves had jet breaks after XRT observations ended or that were buried within the noise of the late-time data. There are a few exceptions to this, particularly in those single power-law light curves mentioned above that would have had to have their jet breaks very early (few $\times 100$ s) and did not break even beyond the expected jet break times. Perhaps these few bursts are fundamentally different from those with jet breaks.

We also included short hard GRBs (SHBs) in our study of jet breaks, treating them the same as the long bursts except in the calculation of $E_{\gamma,\rm iso}$. Only the brightest X-ray afterglows of SHBs were included in our study, which may bias the understanding of this group in terms of the faint and quickly fading subsample that did not meet our minimum requirements. The SHBs were placed into similar jet break subsamples as the long GRBs (i.e., two Prominent, four Possible, three Unlikely, and four nonjet breaks). The SHBs have on average smaller values of $E_{\gamma,\rm iso}$ and E_γ than the long bursts. Those SHBs that show jet breaks and similarity to the canonical model perhaps have some fundamental differences in their environments or physical mechanisms from those that simply fade quickly (Troja et al. 2008; Sakamoto & Gehrels 2009).

Comparing this work to other recent studies of jet breaks in X-ray afterglows (Burrows & Racusin 2007; Willingale et al. 2007; Panaitescu 2007; Kocevski & Butler 2008; Liang et al. 2008; Evans et al. 2008), we find significant overlap with our jet break candidates. Most differences can be attributed to differing interpretation of light curve fitting and flaring and generally more limited jet break definitions in those other studies. Each study used independent jet break criteria and there were several different independent data analysis pipelines. Our work builds upon these other studies with our systematic analysis of the interaction between all of the light curve regions for each burst, broad closure relation model usage, careful searches for jet breaks buried in the data, and characterization of the energetics and limits.

6. CONCLUSIONS

Pre-*Swift* expectations for GRB X-ray afterglows have been substantially revised with the great wealth of XRT observations. While we try to categorize and classify their properties, there is still a wide range of unexplained diversity in GRB afterglow properties. Within the limits of theoretical expectations and observational biases, we have attempted to survey the properties of the X-ray afterglows.

In agreement with some previous studies (Burrows & Racusin 2007; Liang et al. 2008; Willingale et al. 2007; Kocevski & Butler 2008; Evans et al. 2008), we find that only a small fraction ($\sim$12%) of our total sample has a late-time break that is clearly a jet break justified by the closure relations (Prominent). We find an additional $\sim$30% with observational biases that make segments IV nondistinct but with a strong case for post-jet break temporal and spectral properties (Hidden and Possible). Some of the bursts in our sample remain ambiguous in the jet break designation. Despite not being able to make absolute claims about these specific bursts, we demonstrate that there are jet breaks hidden within the data and observational biases. This suggests that there are more jet breaks in XRT afterglows that previous studies have revealed and $\sim$60% of the Unlikely and nonjet breaks could have had jet breaks after the observations ended or buried within the errors and would still be consistent with the jet break time frame expectations from the Prominent jet break sample. Some of our light curves that require energy

injection to continue post-jet break may have been previously misidentified as the end of the energy injection phase.

Evans et al. (2008) also explores the canonical X-ray afterglow form using the XRT sample, where they find that less than half of all light curves behave canonically, and one quarter are "oddballs." Many of these "oddballs" can be explained by the scenarios we use to describe the ambiguous cases discussed in this paper. While their approach is somewhat different, their conclusions are similar to ours.

Our study requires post-jet break energy injection to explain four cases of the Prominent jet break sample and 11 others in the Hidden jet break category. This modification to the canonical X-ray afterglow form alters expectations from simply studying the light curve alone, and adds to the theory needed to explain the diversity of observed properties.

These explanations do not solve all of the remaining problems related to jet breaks. Several afterglow light curves, particularly the ones that can only be fit by a single power law, persist with a constant slope prior to and beyond the times for which we would expect a jet break. These bursts require either an exceptionally early jet break (sometimes before 100 s) or an exceptionally late jet break, requiring a large jet opening angle and an enormous ($\gg 10^{51}$ erg) collimation corrected energy output.

Swift GRBs are on average at higher redshifts, smaller jet opening angles, lower isotropic equivalent energies, and lower collimated γ-ray energies compared to GRBs observed prior to *Swift*. Some of these effects can be attributed to the lower energy coverage and superior sensitivity of the *Swift*-BAT. However, the consequences of these observational biases toward selecting different sorts of bursts is unexpected.

One of the fundamental predictions of the jet break models used in this work is achromatic behavior in a single spectral component. The jet break should be a purely geometrical effect and should therefore not be limited to the X-ray afterglows. Other components of the afterglow geometry may be more closely tied to emission segments and mechanisms making direct afterglow comparison difficult. Modeling of the complete spectral energy distribution would be necessary to understand how the spectral breaks might influence the chromatic light curve behavior. This would be further complicated by uncertainties in the optical extinction and X-ray absorption. These detailed spectral studies, which are beyond the scope of this work, would provide additional information if simultaneous optical, infrared, and radio observations were available to narrow down the closure relation models and better constrain the physical models. Liang et al. (2008) have already made some progress on exploring multi-wavelength approach to this problem, specifically evaluating cases of chromatic versus achromatic breaks.

J.L.R., D.N.B., and A.F. gratefully acknowledge support for this work from NASA contract NAS5-00136. We acknowledge the use of public data from the Swift data archive. B.Z., B.B.Z, and E.-W.L. gratefully acknowledge support from NASA contracts NNG05GB67G, NNX08AN24G, NNX08AE57A, and a President's Infrastructure Award from UNLV. E.-W.L. also acknowledges support from a National Natural Science Foundation of China grant 10873002, National Basic Research Program ("973" Program) of China (grant 2009CB824800), and the research foundation of Guangxi University. This work made use of data supplied by the UK Swift Science Data Centre at the University of Leicester. We thank R. Willingale for his helpful comments.

APPENDIX

To measure $E_{\gamma,\rm iso}$, we must know (or estimate) the shape of the spectrum and integrate it over the desired energy range, correcting for the distance and redshift (k-correction) effects using the method of Amati et al. (2002)

$$E_{\gamma,\rm iso} = \frac{4\pi D_L^2}{(1+z)} \int_{1{\rm keV}/(1+z)}^{10{\rm MeV}/(1+z)} E F(E) dE, \quad \text{(A1)}$$

where $F(E)$ is the functional form of the spectrum and D_L is the luminosity distance.

We assume that the Band function (Band et al. 1993) represents the intrinsic shape of the spectra for long GRBs even if the BAT data are insufficient to constrain a fit to this model. We choose to assume or infer the parameters of the Band function, and use its functional form rather than use the fits to the power law or cutoff power law due to their gross overestimates of the bolometric fluence.

The Band function takes the form

$$F(E) = \begin{cases} K_{50}^B \left(\frac{E}{50\,{\rm keV}}\right)^{\alpha_B} \exp\left(-\frac{E}{E_0}\right) \\ (\alpha_B - \beta_B) E_0 \geqslant E \\ K_{50}^B \left(\frac{(\alpha_B-\beta_B)E_0}{50\,{\rm keV}}\right)^{\alpha_B-\beta_B} \exp(\beta_B - \alpha_B) \left(\frac{E}{50\,{\rm keV}}\right)^{\beta_B} \\ (\alpha_B - \beta_B) E_0 \leqslant E \end{cases} \quad \text{(A2)}$$

where K_{50}^B is the normalization at 50 keV, and α_B and β_B are the spectral slopes below and above the break energy (E_0). When available, we use the measured spectral slopes, otherwise we assume $\alpha_B = -1$ and $\beta_B = -2.5$. The relationship between the spectral peak energy and the Band break energy is $E_p = (2+\alpha_B)E_0$.

Unfortunately, the data are often not sufficient to measure the Band function parameters because of the limited observed bandpass and measurement uncertainties. In some cases, better fits can be obtained using an exponential CPL model, and we can use these fits to estimate E_p for input into the Band function. The CPL takes the form

$$F(E) = K_{50}^{\rm CPL} \left(\frac{E}{50\,{\rm keV}}\right)^{\alpha_{\rm CPL}} \exp\left(\frac{-E(2+\alpha_{\rm CPL})}{E_p}\right), \quad \text{(A3)}$$

where $K_{50}^{\rm CPL}$ is the normalization at 50 keV, and $\alpha_{\rm CPL}$ is the spectral index. If available in the literature, we obtain measurements of the peak energy (E_p) from either Band function or exponential CPL fits to the γ-ray data (Table 8).

An adequate CPL fit and therefore an E_p measurement is available for only ~28% of the GRBs in our sample. For those without a directly measured E_p from either the Band or CPL fits, we infer a value using the correlation between E_p and the spectral index from fitting a single power law ($\alpha_{\rm PL}$) to the BAT data as parameterized by Zhang et al. (2007b) as

$$\log E_p = 2.76\text{–}3.61 \log(-\alpha_{\rm PL}), \quad \text{(A4)}$$

where $\alpha_{\rm PL}$ comes from fitting a simple power-law function of the form

$$F(E) = K_{50}^{\rm PL} \left(\frac{E}{50\,{\rm keV}}\right)^{\alpha_{\rm PL}}, \quad \text{(A5)}$$

and $K_{50}^{\rm PL}$ is the normalization at 50 keV. We use the measurements of $\alpha_{\rm PL}$ and $\alpha_{\rm CPL}$ from Sakamoto et al. (2008). However, this method only works for those GRBs whose E_p is inside the BAT energy band indicated by $-2.3 < \alpha_{\rm PL} < -1.2$. We

are unable to estimate $E_{\gamma,\rm iso}$ for those GRBs with $\alpha_{\rm PL}$ outside this range that do not have a measurement of E_p by another instrument.

Short burst spectra are better characterized by the exponential CPL model than the Band function. They also tend to have harder photon indices ($\sim$0.8) than long bursts. Therefore, we assume the CPL model to describe the gamma-ray spectra for short bursts in this sample used to calculate $E_{\gamma,\rm iso}$ and assume $\alpha_{\rm CPL} = -0.8$ if no measurement is available.

REFERENCES

Achterberg, A., et al. 2001, MNRAS, 328, 393
Amati, L., et al. 2002, A&A, 390, 81
Bagoly, Z., et al. 2006, A&A, 453, 797
Band, D., et al. 1993, ApJ, 413, 281
Bellm, E. C., et al. 2008, ApJ, 688, 491
Berger, E. 2006, GRB Coordinates Network, 5958, 1
Berger, E., & Becker, G. 2005, GRB Coordinates Network, 3520, 1
Berger, E., Fox, D. B., & Cucchiara, A. 2007a, GRB Coordinates Network, 6470, 1
Berger, E., et al. 2005a, ApJ, 629, 328
Berger, E., et al. 2005b, ApJ, 634, 501
Berger, E., et al. 2006a, GRB Coordinates Network, 4815, 1
Berger, E., et al. 2006b, ApJ, 642, 979
Berger, E., et al. 2007b, ApJ, 664, 1000
Bhattacharya, D. 2001, Bull. Astron. Soc. India, 29, 107
Bloom, J. S., Frail, D. A., & Kulkarni, S. R. 2003, ApJ, 594, 674
Bloom, J. S., Frail, D. A., & Sari, R. 2001, AJ, 121, 2879
Bloom, J. S., Perley, D. A., & Chen, H. W. 2006a, GRB Coordinates Network, 5826, 1
Bloom, J. S., et al. 2006b, GRB Coordinates Network, 5217, 1
Burrows, D. N., & Racusin, J. 2007, Il Nuovo Cimento B, 121, 1273
Burrows, D. N., et al. 2005, Science, 309, 1833
Burrows, D. N., et al. 2006, ApJ, 653, 468
Campana, S., et al. 2006, Nature, 442, 1008
Castro-Tirado, A. J., et al. 2006, GRB Coordinates Network, 5218, 1
Cenko, S. B., et al. 2006, GRB Coordinates Network, 5155, 1
Cenko, S. B., et al. 2007a, GRB Coordinates Network, 6888, 1
Cenko, S. B., et al. 2007b, GRB Coordinates Network, 6322, 1
Cenko, S. B., et al. 2008, ApJ, 677, 441
Chen, H.-W., et al. 2005, ApJ, 634, L25
Chevalier, R. A. 2007, arXiv:0706.0461
Chevalier, R. A., & Li, Z.-Y. 2000, ApJ, 536, 195
Chincarini, G., et al. 2007, ApJ, 671, 1903
Cucchiara, A., Fox, D. B., & Berger, E. 2006a, GRB Coordinates Network, 4729, 1
Cucchiara, A., Fox, D. B., & Cenko, S. B. 2007a, GRB Coordinates Network, 7124, 1
Cucchiara, A., et al. 2006b, GRB Coordinates Network, 5052, 1
Cucchiara, A., et al. 2007b, GRB Coordinates Network, 6665, 1
Cucchiara, A., et al. 2007c, GRB Coordinates Network, 6083, 1
Curran, P. A., van der Horst, A. J., & Wijers, R. A. M. J. 2008, MNRAS, 386, 859
Dai, Z. G., & Cheng, K. S. 2001, ApJ, 558, L109
Dai, Z. G., & Lu, T. 1998, A&A, 333, L87
D'Avanzo, P., et al. 2009, arXiv:0901.4038
de Pasquale, M., et al. 2008, MNRAS, 392, 153
de Pasquale, M., et al. 2006, A&A, 455, 813
Della Valle, M., et al. 2006, ApJ, 642, L103
Eichler, D., & Waxman, E. 2005, ApJ, 627, 861
Elíasdóttir, Á., et al. 2008, arXiv:0810.2897
Evans, P. A., et al. 2007, A&A, 469, 379
Evans, P. A., et al. 2008, arXiv:0812.3662
Falcone, A. D., et al. 2007, ApJ, 671, 1921
Ferrero, P., et al. 2008, arXiv:0804.2457
Fiore, F., et al. 2007, A&A, 470, 515
Frail, D. A., et al. 2001, ApJ, 562, L55
Fugazza, D., et al. 2005, GRB Coordinates Network, 3948, 1
Fugazza, D., et al. 2006, GRB Coordinates Network, 5513, 1
Fynbo, J. P. U., et al. 2005, GRB Coordinates Network, 3749, 1
Fynbo, J. P. U., et al. 2006a, GRB Coordinates Network, 5809, 1
Fynbo, J. P. U., et al. 2006b, A&A, 451, L47
Fynbo, J. P. U., et al. 2006c, Nature, 444, 1047
Gal-Yam, A., et al. 2006, Nature, 444, 1053
Gehrels, N., et al. 2004, ApJ, 611, 1005
Genet, F., Daigne, F., & Mochkovitch, R. 2007, MNRAS, 381, 732
Ghisellini, G., Ghirlanda, G., & Tavecchio, F. 2007a, MNRAS, 375, L36
Ghisellini, G., et al. 2007b, ApJ, 658, L75
Gmpe, D., et al. 2009, ApJ, submitted (arXiv:0903.1250)
Godet, O., et al. 2006, A&A, 452, 819
Golenetskii, S., et al. 2005a, GRB Coordinates Network, 3518, 1
Golenetskii, S., et al. 2005b, GRB Coordinates Network, 4238, 1
Golenetskii, S., et al. 2005c, GRB Coordinates Network, 4394, 1
Golenetskii, S., et al. 2006a, GRB Coordinates Network, 5837, 1
Golenetskii, S., et al. 2006b, GRB Coordinates Network, 5264, 1
Golenetskii, S., et al. 2006c, GRB Coordinates Network, 5460, 1
Golenetskii, S., et al. 2006d, GRB Coordinates Network, 5722, 1
Golenetskii, S., et al. 2006e, GRB Coordinates Network, 5890, 1
Golenetskii, S., et al. 2006f, GRB Coordinates Network, 4989, 1
Golenetskii, S., et al. 2007a, GRB Coordinates Network, 6849, 1
Golenetskii, S., et al. 2007b, GRB Coordinates Network, 6879, 1
Golenetskii, S., et al. 2007c, GRB Coordinates Network, 6960, 1
Golenetskii, S., et al. 2007d, GRB Coordinates Network, 6403, 1
Golenetskii, S., et al. 2007e, GRB Coordinates Network, 7114, 1
Gomboc, A., et al. 2008, ApJ, 687, 443
Graham, J. F., et al. 2008, arXiv:0808.2610
Granot, J., & Kumar, P. 2006, MNRAS, 366, L13
Granot, J., & Sari, R. 2002, ApJ, 568, 820
Grupe, D., et al. 2006, ApJ, 653, 462
Grupe, D., et al. 2009, ApJ, submitted (arXiv:0903.1258)
Harrison, F. A., et al. 2001, ApJ, 559, 123
Jakobsson, P., et al. 2006a, A&A, 460, L13
Jakobsson, P., et al. 2006b, A&A, 447, 897
Jakobsson, P., et al. 2007a, GRB Coordinates Network, 6398, 1
Jakobsson, P., et al. 2007b, GRB Coordinates Network, 7117, 1
Jakobsson, P., et al. 2007c, GRB Coordinates Network, 7076, 1
Jakobsson, P., et al. 2007d, GRB Coordinates Network, 6283, 1
Jakobsson, P., et al. 2007e, GRB Coordinates Network, 6952, 1
Jaunsen, A. O., et al. 2007a, GRB Coordinates Network, 6216, 1
Jaunsen, A. O., et al. 2007b, GRB Coordinates Network, 6010, 1
Jaunsen, A. O., et al. 2008, ApJ, 681, 453
Kalberla, P. M. W., et al. 2005, A&A, 440, 775
Kawai, N., et al. 2006, Nature, 440, 184
Klose, S., et al. 2004, AJ, 128, 1942
Kocevski, D., & Butler, N. 2008, ApJ, 680, 531
Kulkarni, S. R., et al. 1999, Nature, 398, 389
Kumar, P., Narayan, R., & Johnson, J. L. 2008, MNRAS, 388, 1729
Kumar, P., & Panaitescu, A. 2000, ApJ, 541, L51
La Parola, V., et al. 2006, A&A, 454, 753
Ledoux, C., et al. 2006, GRB Coordinates Network, 5237, 1
Ledoux, C., et al. 2007, GRB Coordinates Network, 7023, 1
Liang, E.-W., Zhang, B.-B., & Zhang, B. 2007, ApJ, 670, 565
Liang, E.-W., et al. 2006, ApJ, 646, 351
Liang, E.-W., et al. 2008, ApJ, 675, 528
Liang, E.-W., et al. 2009 (arXiv:0902.3509)
Malesani, D., et al. 2007, GRB Coordinates Network, 6651, 1
Mészáros, P. 2002, ARA&A, 40, 137
Mészáros, P., & Rees, M. J. 1997, ApJ, 476, 232
Mineo, T., et al. 2007, A&A, 469, 663
Mirabal, N., & Halpern, J. P. 2006, GRB Coordinates Network, 4591, 1
Mirabal, N., Halpern, J. P., & O'Brien, P. T. 2007, ApJ, 661, L127
Mirabal, N., et al. 2006, ApJ, 643, L99
Nousek, J. A., et al. 2006, ApJ, 642, 389
Oates, S. R., et al. 2007, MNRAS, 380, 270
Ohno, M., et al. 2007, GRB Coordinates Network, 6638, 1
Osip, D., Chen, H.-W., & Prochaska, J. X. 2006, GRB Coordinates Network, 5715, 1
Page, K. L., et al. 2007, ApJ, 663, 1125
Panaitescu, A. 2005, MNRAS, 362, 921
Panaitescu, A. 2007, MNRAS, 380, 374
Panaitescu, A. 2008, MNRAS, 383, 1143
Panaitescu, A., & Kumar, P. 2001, ApJ, 560, L49
Panaitescu, A., et al. 2006, MNRAS, 366, 1357
Pellizza, L. J., et al. 2006, A&A, 459, L5
Perley, D. A., et al. 2006, GRB Coordinates Network, 5387, 1
Perley, D. A., et al. 2008, ApJ, 672, 449
Piran, T. 2005, Rev. Mod. Phys., 76, 1143
Piranomonte, S., et al. 2006a, GRB Coordinates Network, 4520, 1
Piranomonte, S., et al. 2006b, GRB Coordinates Network, 5626, 1
Price, P. A., et al. 2007, ApJ, 663, L57
Prochaska, J. X., Chen, H.-W., & Bloom, J. S. 2006a, ApJ, 648, 95

Prochaska, J. X., et al. 2006b, ApJ, 642, 989
Prochaska, J. X., et al. 2007a, ApJS, 168, 231
Prochaska, J. X., et al. 2007b, GRB Coordinates Network, 6864, 1
Qin, Y.-P., et al. 2004, ApJ, 617, 439
Quimby, R., et al. 2005, GRB Coordinates Network, 4221, 1
Rees, M. J., & Mészáros, P. 1994, ApJ, 430, L93
Rees, M. J., & Mészáros, P. 1998, ApJ, 496, L1
Rhoads, J. E. 1999, ApJ, 525, 737
Rol, E., et al. 2006, GRB Coordinates Network, 5555, 1
Romano, P., et al. 2006, A&A, 456, 917
Ruiz-Velasco, A. E., et al. 2007, ApJ, 669, 1
Sakamoto, T., & Gehrels, N. 2009, arXiv:0901.4920
Sakamoto, T., et al. 2006, ApJ, 636, L73
Sakamoto, T., et al. 2008, ApJS, 175, 179
Sari, R., & Mészáros, P. 2000, ApJ, 535, L33
Sari, R., Piran, T., & Halpern, J. P. 1999, ApJ, 519, L17
Sari, R., Piran, T., & Narayan, R. 1998, ApJ, 497, L17
Schady, P., et al. 2006, ApJ, 643, 276
Schady, P., et al. 2007, MNRAS, 380, 1041
Shao, L., & Dai, Z. G. 2007, ApJ, 660, 1319
Soderberg, A. M., Berger, E., & Ofek, E. 2005, GRB Coordinates Network, 4186, 1
Soderberg, A. M., et al. 2006, ApJ, 650, 261
Soderberg, A. M., et al. 2007, ApJ, 661, 982
Sollerman, J., et al. 2007, A&A, 466, 839
Still, M., et al. 2005, ApJ, 635, 1187
Stratta, G., et al. 2007, A&A, 474, 827
Thöne, C. C., Perley, D. A., & Bloom, J. S. 2007a, GRB Coordinates Network, 6663, 1
Thöne, C. C., et al. 2006a, GRB Coordinates Network, 5812, 1
Thöne, C. C., et al. 2006b, GRB Coordinates Network, 5373, 1
Thöne, C. C., et al. 2007b, GRB Coordinates Network, 6379, 1
Thöne, C. C., et al. 2007c, GRB Coordinates Network, 6499, 1
Thöne, C. C., et al. 2007d, GRB Coordinates Network, 6741, 1
Troja, E., et al. 2008, MNRAS, 385, L10
Uhm, Z. L., & Beloborodov, A. M. 2007, ApJ, 665, L93
van Marle, A. J., et al. 2006, A&A, 460, 105
Watson, D., et al. 2006, ApJ, 652, 1011
Willingale, R., et al. 2007, ApJ, 662, 1093
Zeh, A., Klose, S., & Kann, D. A. 2006, ApJ, 637, 889
Zhang, B.-B., Liang, E.-W., & Zhang, B. 2007a, ApJ, 666, 1002
Zhang, B., & Mészáros, P. 2001, ApJ, 552, L35
Zhang, B., & Mészáros, P. 2004, Int. J. Mod. Phys. A, 19, 2385
Zhang, B., et al. 2006, ApJ, 642, 354
Zhang, B., et al. 2007b, ApJ, 655, 989
Zhang, B.-B., et al. 2009, ApJ, 690, L10